PROTEIN STRUCTURE, STABILITY AND DYNAMICS IN CELLS AND CELL-LIKE ENVIRONMENTS

Austin E. Smith

A dissertation submitted to the faculty of the University of North Carolina at Chapel Hill in partial fulfillment of the requirements for the degree of Doctor of Philosophy in the Department of Chemistry.

Chapel Hill
2015

Approved by:

Gary J. Pielak

Nancy L. Thompson

Andrew L. Lee

Linda L. Spremulli

Max L. Berkowitz

ABSTRACT

Austin E. Smith: Protein Structure, Stability and Dynamics in Cells and Cell-Like Environments
(Under the direction of Gary J. Pielak)

The intracellular milieu is filled with small molecules, nucleic acids, lipids and proteins. Theories have attempted to explain how macromolecules react to this environment for over 30 years. Recent experiment-based studies have shown that protein stability and dynamics are altered in this environment. I used the loop of chymotrypsin inhibitor 2 and two unfolded proteins (α-synuclein and FlgM) to show that the crowded cellular matrix does not necessarily cause structuring of these dynamic regions. Most importantly, I have shown the thermodynamic and mechanistic basis for how protein stability is changed in the cellular environment. To do this I use a marginally stable globular protein (an isolated SH3 domain) to measure stability, dynamics, and folding rates in cells and cell-like environments. Proteins are enthalpically destabilized in cells. The destabilization arises from charge-charge interactions of the cellular environment with the unfolded ensemble of the protein. These interactions also slow folding of the protein. This work will allow creation of a more complete picture of protein thermodynamics inside the cell. Furthermore, the SH3 domain is amenable to studying *in vitro* protein stability over a broad range of pH values, and allows acquisition of folding and unfolding rates with a variety of crowders. Future efforts will facilitate a better understanding of surface

charge interactions and will allow elucidation of a crowder's interaction with the transition state.

“Basic research is what I’m doing when I don't know what I’m doing.”

- Wernher von Braun

ACKNOWLEDGEMENTS

I would have never even started this journey if it were not for all those afternoons growing up when my Grandmother, Helen Clapp Greene, made me sit down and do my homework before I could go outside and play. She taught me to work hard, to have pride in what I do, and to persevere, through any task, until the job was done (then to clean up after myself!). That mentality defines me as a person; I owe all that to her. The rest of my family and my friends have supported me no matter what and I thank all of them for being there for me.

Scientifically, I want to thank both my mentors, Karen L. Buchmueller and Gary J. Pielak for teaching me how to do science. Furman University was a wonderful environment to learn how to think and discussions with Dr. B always pushed me and taught me how to approach both people and problems. She gave me a good base in NMR that allowed me to excel here at UNC. Gary has been the best mentor anyone can hope for. I came to UNC with a good hold on how to tackle tough problems. Gary taught me how to discuss problems, come up with ideas, and work with other people to come up with answers. He also taught me to believe in myself, something I am very grateful for.

I want to thank Greg B. Young for always helping me with the more technical NMR questions. He runs a great facility and I always enjoy going over to do science (means, talk to Greg).

Finally, I want to thank members of the Pielak lab. I came into lab knowing almost nothing about bacterial overexpression of proteins. Drs. Will Monteith, Mohona Sarkar, Jillian Tyrell, and Yaqiang Wang taught me everything from molecular biology to running a FPLC. Talking science with Will and Mohona helped me come up with the ideas that are the foundation for Chapter 4; my most important work. At the same time, spending time after lab with Will, Mohona and Rachel Cohen kept me sane through life's roller coaster.

Thank you all, you made this possible.

TABLE OF CONTENTS

LIST OF TABLES

LIST OF FIGURES

LIST OF ABBREVIATIONS

$\Delta C^{\circ}_{p,U}$	Standard heat capacity of unfolding
$\Delta G^{\circ\prime}_{U}$	Standard, modified free energy of unfolding
$\Delta\Delta G^{\circ\prime}_{U}$	Change in the standard, modified free energy of unfolding
$\Delta H^{\circ\prime}_{U}$	Standard, modified enthalpy of unfolding
$\Delta S^{\circ\prime}_{U}$	Standard, modified entropy of unfolding
η	Viscosity
ρ_f	Population of folded state
ρ_u	Population of unfolded state
τ_m	Rotational correlation or tumbling time
τ_{mix}	Mixing time
°C	Degree Celcius
ATP	Adenosine triphosphate
BSA	Bovine serum albumin
CI2	Chymotrypsin inhibitor 2
CLEANEX	Phase-modulated CLEAN chemical exchange
CPMG	Carr-Purcell-Meiboom-Gill
E_a	Activation energy
EDTA	Ethylene diamine tetraacetic acid
FPLC	Fast protein liquid chromatography
g	Gram
GB1	B1 domain on protein G
h	Hour

HEPES	4-(2-hydroxyethyl)-1-piperazineethanesulfonic acid
HSQC	Heteronuclear single quantum correlation
ILVA	Isoleucine, leucine, valine, alanine enrichment
IPTG	Isopropyl β-D-1-thiogalactopyranoside
J_{NH}	Proton-nitrogen coupling constant
K	Kelvin
$k_{b,ref}$	Reference rate of base catalyzed amide proton exhange
kcal/mol	Kilocalories per mole
k_{cl}	Closing rate constant
kDa	Kilodalton
k_{int}	Rate of amide proton exchange in absence of structure
k_{obs}	Observed rate of amide protein exchange
K_{op}	Opening equilibrium constant
k_{op}	Opening rate constant
L	Liter
LB	Lennox Broth
M	Molar
MIMS	Mitochondrial intermembrane space
min	Minute
Nat	N-α-acetyltransferase
NMR	Nuclear magnetic resonance
NOESY	Nuclear Overhauser effect spectroscopy
PEG	Polyethylene glycol
PF	Protection factor

pI	Isoelectric point
PVP	Polyvinylpyrrolidone
R	Gas constant
s	Second
SASA	Solvent accessible surface area
SH3	*N*-terminal SH3 of *Drosophila* protein drk
SOD	Superoxide dismutase
SOLEXSY	Solvent exchange spectroscopy
T_1	Spin-lattice relaxation time
T_2	Spin-spin relaxation time
T_m	Melting temperature
TMAO	Trimethylamine N-oxide
TPPI	Time-proportional phase incrementation
T_{ref}	Reference temperature
TROSY	Transverse relaxation optimized spectroscopy
T_s	Temperature of maximum stability

CHAPTER 1: NMR STUDIES OF PROTEIN FOLDING AND BINDING IN CELLS AND CELL-LIKE ENVIRONMENTS

Edited from: Smith AE, Zhang Z, Pielak GJ, Li C. *Current Opinion in Structural Biology*. **30**,7-16 (2015)

Abstract

Proteins function in cells where the concentration of macromolecules can exceed 300g/L. The ways in which this crowded environment affect the physical properties of proteins remain poorly understood. We summarize recent NMR-based studies of protein folding and binding conducted in cells and *in vitro* under crowded conditions. Many of the observations can be understood in terms of interactions between proteins and the rest of the intracellular environment (*i.e.*, quinary interactions). Nevertheless, NMR studies of folding and binding in cells and cell-like environments remain in their infancy. The frontier involves investigations of larger proteins and further efforts in higher eukaryotic cells.

Introduction

The cytoplasm is a complex environment where macromolecules can reach concentrations greater than 300g/L and occupy 30% of the cellular volume.[1,2] Organelles can be even more crowded.[3] These high concentrations of macromolecules define the environment where proteins function. Furthermore, the surfaces of biological macromolecules (*e.g.*, proteins, nucleic acids) are covered with groups capable of forming hydrogen bonds and attractive or repulsive charge-charge interactions.[4] The crowded nature of the cellular interior puts these groups in close contact.

Multi-dimensional NMR spectroscopy provides information about protein structure, dynamics, stability and interactions at the level of individual atoms. The main advantage of NMR for studying crowding effects is that the introduction of NMR-active isotopes (*e.g.*, ^{15}N, ^{13}C, ^{19}F) allows the protein of interest (the test protein) to be examined in the presence of unenriched crowding agents, even when the agents are present at biologically relevant concentrations. The main downside of NMR is its insensitivity; in general, test protein concentrations must be greater than 10^{-5} M. This insensitivity means that NMR detection of proteins in cells relies mostly on promoter-driven overexpression of test proteins or their delivery into cells. We use the term in-cell NMR rather than *in vivo* NMR for several reasons: expression levels are hundreds of times larger than native levels, many of test proteins are not native to the cells in which they are studied and dense cell slurries alter intracellular pH (Chapters 3 and 4).[5]

The birth of in-cell NMR

Three publications in between 1975-1989 gave rise to in-cell protein NMR by utilizing NMR active-isotopes. First, to elucidate the viscosity of the intracellular matrix in red cells, Bob London used [2-^{13}C]-histidine to label mouse hemoglobin.[6] London measured the labeled proteins T_1 relaxation time to determine the rotational correlation time in the cytoplasm. He discovered the intracellular viscosity is less than two times that of water. Later in 1975, Llinas pioneered the use of ^{15}N to label peptides in *Ustilago sphaerogen*.[7] 14 years later, Brindle grew yeast with 5-fluorotyptophan to produce fluorine labeled phosphoglycerate kinase.[8] Two distinct ^{19}F resonances were observable and dependent on the metabolic state of the cells. These seminal papers showed how efficient labeling strategies produce in-cell NMR spectra even when NMR methodology and hardware were far from what we have today.

In 1976, Daniels used the different T_2 relaxation properties of small molecules and macromolecules to filter out the ^{1}H signal of macromolecules; leaving behind only the signal associated with the small molecule, adrenaline.[9] A year later, Brown used a similar spin-echo strategy to measure the internal pH of red cells.[10] While these two systems did not focus on protein NMR, they show an important result, proteins tumble slowly in cells, have short transverse relaxation times and result in broad resonances. On the contrary, small molecules tumble quickly, have long transverse relaxation times and can readily be seen in cells.

In 2001, Volker Dötsch's group brought isotopic labeling, *Escherichia coli* and NMR together. Serber used ^{15}N-enrichment and ^{1}H-^{15}N correlation spectroscopy to observe the small protein, NmerA in living *E. coli.*[11] Another paper outlined different growth strategies and showed selective labeling could produce high quality results for the protein calmodulin.[12] These papers signified the beginning of high-resolution multi-nuclear in-cell NMR.

Hereafter, we focus on high-resolution solution NMR studies published since 2011 conducted in cells and under crowded *in vitro* conditions. We have not reviewed NMR-based studies of membrane proteins under physiological conditions or enzyme activity in cells, but direct the reader to several recent contributions.[13-17]

Quinary interactions and NMR

In 1973, Anfinsen stated that weak surface contacts play a role in protein chemistry.[18] In 1983, McConkey realized that such interactions are above primary, secondary, tertiary and quaternary structure.[19] He coined the term quinary structure to define the interactions between proteins and the rest of the intracellular environment. These contacts organize the cytoplasm and play key roles in metabolism[20] and signal transduction. Interest in quinary interactions languished, however, until recent in-cell NMR studies returned them to the fore.[21,22]

Much of the data reviewed here can be understood in terms of quinary structure. We consider attractive quinary structure in terms of binding interactions. This binding is neither as specific nor as strong as, for instance, the interaction

between a protein-based protease inhibitor and its protease, but it is binding nonetheless.

Attractive quinary interactions can adversely affect NMR spectra. Fast tumbling (*i.e.*, rotational motion) is key to acquiring high-resolution protein NMR data in solution. Increasing the molecular weight of a globular protein or solvent viscosity with small viscogens degrade tumbling rates, increasing the width of protein resonances. It was recognized several years ago that spectra of globular proteins tend to be broader in cells than they are when the protein is studied in buffer alone[23] and that broadening did not arise from increased viscosity alone. For globular test proteins, especially in *Escherichia coli* cells, broadening is often so severe that the test protein spectrum is undetectable. This situation can lead to dangerous misinterpretations when spectra attributed to the test protein inside cells are actually from test protein that has leaked from the cells into the surrounding media.[24] Along these lines, the Christodoulou group has recently applied NMR-diffusion methods to separate signals from inside cells from those in the surrounding media.[25]

The Spicer[26] and Ito[27] groups have identified important exceptions to the observation that heteronuclear multidimensional spectra from globular proteins in *E. coli* are too broad to be useful. One of these proteins, the B1 domain of protein G (GB1, 6 kDa), has come to serve as a test bed for in-cell NMR.[26,28-34]

Lila Gierasch's lab examined the effects of increased viscosity on several properties, including the width of crosspeaks in ^{1}H-^{15}N HSQC spectra of small globular proteins in simple buffered solutions.[32] The widths were compared to those

obtained for the same proteins in *E. coli* cells. The data indicate that the large line widths in cells cannot be completely explained by a higher viscosity. The authors concluded that the extra broadening comes from weak transient interactions (*i.e.*, quinary interactions) with components of the cytosol.

Peter Crowley's group obtained direct evidence for these interactions by examining HSQC spectra of overexpressed cytochrome *c* (12 kDa) in *E. coli* lysates (severe broadening prevented acquisition of in-cell spectra).[28] Size exclusion chromatography as a function of salt concentration in combination with SDS-PAGE was used to show that the broadening is due to weak interactions. Mutating positively-charged residues to negatively-charged residues resulted in crosspeak narrowing and smaller SDS-PAGE-measured molecular weights, indicating that the quinary contacts involve interactions of positively-charged residues on the cytochrome with negatively-charged moieties on macromolecules in the lysate. This important study has placed the focus on charge-charge interactions. Other types of polar interaction as well as hydrophobic contacts may also play key roles, but systematic studies have yet to be performed.

Volker Dötsch's group moved work on quinary interactions into eukaryotic cells.[35] They injected ^{15}N-enriched protein into *Xenopus laevis* oocytes and again found that quinary interactions resulted in broad HSQC spectra. Specific phosphorylation of one of the proteins (the 19 kDa WW domain of peptidyl-prolyl isomerase Pin1) abrogated the interactions, resulting in observation of the test protein spectrum in oocytes.

Lewis Kay's group tackled quinary interactions with the test protein calmodulin (17 kDa) in *E. coli* lysates. The system provides information about nonspecific interactions because neither calmodulin nor its specific binding partners are found in bacteria. The interactions between components of the cytosol and calmodulin affect protein dynamics on the ps to ns and ms timescales.[36] They measured a lower bound of ~0.2 mM for the binding constant of calmodulin with cytosolic components (Figure 1.1 a,b).[37] These results show that quinary interactions are strong even in the absence of natural selection. The team also examined what happens when calmodulin is immersed in yeast lysate. This system has both biological and physiological relevance because yeast lysate harbors proteins that specifically bind calmodulin. The specific interactions caused further broadening resulting in complete loss of the spectrum (Figure 1.1 c).

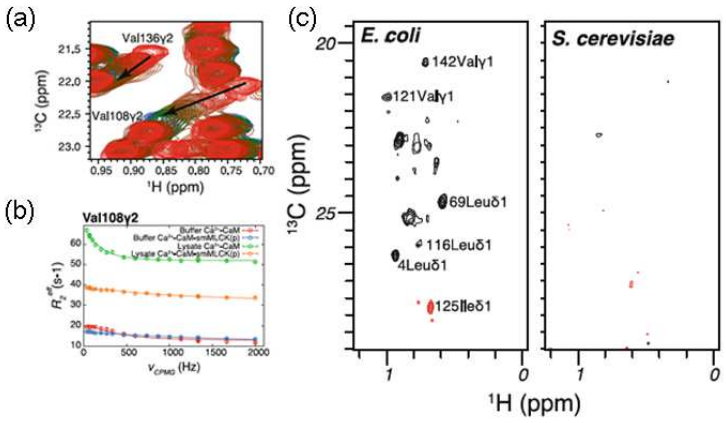

Figure 1.1. Equilibrium thermodynamic effects of quinary interactions.[37] a) Changes in calmodulin methyl chemical shifts as a function of *E. coli* lysate concentration indicate nonspecific interactions with lysate constituents on the fast NMR timescale. b) Methyl relaxation data showing the higher viscosity of lysate (100 g/L, orange and green) compared to buffer (red and blue) and the competition between nonspecific biding and specific peptide binding (green and orange). c) HSQC spectra showing that specific binding in *Saccharomyces cerevisiae* (yeast) lysate replaces nonspecific binding in *E. coli* lysate resulting in disappearance of the calmodulin spectrum.

As discussed above, some proteins have such strong quinary interactions that tumbling is too slow for solution NMR. However, lack of rotational motion need

not be a barrier; solid state NMR with magic angle spinning is the tool of choice under these conditions. Reckel *et al.* used solid-state NMR to examine two rotationally challenged proteins in *E. coli* cells.[38] Selective ^{13}C- enrichment in combination with uniform ^{15}N enrichment provided interpretable spectra. Although solid-state spectra are not yet as informative as solution spectra, solid state NMR of biological macromolecules is advancing quickly.[39]

Folding intermediates and crowding

Latham and Kay studied the effects of biologically relevant crowders on protein folding intermediates.[40] They chose an 8 kDa four-helix bundle (the FF domain) as the test protein and assessed its folding dynamics in *E. coli* and yeast lysates (Figure 1.2 a-c). The same intermediate is found in buffer and lysates, but it is more highly populated in lysates. Further, the exchange rate between native and intermediate states is slowed. Thus, crowding can affect folding pathways, which suggests we may not learn all there is to know about physiologically relevant folding by studying proteins in buffer alone.

We close this section with a warning. A classic approach to understanding the solvent-protein friction of folding dynamics is to quantify the conversion between states as a function of viscosity. Using the same four-helix bundle, Sekhar *et al.*[41] showed that a small molecule viscogen (glycerol) and a macromolecular viscogen (bovine serum albumin) give different results. The discrepancy arises from the sizes of the viscogens compared to the folding species; only small viscogens yield correct

values because, for molecules much smaller than the test protein, the macroscopic viscosity equals the microscopic viscosity.[42]

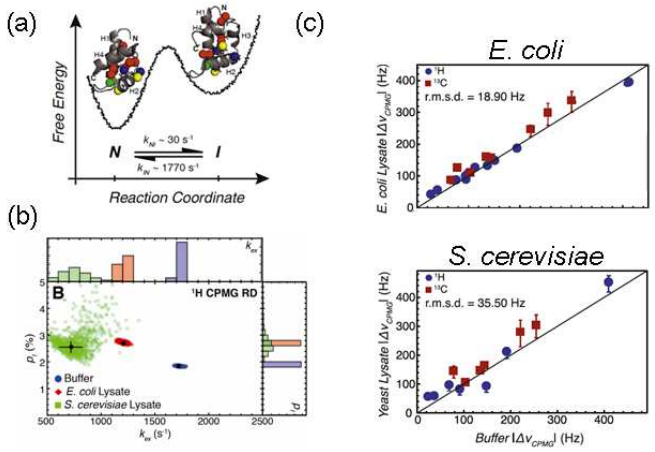

Figure 1.2. Kinetic effects of quinary interactions.[40] a) Free energy diagram of the equilibrium between the native state and the intermediate of the FF domain. b) Percent population *versus* rate plot showing that the intermediate is more highly populated in *E. coli* lysate and yeast lysate than it is in buffer. **c)** Plots of shift changes in lysate (upper, *E. coli*; lower, yeast) showing that lysates do not affect the structure of the intermediate.

Disordered proteins are different

The interior of a globular protein is similar to that of a billiard ball in that both are rigid. That is, the parts that comprise the interior of these objects move as a group. On the other hand, disordered proteins[2] are similar to spaghetti in that they have local, internal motions that are independent of global motion. In cells, the internal motions are not affected to the same extent as the global motion of globular proteins. Thus, disordered proteins tend to give higher quality HSQC spectra in cells. Barnes *et al.*[2] showed this differential effect in a simple experiment by fusing the disordered protein, α-synuclein (14 kDa), to the small globular protein, ubiquitin (9 kDa). An in-cell HSQC spectrum of the fusion showed only crosspeaks from the disordered protein. When the cells were lysed and the lysate diluted, loosening ubiquitin's quinary interactions, the spectra of both proteins were visible. By

examining secondary shifts, Waudby *et al.* showed that α-synuclein appears to remain unfolded even in *E. coli*.[5] By monitoring the shift of the protein's histidine resonance, these authors also showed that the internal pH of *E. coli* in dense slurries acidified to pH 6.2 instead of 7.6. (For further information see Chapter 3.)

Majumber *et al.* exploited the differential dynamic effect on globular and disordered proteins to probe binding.[43] First, they induced expression of a disordered protein in ^{15}N-containing media and obtained the expected in-cell spectrum. Next, they induced expression of its unenriched globular partner. Binding of the two proteins hindered the local motion of the previously disordered protein, broadening its resonances into the background. Application of principle component analysis even allowed the authors to define the binding site on the disordered partner.

Minimizing effects of attractive quinary interactions on spectra

Methods for obtaining high-resolution spectra of globular proteins in cells are desirable because attractive quinary interactions broaden resonances. We discuss two approaches: ^{19}F incorporation and optimization of conventional multidimensional experiments.

^{19}F is a wonderful in-cell NMR nucleus for eight reasons. First, fluorine is rare in biological systems,[44] which eliminates background. Second, it is 100% abundant. Third, the NMR sensitivity of ^{19}F is 83% that of ^{1}H, making it one of the most sensitive nuclei. Fourth, its chemical shift range is large. Fifth, as a spin-1/2 nucleus, its relaxation properties are similar to those of the proton. Sixth, cells can be coaxed

into incorporating aromatic fluorine-labeled amino acids.[29] Seventh, replacing a few hydrogen atoms with fluorine atoms has a minimal effect on structure and stability.[45]

The eighth advantage is subtle. It might be considered a disadvantage that only a *few* fluorine-labeled amino acids are incorporated. However, this situation is advantageous for studying globular proteins in cells. Simply put, it is easier to observe a few broad resonances in a one-dimensional spectrum of an ^{19}F-labeled proteins than it is to observe tens to hundreds of closely packed broad crosspeaks in a typical multidimensional spectrum of protein uniformly enriched with ^{15}N or ^{13}C.[31] Not only can 'less mean more' with ^{19}F, the Crowley lab has shown how to make ^{19}F labeling of tryptophan residues in *E. coli* an inexpensive endeavor.[29] They showed 5-fluorindole and 6–fluoroindole are incorporated into GB1. The method represents a 15-fold savings compared to the usual scheme for labeling aromatic residues, which involves, for tryptophan labeling, growth of cells in minimal media containing labeled tryptophan, an inhibitor of aromatic amino acid synthesis (glyphosate, *i.e.*, Roundup™) and unlabeled phenylalanine and tyrosine.[46]

In one of the first studies to demonstrate the effect of attractive interactions in cells, Schlesinger *et al.*[47] exploited ^{19}F labeling to show that crowding is not always stabilizing, because, as explained in the next section, attractive quinary interactions can overcome crowding-induced short-range repulsions. Ye *et al.* went on to use ^{19}F to show that the viscosity in cells is only two-to-three times that in buffer alone, but quinary interactions make the protein appear much larger than it is. Their work also emphasizes the fact that care is required in interpreting NMR-relaxation derived in-cell viscosity measurements, because both quinary interactions and viscosity affect

relaxation.

Despite the favorable aspects of ^{19}F labeling, enrichment with ^{15}N and ^{13}C can yield more detailed information about structure and dynamics. One way to overcome the broadening-induced overlap is to use selective enrichment.[36,37] Latham and Kay showed that incorporating ^{13}C and ^{2}H methyl-enriched Ile, Leu, Val, or Met gave interpretable ^{13}C–^{1}H correlation spectra in *E. coli* and yeast lysates.[36,37] There are, however, many combinations of enrichment schemes and NMR experiments. To define a strategy for optimizing in-cell NMR in *E. coli*, Xu *et al.* explored the in-cell NMR of four highly-expressed small (*i.e.*, <20 kDa) globular proteins in combination with several enrichment methods, including uniform ^{15}N enrichment with and without deuteration, selective ^{15}N-leucine enrichment, ^{13}C methyl enrichment of isoleucine, leucine, valine, and alanine (ILVA), fractional ^{13}C enrichment, and ^{19}F labeling.[33] ^{19}F labeling gave acceptable results in all instances, as did ^{13}C ILVA labeling with one-dimensional ^{13}C direct detection in a cryogenic probe. ILVA enrichment, however, is expensive and such simple spectra might yield little insight relative to their cost. Xu *et al.* suggest that uniform ^{15}N enrichment and ^{19}F labeling, both of which are low cost, be tried first. If enrichment yields high quality HSQC spectra, other approaches will probably work. If an HSQC spectrum of the protein in cells is not observed, but reasonable ^{19}F spectra are, ILVA enrichment is worth trying. If both experiments fail, one might try weakening protein-cytoplasm interactions by exploring charge-change variants.[28]

Quinary interactions and globular protein stability

The effects of crowding on protein stability arise from two phenomena: short range (steric) repulsions and longer-range interactions. Repulsions stabilize globular proteins for the simple reason that the crowders take up space, favoring the compact native state over the expanded denatured state. Longer-range interactions (also called soft- or chemical- interactions) include hydrogen bonding and charge-charge interactions. Charge-charge interactions can be stabilizing or destabilizing. Charge-charge repulsions are stabilizing because they require the crowders to stand off from the test protein making them occupy even more space. Attractive interactions between the test protein surface and the crowders, on the other hand, are destabilizing because unfolding of the test protein exposes more interacting surface.

NMR-detected amide proton exchange is a tool for quantifying the free energy required to expose backbone amide protons to solvent.[48] The largest opening free energies reflect global protein stability, *i.e.*, the free energy of denaturation. Although the method provides opening free energies at the residue level, we focus on the global free energy of opening because interpretation of smaller opening free energies remains controversial.[49,50] Importantly, exchange experiments provide this information without the addition of heat or denaturing co-solutes, which is important for systems containing protein crowders because it means crowder stability is unaffected by the experiment. Several controls are required to ensure that the rate data yield equilibrium thermodynamic data.[51]

Work in the Pielak lab has been conducted with the small globular proteins, chymotrypsin inhibitor 2 (CI2, 6 kDa) and GB1. One of the control experiments mentioned above is to demonstrate that the crowding agent does not affect the intrinsic rate of exchange in a disordered peptide. This assumption is true for a number of crowders, including the *E. coli* cytoplasm (See Chapters 2 and 3).[52-54]

Synthetic crowders such as Ficoll and polyvinylpyrrolidone have minimal attractive interactions with CI2. Thus, these crowders stabilize CI2 and other test proteins.[42,53,55,56] CI2, however, is destabilized by protein crowders and the constituents of *E. coli* lysate.[57] The destabilization suggests the presence of attractive crowder-test protein interactions, which is consistent with other NMR experiments on CI2.[42] Inomata *et al.*[58] have observed an increase in amide-proton exchange rates for the test protein ubiquitin in human cells, a result that is also consistent with the presence of attractive quinary interactions.

Sarkar *et al.* hypothesized that the interactions involve charge-charge contacts.[59] To test this idea, they refined the lysate by removing the anionic nucleic acids and negatively charged proteins; CI2 was still destabilized. The result indicates there remains much to be learned about longer-range interactions and crowding. Sarkar and Pielak have also shown that the osmolyte glycine betaine can mitigate the lysate's destabilizing effect on CI2.[60]

Monteith *et al.*[61] used amide proton exchange to measure the stability of GB1 in living *E. coli* cells (Figure 1.3). There are two reasons one might think this would be an easy experiment. First, GB1 is one of the few globular proteins whose ^{1}H-^{15}N

HSQC spectrum can be directly observed in *E. coli.*[26] Second, D_2O diffuses quickly into cells.[62] Unfortunately, the low signal-to-noise ratio of the in-cell HSQC spectra prevents quantification of exchange rates. Instead, the authors employed a quenched-lysate method.[62] They showed that GB1 is destabilized in cells compared to buffer by approximately 1 kcal/mol, which is significant given the free energy of unfolding in buffer is 7 kcal/mol.[63]

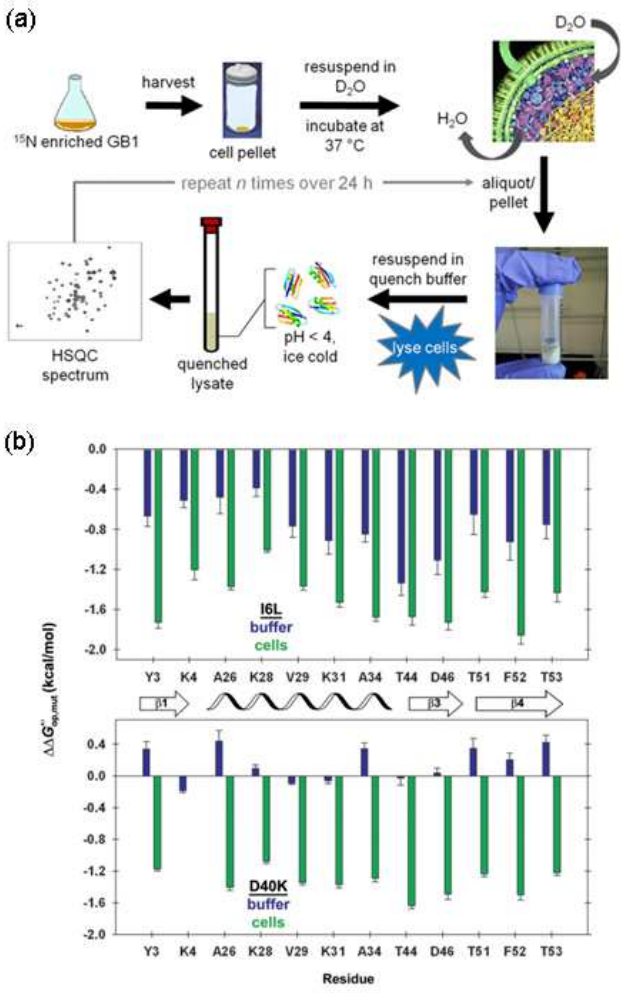

Figure 1.3. Quantifying residue-level protein stability in living cells.[61,63] a) Procedure used to acquire in- cell NMR-detected amide ^{1}H exchange data. b) Bar graphs showing the free energy of opening *versus* residue number of GB1 showing that protein variants are destabilized with respect to buffer in cells.

The stability change of GB1 in cells appears to be related to protein charge, but the story is not yet clear. As mentioned above, the majority of proteins in *E. coli* are anionic, and so are CI2 and GB1. The resulting net repulsive interactions should allow both proteins to retain their rotational motion resulting in acceptably narrow crosspeaks.[28] The decreased stability of GB1 in cells compared to buffer suggests interactions between the test protein and the cytoplasm. Interactions, however, are inconsistent with the fact we can observe its

HSQC spectrum in cells.[28,31-33] CI2 and GB1, show similar responses to the cytosol. CI2 is negatively charged, its ^{15}H-^{1}H HSQC spectrum cannot be observed in *E. coli*[24] and the protein is destabilized by reconstituted cytosol.[57,59] This response of similarly charged proteins to the cytosol, in addition to the research presented in Chapter 4, show that anionic proteins are destabilized in cells. However, we still have a great deal to learn about the nature of these quinary interactions.

NMR in eukaryotic cells

Eukaryotic cells are at the cutting edge of in-cell NMR. Although *E. coli* is a good test bed because it is easy to grow and can be coaxed into expressing the large amounts of test protein required for NMR, the more complex features of eukaryotic cells make them an important subject for in-cell NMR.

Insect cells and the yeast *Pichia pastoris* are commonly used to express large quantities of eukaryotic proteins. Bertrand *et al.* tested this yeast as a subject for in-cell NMR using ubiquitin as the test protein.[64] Their results are especially informative about what can happen when proteins are highly expressed. The authors compared ^{1}H-^{15}N HSQC spectra after expression from a methanol inducible promoter under two conditions. Methanol as the carbon source gave high expression and usable spectra. A combination of methanol and glucose gave even higher expression, but the ubiquitin was trapped in expression vesicles, making it essentially a solid. The resulting diminution of rotational motion broadened its resonances into the background. Hamatsu *et al.* have shown that insect cells are also amenable to in-cell protein NMR with a baculovirus expression system, reporting both ^{15}N-^{1}H HSQC

spectra and three dimensional spectra of four small globular proteins, including GB1 and calmodulin.[30] Thus, these eukaryotes should prove useful for in-cell NMR, especially for studies of eukaryotic-specific post-translational modifications.

Higher eukaryotic cells are fussier than *E. coli*. For instance, *E. coli* can be examined under anaerobic conditions, but most higher-eukaryotic cells are sensitive to nutrient depletion and require oxygenation. Kubo *et al.* developed a clever bioreactor that solves these problems.[65] Cells are fixed in a gel in the sensitive part of the probe where they can be easily perfused with fresh oxygenated media (Figure 1.4). The authors tested the bioreactor by using ^{31}P NMR to examine ATP levels. Without the bioreactor, ATP depletion was complete in 30 min. With the bioreactor, cells maintained their ATP levels for the duration of the experiment (5 h). They also investigated the in-cell ^{1}H-^{13}C HMQC spectra of a 9- kDa methyl ILV ^{13}C-enriched microtubule binding protein. The protein was introduced into the cells *via* a pore-forming toxin. Transferred cross saturation experiments and competition experiments with unenriched protein helped define the binding site and showed specific microtubule binding. Importantly, the binding site in cells is similar to that discovered *in vitro*. These experiments also illuminate an important point about protein leakage. In the absence of the bioreactor only 10-20% of the protein leaked, but almost all the signal arose from the leaked protein because the quinary interactions in cells led to severe broadening.

The Banci group has characterized the maturation of the mitochondrial intermembrane space (MIMS) protein, Mia40 (16 kDa) in human cells.[66] To reach their destination, MIMS proteins must be transported through the outer membrane in

a disulfide-reduced, unfolded state. Overexpression resulted in accumulation of the fully folded form in the cytoplasm because the transporter and reductive apparatus were overwhelmed. This lack of a physiological outcome with a physiologically relevant protein is one reason why such studies should be called in-cell, not *in-vivo*, NMR. As expected, simultaneous overexpression of the reductive machinery resulted in more unfolded, ready-to-be-transported protein.

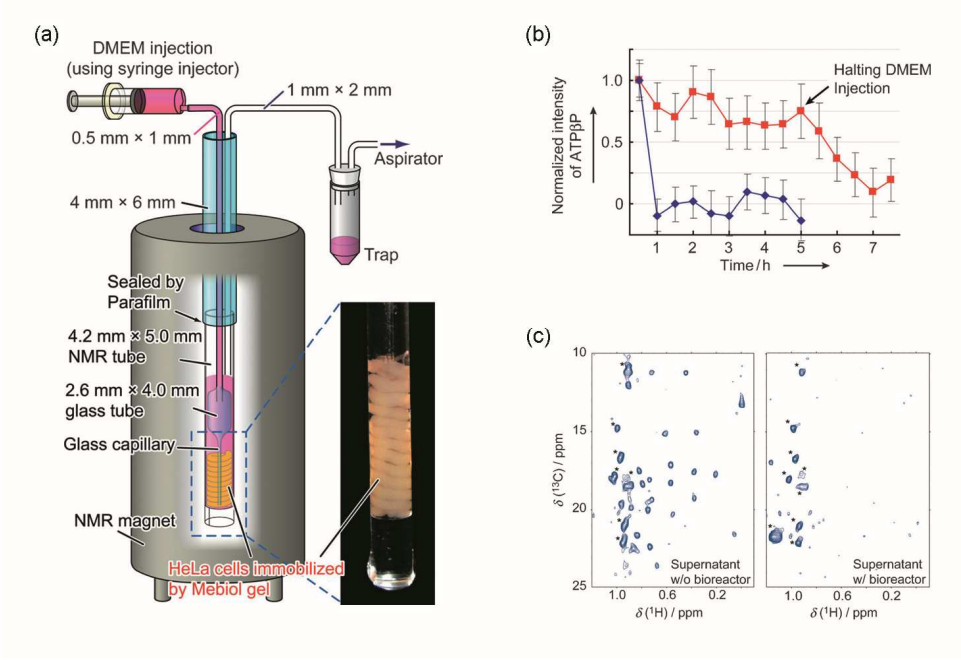

Figure 1.4. a) Bioreactor for protein NMR in eukaryotic cells.[65] b) Plots of relative ATP concentration *versus* time showing that the bioreactor maintains ATP levels. c) TROSY spectra showing the bioreactor prevents test protein leakage.

Banci *et al.* also investigated the maturation of superoxide dismutase (SOD) in human cells.[67] The wealth of detail available from their spectra is remarkable. The authors could detect the monomeric partially unfolded apo form, the Zn-bound monomer and dimer as well as the Cu-Zn form. Furthermore, both oxidized and reduced cysteines could be detected by [^{15}N]-cysteine enrichment. This group also attached a sequence to target Mia40 and superoxide dismutase for import into the MIMS[68] and showed it is possible to acquire high-resolution data from proteins in the

inter-membrane space of intact mitochondria.

Continuing with SOD, Danielsson *et al.* took a different approach.[69] Instead of expressing the protein in human cells, they expressed and purified the isotopically-enriched protein from *E. coli* and covalently attached a cell penetrating peptide to an engineered cysteine on SOD. Initial attempts to introduce sufficient amounts into HeLa cells were unsuccessful. Success came after increasing the positive charge on SOD. The success of the charge changes makes sense considering our knowledge of cell penetrating proteins: they must overcome the negative charge on the test protein to which they are attached. Another key point involving a pre-enriched protein[65] is that the NMR-active nuclei are less likely to find their way into metabolites and other proteins that obscure the test-protein spectrum.

We close this section by comparing the quality of in-cell spectra from bacterial and eukaryotic cells. With rare exceptions,[26,27] multidimensional spectra from globular protein are difficult to observe in *E. coli*. As discussed above, the situation is better in eukaryotic cells. It is not entirely clear why this should be the case, but one clue may be the lower concentration of protein plus nucleic acid in eukaryotic cells (100-300 g/L) compared to *E. coli* cells (300-500 g/L).[2] It is important to bear in mind, however, that eukaryotic cells are far from a panacea because not all proteins that should be observable by in-cell NMR in eukaryotes are observed.[66] The difference between what should happen and what does happen extends to methods for getting isotopically enriched proteins into higher eukaryotic cells. Besides injection, which is only reasonable for oocytes, the most common methods are attachment of a cell-penetrating peptide, use of a toxin to open pores in the

membrane and electroporation.[70] It is unclear, however, which method will work best in any particular combination of test protein and cell.

Summary and closing thoughts

NMR has taken the lead in adding to our understanding of how quinary structure affects protein stability, folding pathways, ligand binding and side chain dynamics. Selective labeling strategies have been shown to be useful when these interactions broaden protein resonances into the baseline. In addition, sophisticated NMR strategies are being applied to not only *E. coli* proteins, but also to several types of eukaryotic cells. Nevertheless, the field remains in its infancy. We are picking the low hanging fruit: typical test proteins have molecular weights of approximately 10 kDa, but the average molecular weight an *E. coli* protein is 30 kDa. The average eukaryotic protein is even larger.[71] In addition, we need models to explain how proteins of similar size, shape and surface properties interact differently with the cytosol. Therefore, the most important and challenging frontier is the study of larger test proteins, because crowding effects are predicted to scale with molecular weight.[72]

CHAPTER 2: AMIDE PROTON EXCHANGE OF A DYNAMIC LOOP IN CELL EXTRACTS

Edited from: Smith AE, Sarkar M, Young GB, Pielak GJ. *Protein Science.* **22**,1313-1319 (2013)

Abstract

Intrinsic rates of exchange are essential parameters for obtaining protein stabilities from amide ^{1}H exchange data. To understand the influence of the intracellular environment on stability, one must know the effect of the cytoplasm on these rates. We probed exchange rates in buffer and in *Escherichia coli* lysates for the dynamic loop in the small globular protein chymotrypsin inhibitor 2 using a modified form of the solvent exchange NMR experiment, SOLEXSY. No significant changes were observed, even in 100 g dry weight L^{-1} lysate. Our results suggest that intrinsic rates from studies conducted in buffers are applicable to studies conducted under cellular conditions.

Introduction

The cytoplasm of *Escherichia coli* is a milieu of macromolecules whose total concentration can exceed 300 gL^{-1}.[1,73] This crowded environment is expected to affect biophysical properties, such as protein stability.[74] Quantifying these changes is key to understanding protein chemistry in cells.[75]

$^1H/^2H$ exchange has been used to assess protein stability since Linderstrøm-Lang and colleagues laid the theoretical framework in the 1950s.[76-78] Native globular proteins exist in equilibrium with a large ensemble of less structured states.[48] When a protein in H_2O is transferred to ^2H_2O, solvent-exposed amide protons in the native state can, in most cases,[79] exchange freely with deuterons. Hydrogen-bonded and other protected protons, however, exchange only upon exposure to solvent during a transient opening (equation 1),

$$N^1H\ (\text{closed}) \underset{}{\overset{K_{op}}{\rightleftharpoons}} N^1H\ (\text{open}) \xrightarrow{k_{int}} N^2H\ (\text{open}) \qquad (1)$$

where $K_{op}=k_{op}/k_{cl}$ is the opening equilibrium constant, k_{op} and k_{cl} are the opening and closing rate constants, respectively, and k_{int} is the intrinsic rate of amide ^1H exchange in an unstructured peptide. When intrinsic exchange is rate limiting ($k_{cl} > k_{int}$), the observed exchange rate of a protonated amide (k_{obs}) can be used to determine the modified standard free energy of opening (*i.e.*, the stability), because $k_{obs} = K_{op}k_{int}$ (equation 2).[51,78,80]

$$\Delta G^{\circ'}_{op} = -RT\ln K_{op} = -RT\ln \frac{k_{obs}}{k_{int}} \qquad (2)$$

This approach is valid for protons that are exposed on global unfolding, so called "globally exchanging residues," because maximum values of $\Delta G^{o'}_{op}$ often equal the free energy of denaturation measured by using independent techniques.[78,81,82]

To validate the $^1H/^2H$ exchange results, one must know if k_{int} changes under crowded conditions. k_{int} values in buffer can be calculated as a function of primary structure, pH, and temperature[83-85] using the online resource, SPHERE.[86] These values have also been used to measure protein stability in solutions crowded by synthetic polymers and proteins, because as described below, these crowding agents do not affect k_{int}.[53,87-89] Saturation transfer NMR was used to show that the k_{int} of poly-DL-alanine does not change in 300 gL^{-1} 70 kDa of Ficoll or its monomer, sucrose.[53,90] Information about crowding induced changes in intrinsic rates can also be gleaned from dynamic loops of globular proteins.

Chymotrypsin inhibitor 2 (CI2; Figure 2.1A) is a globular protein[91] (Figure 2.1A) that has been extensively studied by amide $^1H/^2H$ exchange.[82,87,92,93] Residues in its reactive loop are potential models for assessing k_{int}, because they possess few hydrogen bonds, lower than average order parameters,[94] high B-factors,[91] and large solvent accessible surface areas (SASAs; Figure 2.1B). Phase-modulated CLEAN chemical exchange (CLEANEX) experiments[95] conducted in buffer and under crowded conditions show that exchange rates in the loop do not change in solutions containing 300 gL^{-1} 40-kDa poly-vinyl-pyrrolidone (PVP),[87] 100 gL^{-1} lysozyme and 100 gL^{-1} bovine serum albumin.[88] These observations suggest that k_{int} values in buffer can be applied to experiments conducted with these crowding agents.

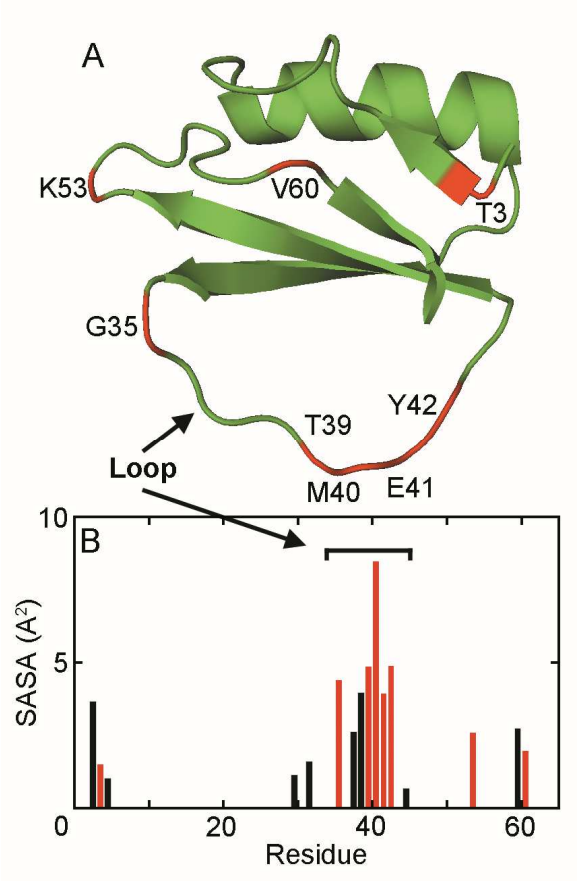

Figure 2.1. Exposed and fast exchanging backbone amide protons in CI2. Residues whose backbone amide protons exhibit reliable exchange using SOLEXSY (293 K, 50 mM sodium phosphate, pH_{read} 6.7) are shown in red. A) Ribbon diagram (PDB: 2CI2 made with PyMOL[96]). B) Histogram of SASAs of backbone amide nitrogens *versus* residue number. Residues whose backbone amide hydrogens form a hydrogen bond to a backbone carbonyl oxygen, a side chain oxygen or the oxygen of structured water are not shown, with one exception (see text). SASAs were calculated with the program POPS.[97]

To understand protein stability under native cellular conditions we must understand how the cytoplasm affects k_{int}. This goal is challenging because ^{15}N-^{1}H heteronuclear single quantum correlation (HSQC) spectra cannot be observed from most globular proteins, including CI2, in cells.[23,98] Furthermore, proteins often begin to leak from cells after 1.5 h,[24] or less, whereas the experiments used to measure exchange require at least an order of magnitude longer.[95,99] For these reasons, we chose *E. coli* cell lysates as a reasonable mimic of the cytoplasm.

We used a modified $^{15}N^{H/D}$-SOLEXSY[99] experiment to measure k_{int}. The experiment is performed on a $^{15}N/^{13}C$ doubly labeled protein, in 50% $^{1}H_2O$:50% $^{2}H_2O$. SOLEXSY bypasses problems such as radiation damping artifacts, long recycle delays, nuclear Overhauser effect- and total correlation spectroscopy- type transfers between $^{1}H^{\alpha}$ and $^{1}H^{N}$, and relayed transfer that arise from selective water excitation.[99] Instead, magnetization is transferred from the $^{1}H^{\alpha}$ through the $^{13}C^{\alpha}$ and

carbonyl carbon to the amide ^{15}N. The ^{15}N chemical shift is then encoded to produce two signals, $^{15}N^{D}$ and $^{15}N^{H}$.

After encoding, a variable mixing time monitors the exchange of $^{15}N^{D}$ and $^{15}N^{H}$ for each hydrogen isotope, and magnetization is transferred to ^{1}H for detection. At short mixing times, only protonated species are observed, because only protonated amide nitrogens are detected at the ^{1}H frequency (Figure 2.2). The chemical shift of $^{15}N^{D}$ is also recorded, but at short mixing times no signal is detected because little ^{1}H has exchanged onto the deuterated amide. At longer times, exchange of ^{1}H onto the initially deuterated ($^{15}N^{D}$) site causes an increase in the volume of the $^{15}N^{D}/^{1}H$ crosspeak, producing a buildup curve (Figure 2.2B). The exchange of deuterons onto the initially protonated site causes a decrease in volume, and a corresponding decay with time (Figure 2.2B). Plots of peak volume *versus* time can be fitted to yield k_{int}. High quality data can be obtained for rates of between 0.3 and 5.0 s^{-1}.[99]

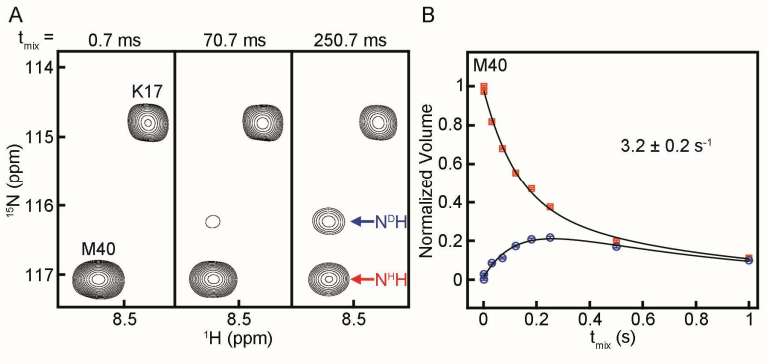

Figure 2.2. Region of $^{15}N^{H/D}$-^{1}H correlation spectra showing an exchangeable (M40) and a non-exchangeable (K17) residue from CI2 and the corresponding exchange curves for M40. Buildup of the deuterated amide ($N^{D}H$) and decay of the protonated amide ($N^{H}H$) occur as the mixing time (t_{mix}) increases. Spectra were acquired with a modified SOLEXSY pulse sequence (see Methods).

We crowded CI2 with up to 100 g dry weight L^{-1} ($g_{dry}L^{-1}$) of *E. coli* lysate and used $^{15}N^{H/D}$-SOLEXSY[99] to measure exchange in the dynamic loop and other

exposed regions. Exchange rates are largely unchanged in lysates compared to buffer alone. Our results suggest that k_{int} values from buffer based experiments (*i.e.*, from SPHERE) are valid for quantifying protein stability under cellular conditions.

Results

Lysate solutions are problematic for two reasons. First, at high concentrations they are not stable enough to allow acquisition of a full 60-h SOLEXSY experiment (Figure 2.3). Second, weak interactions between constituents of the lysate and the protein being studied result in a shorter transverse relaxation time (T_2), leading to broad resonances that degrade the quality of the spectra used to create buildup and decay curves.[42,98,100]

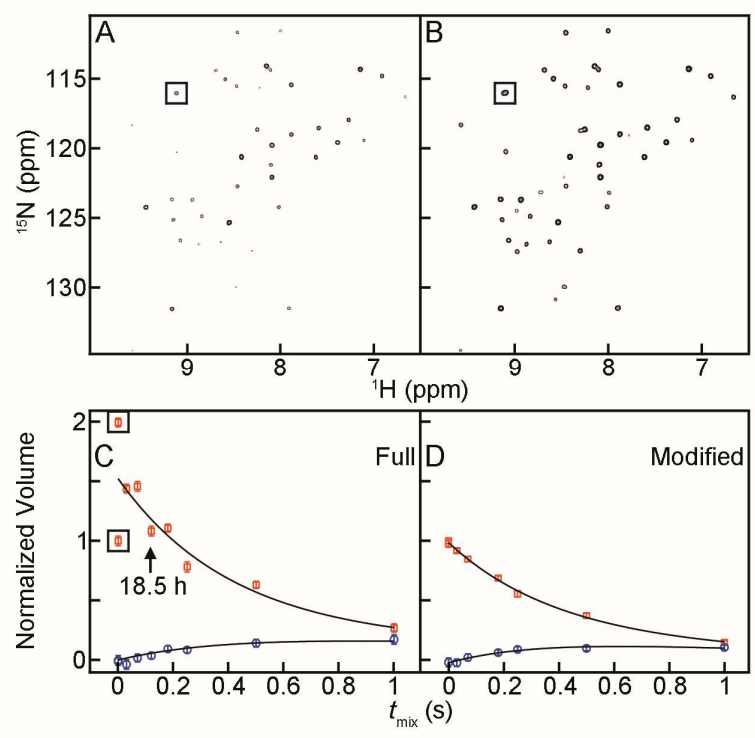

Figure 2.3. Reconstituted lysate (100 $g_{dry}L^{-1}$) is stable for 15 h, but is compromised in less than 59 h. t_{mix} values were acquired in random order. The SOLEXSY dataset for the shortest t_{mix}, 0.7 ms, was acquired twice; the second time at the end of the experiment. The full SOLEXSY experiment required ~59 h, whereas the modified experiment required <15 h. A) Spectrum recorded with the full SOLEXSY experiment (t_{mix} = 0.7 ms) at 6 h. The G35 crosspeak is boxed. B) Repeat spectrum (*i.e.*, t_{mix} = 0.7 ms) recorded to assess stability at the end of the experiment, 59 h, 16 m. Peak volumes are larger at the end of the experiment. The increased volume suggests precipitation of the lysate, allowing CI2 more rotational freedom, lengthening T_2, which sharpens the resonances. C) Fit for G35 from the full

SOLEXSY experiment, which required 59 h. Instead of decaying, the volume of the 120 ms point (vertical arrow, acquired at ~19 h) is greater than that for the 0.7 ms point, acquired at 6 h, indicating breakdown of the lysate. Consistent with this idea, precipitate was visible at ~60 h. D) G35 data acquired with the modified experiment, which required only ~15 h. The repeated t_{mix} point, acquired at 14 h, is on top of the point acquired at 1 h, suggesting that the lysate was stable over the course of the modified experiment. Consistent with this idea, no precipitate was observed at the end of the experiment.

In an attempt to overcome the stability problem, we decreased the acquisition time by reducing the number of scans, but this approach exasperated the broadening problem. We then tried removing the sign-coding portion of the SOLEXSY experiment. In combination with acquiring fewer t_1 points, this change enabled us to acquire a complete experiment in 15 h. Furthermore, the consequent removal of 10.6 ms ($\sim\frac{1}{J_{NH}}$) from the pulse sequence resulted in a mean increase in signal to noise ratio of 25% in buffer (depending on the resonance, Supplementary Figure 2.1A), which helped compensate for the decreased sensitivity arising from the shorter T_2 values in lysate (Supplementary Figure 2.1B). The original and modified SOLEXSY experiments were validated by comparing rates acquired in buffer to mathematical predictions and to values obtained with CLEANEX[79,88] (Supplementary Table 2.1).

Residues useful for assessing k_{int} values should lack stable hydrogen bonds. Backbone amide hydrogens from 15 residues of CI2 do not form hydrogen bonds to a backbone carbonyl oxygen, a side chain oxygen or the oxygen of structured water.[91] These residues are in loops, and as expected, exhibit significant SASAs (Figure 2.1B). We also included E41, whose backbone amide ^{1}H is within hydrogen

bonding distance (2.6 Å for the heavy atoms) of the carbonyl oxygen of T39, in our analysis because loop motion likely makes any hydrogen bond transient.

Nine of these 16 hydrogens exhibit amide exchange on the SOLEXSY (i.e., 0.3 - 5.0 s^{-1})[99] timescale (Supplementary Table 2.1, Figures 2.4A, and Supplementary figures 2.2 and 2.3). Data from K2, were not included because its exchange is faster than that which can be reliably measured by SOLEXSY.[99] k_{obs} values obtained in buffer and in 100 $g_{dry}L^{-1}$ lysate are within error of one another, and are similar to the values calculated and predicted by SPHERE (Figure 2.4A, Supplementary Table 2.1).

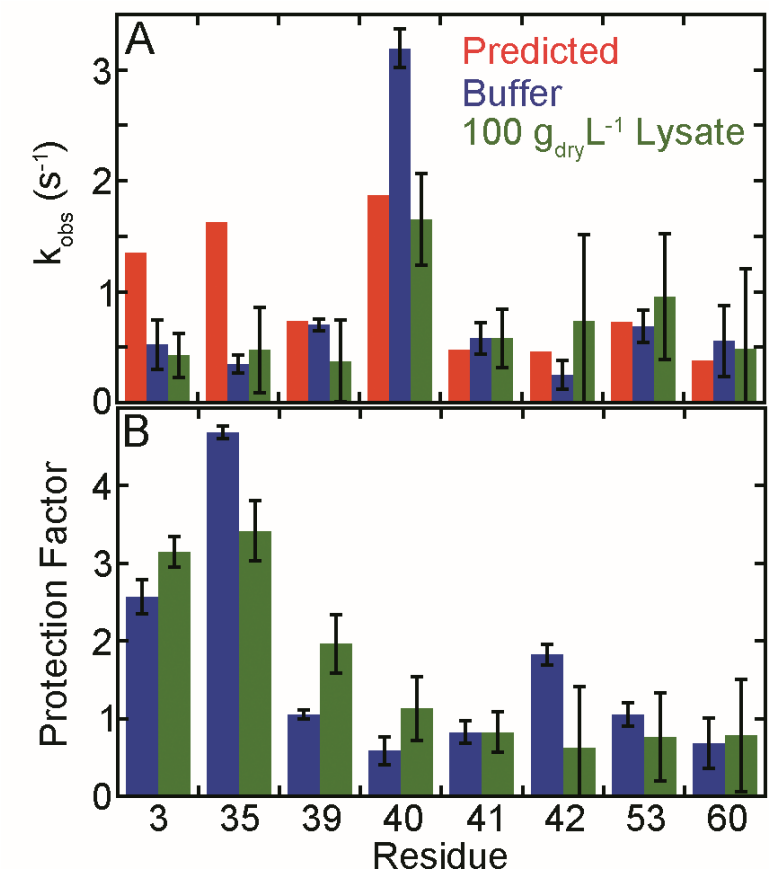

Figure 2.4. *E. coli* lysate (100 $g_{dry}L^{-1}$, green) and buffer alone (blue) yield similar amide backbone ^1H exchange rate constants, k_{obs}, for solvent accessible residues. A) Predicted values[83,84] are shown in red. Values from modified SOLEXSY data are the average of 20 Monte Carlo noise simulations. Error bars represent the standard deviation. B) Protection factors ($k_{int,predicted}/k_{obs,buffer}$ and $k_{int,predicted}/k_{obs,lysate}$). Error bars are from the uncertainties in Panel A. Conditions are given in the caption of Figure 2.1.

Seven of the 16 residues do not show exchange on the SOLEXSY timescale at pH_{corr} 6.9 (Figure 2.1). Residues E4 and Q59 exchange slow enough to be detected by conventional

$^{1}H_2O$-to-$^{2}H_2O$ transfer experiments.[53,82] The other five residues (A29, V31, H37, V38, I44) show chemical exchange using CLEANEX, but these data were acquired at higher pH.[79] Extrapolating these data to our conditions (pOH = 7.71)[101] and using an Arrhenius activation energy (E_a)[83]of 17 kcalmol^{-1}, leads to k_{int} values between 0.001 s^{-1} and 0.04 s^{-1}, which are too small to be accurately assessed with SOLEXSY.

Discussion

Knowing how the cytoplasm affects $^{1}H/^{2}H$ amide exchange of exposed residues is vital to calculating opening free energies and global stabilities.[51,53,87] Although these values are normally obtained from SPHERE, the server only predicts values in solutions made with 100% $^{1}H_2O$ or $^{2}H_2O$. The SOLEXSY experiment, however, is conducted in a 1:1 $^{2}H_2O$:$^{1}H_2O$ mixture. To obtain a direct comparison to our solution conditions we calculated the rates using the equations that drive SPHERE, but with different parameters. Rates were calculated stipulating a buffer made from 1:1 $^{2}H_2O$:$^{1}H_2O$ (pH_{corr} 6.9, pK_W 14.61), with poly-DL-alanine as the reference molecule and $k_{b,ref}$ for N^D exchanging in $^{1}H_2O$.[83-85,101] These rates were then halved[99] to make them comparable to those from experiment and SPHERE. This manipulation accounts for the fact that exchange onto $^{15}N^D$ is only visible by SOLEXSY when ^{1}H exchanges. In other words, ^{2}H exchange onto initially deuterated amides is undetected, because only ^{1}H is visible at the ^{1}H frequency, making the predicted rate twice that measured by SOLEXSY. These corrected values closely match those obtained from SPHERE by using the poly-DL-alanine rate basis, with a pH_{read} 6.5, in 100% $^{2}H_2O$ (Supplementary Table 2.1).

The corrected rates are also similar to rates measured in buffer (Figure 2.4A) and obtained with CLEANEX (Supplementary Table 2.1).[79,88] Slight deviations from the CLEANEX results are likely due to differences in solvent condition; the SOLEXSY experiments used 1:1 $^{2}H_2O$:$^{1}H_2O$ and a different ionic strength. Taken together these results suggest that SOLEXSY is a useful experiment for measuring exchange rates in disordered loops of globular proteins.

The rates are also similar to those measured in lysate (Figure 2.4), indicating that lysate at 100 $g_{dry}L^{-1}$ has an insignificant effect on exchange. Protection factors (k_{int}/k_{obs}) of less than five are an unreliable indicator of secondary structure,[102] whereas residues that exchange only on complete unfolding (*i.e.*, globally exchanging residues) can have protection factors greater than 10^5.[53,55,82,87,93] Protection factors based on the SOLEXSY data ($k_{int,predicted}/k_{obs,buffer}$ and $k_{int,predicted}/k_{obs,lysate}$), are no larger than five for the loop region (Figure 2.4), and even these may reflect small errors in the parameters used to drive SPHERE. Taken together, the data indicate that small differences in k_{obs} values between lysate and buffer will have small effects on protein stability studies conducted in lysates.

The concentration of macromolecules in the cytoplasm of *E. coli* is 300 gL^{-1}, or even higher.[1,73] Our attempts to acquire SOLEXSY data at these concentrations were unsuccessful for the reasons discussed above: chemical instability of the lysate and interaction-induced resonance broadening. Nevertheless, rates obtained in 0, 25, 50 and 100 $g_{dry}L^{-1}$ lysate show no general and consistent trend (Figures 2.5 and Supplementary Figure 2.4), suggesting our results are applicable to the dense interior of the bacterial cell.

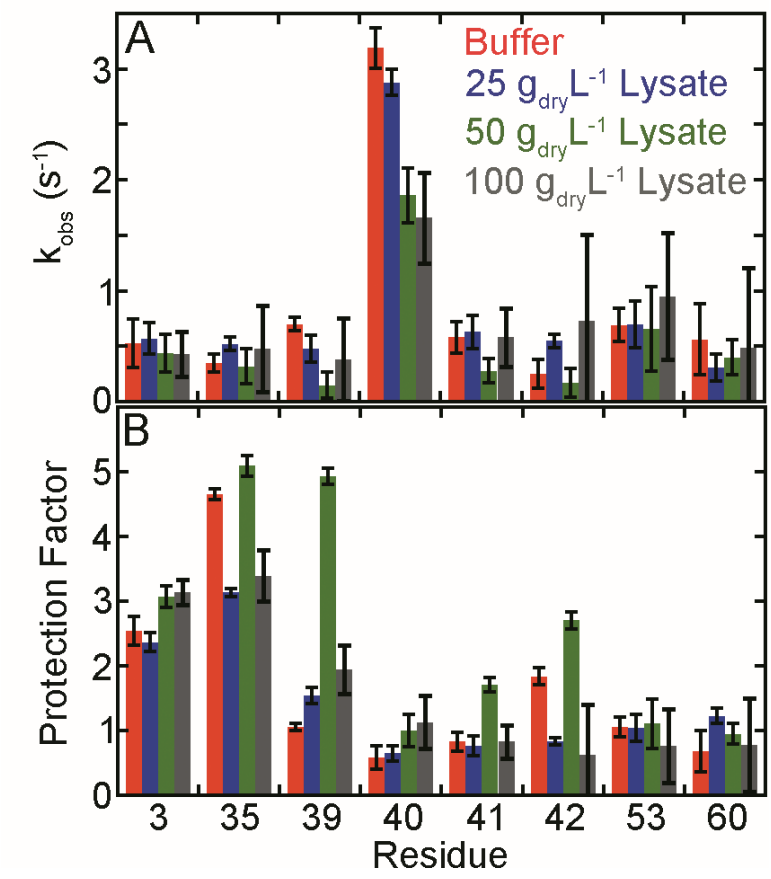

Figure 2.5. Comparison of 0 - 100 $g_{dry}L^{-1}$ lysate show no general and consistent trend. A) Values from SOLEXSY data are the average of 20 Monte Carlo noise simulations. Error bars represent the standard deviation. Data were acquired with the modified SOLEXSY experiment for buffer and 100 $g_{dry}L^{-1}$ lysate. The full experiment was used for 25 and 50 $g_{dry}L^{-1}$ lysate. B) Protection factors ($k_{int,predicted}/k_{obs,SOLEXSY}$). Predicted values were calculated as described in the footnote to Table S1. Error bars are the same as in Panel A. Protection factors of less than 5 are not a reliable predictor of structure.[102]

Methods

Protein. ^{13}C glucose (2.0 gL^{-1}) and $^{15}NH_4Cl$ (1.0 gL^{-1}) were used to produce purified CI2.[42,87] Purity was assessed by SDS-PAGE.

Lysate. Lysates were obtained by modifying the method described by Wang et al.[42] Competent BL21-DE3 (Gold) *E. coli* were transformed with the pET28a vector harboring the kanamycin resistance gene. The transformants were plated on Luria-Bertani (LB) agar plates containing 60 µg/ml kanamycin. The plates were incubated overnight at 37 °C. A single colony was added to 60 mL of LB liquid media containing 60 µg/ml kanamycin. The culture was shaken overnight (New Brunswick Scientific, Innova, I26) at 225 rpm and 37 °C, then equally divided into four, 2.8 L baffled flasks, each containing 1 L of LB and 60 µg/ml kanamycin. This culture was

grown to saturation (9 h). The cells were pelleted at 6500 *g* for 30 min and the pellets stored at -20 ^{o}C.

Each frozen cell pellet was thawed, resuspended and lysed in 25 mL of 25 mM Tris-HCl (pH 7.6) containing a cocktail of protease inhibitors [Sigma-Aldrich: 0.02 mM 4-(2-aminoethyl) benzenesulfonyl fluoride, 0.14μM E-64, 1.30 μM bestatin, 0.01 μM leupeptin, 3.0 nM aprotinin and 0.01 mM sodium EDTA, 0.01 mM, final concentrations]. Lysis was accomplished by sonic dismembration on ice for 6 min (Fischer Scientific, Sonic Dismembrator Model 500, 20% amplitude, 2 s on, 2 s off). After lysis, cell debris was removed by centrifugation (14000 *g* at 10 ^{o}C for 40 min). The supernatant was filtered through a 0.22 μm Durapore® PVDF membrane (Millipore).

The filtrates were pooled (~ 37 mL per L culture) and dialyzed (Thermo Scientific, SnakeSkin, 3K MWCO) at 4 ^{o}C against 5 L of 10 mM Tris-HCl, 0.1% NaN_3 (pH 7.6) for 72 h. The buffer was changed every 24 h. The inhibitor cocktail was added to each dialysate. After lyophilization (Labconco, Freezone Plus 2.5), the straw-colored powder was stored at -20 ^{o}C. To ensure that the lysate contained 50% exchangeable protons and 50% exchangeable deuterons, the powder was resuspended in 50% D_2O (Cambridge Isotopes Laboratories), incubated at room temperature for 8 h and lyophilized. The process was performed twice and the resultant powder (300.0 mg) was resuspended in sufficient 50% deuterated sodium phosphate buffer (50 mM, pH_{read} 6.7) to give 3.0 mL of solution with a final concentration of 1.0 x 10^2 $g_{dry\ weight}$ L^{-1}. The pH_{read} was adjusted to 6.7. The solution was centrifuged at 14000 *g* for 10 min. The supernatant contained 52 ± 4 gL^{-1} of

protein as determined by a modified Lowry assay sing bovine serum albumin as the standard (Thermo Scientific). The uncertainty in the concentration is the standard deviation of the mean from triplicate measurements.

NMR. ^{13}C, ^{15}N enriched CI2 was added to sodium phosphate buffer (50 mM, 50% $^{1}H_2O$:50% $^{2}H_2O$, pH_{read} 6.7) with and without lysate. The final CI2 concentration was ~1 mM for samples acquired in buffer alone with the modified SOLEXSY experiment. A concentration of 1.5 mM was used for all other experiments. The concentrations in buffer were verified by measuring the absorbance at 280.0 nm ($\varepsilon = 7.04 \times 10^3\ M^{-1}\ cm^{-1}$).[103]

A modified SOLEXSY experiment[99] was used to measure exchange rates (Appendix 1). Sign coding was originally used to facilitate data acquition on intrinsically disordered proteins by reducing the number of crosspeaks.[99] The spectra of globular proteins like CI2 are well dispersed, elimiating the need for this feature. We removed the 10.6 ms sign coding period,

$$\left(\frac{1}{2J_{NH}}\right)\text{-}90^{\circ}_{x}90^{\circ}_{\pm x}(^{1}H),180^{\circ}_{x}(^{15}N)\text{-}(\frac{1}{2J_{NH}}).$$

Data were acquired at 293 K on a 600 MHz Bruker Avance III HD spectrometer equipped with a HCN triple resonance cryoprobe (Bruker TCI) and Topspin Version 3.2 software. Sweep widths were 9600 Hz in the ^{1}H dimension and 2300 Hz in the ^{15}N dimension. Twenty-four transients were collected using 1024 complex points in t_2 with 128 TPPI points in t_1 for each mixing time. Data were collected in a pseudo-3D mode with mixing times of 0.7, 1000.7, 250.7, 120.7, 30.7, 180.7, 70.7, 500.7 ms. An additional spectrum with a 0.7 ms mixing time was

collected at the end of the experiment to assess lysate stability. The 120.7 ms data point was omitted for the 100 $g_{dry}L^{-1}$ lysate. Acquisition required approximately 15 h per sample. The full experiment used the same parameters, except that 256 points in t_1 were used for each mixing time, and required ~60 h per sample.

Data processing. Data were processed with NMRPipe.[104] The t_2 data were subjected to a 60° shifted squared sine bell function (800 complex points for buffer alone and 512 complex points for lysate) prior to zero-filling to 8096 points and Fourier transfomation. The t_1 data were linear predicted to 256 points prior to application of a 60°-shifted squared sine bell. The t_1 data were then zero-filled to 2048 points and Fourier-transformed. The spectra were peak picked and integrated using the built in automated routines. Peak volumes were fitted as described.[99] When the full experiment was used similar routines were followed without linear prediction. Sign encoded spectra were added or subtracted to create buildup and decay spectra, respectively.

Supplementary Information for Chapter 2

Supplementary Table 2.1. Exchange rates (s^{-1}) in buffer.

			SOLEXSY[c]		CLEANEX-PM	
Residue	SPHERE[a]	Prediction[b]	Full	Modified	M et al.[d]	H et al.[e]
3	1.49	1.35	0.7 ± 0.2	0.5 ± 0.2	NR[f]	0.3
35	1.79	1.63	0.56 ± 0.04	0.35 ± 0.08	NR	0.5
39	0.82	0.74	0.4 ± 0.2	0.70 ± 0.06	0.5 ± 1	0.2
40	2.05	1.87	2.58 ± 0.04	3.2 ± 0.2	NR	1.8
41	0.53	0.48	0.5 ± 0.1	0.6 ± 0.1	0.5 ± 1	NR
42	0.51	0.46	0.57 ± 0.02	0.3 ± 0.1	0.4 ± 0.2	0.1
53	0.80	0.73	0.67 ± 0.03	0.7 ± 0.1	1 ± 1	0.4
60	0.42	0.38	0.35 ± 0.08	0.6 ± 0.3	NR	0.4

Footnotes

[a]based on CI2 sequence using the online server SPHERE, poly-DL-alanine rate basis, pH 6.5, 100% D_2O[83,84,86]

[b]Rates were calculated as described[99] using the method introduced by Bai, et al.[83,85] $\log k_{b,ref}$ and $\log k_{w,ref}$ are from Connelly, et al.[84] pOH was calculated taking into account the 50% H_2O:50% D_2O solution.[101] After calculation, rates were halved, as discussed in the main text.

[c]fitted as described.[99] Averages from Monte Carlo analysis along with their uncertainties. pH_{corr} 6.9, 50 mM $NaPO_4$,293 K, 50% D_2O

[d]CLEANEX[95] data from Miklos, et al.[88] pH 6.5, 50 mM $NaPO_4$, 293 K, 10% D_2O. Rates halved to account for H_2O concentration.

[e]Relaxation compensated[105] CLEANEX[95] data from Hernandez, et al.[79] pH 7: 20 mM $NaPO_4$, total ionic strength 150 mM, 298 K. To mimic our experimental conditions: pOH (7.71, as calculated)[101] was subtracted from $\log k_{OH}$ to obtain $\log k_{int}$. These values were then extrapolated to 293 K using the Arrhenius equation and an activation energy of 17 kcal/mol.[83] Rates halved to account for H_2O concentration.

[f]Not Reported

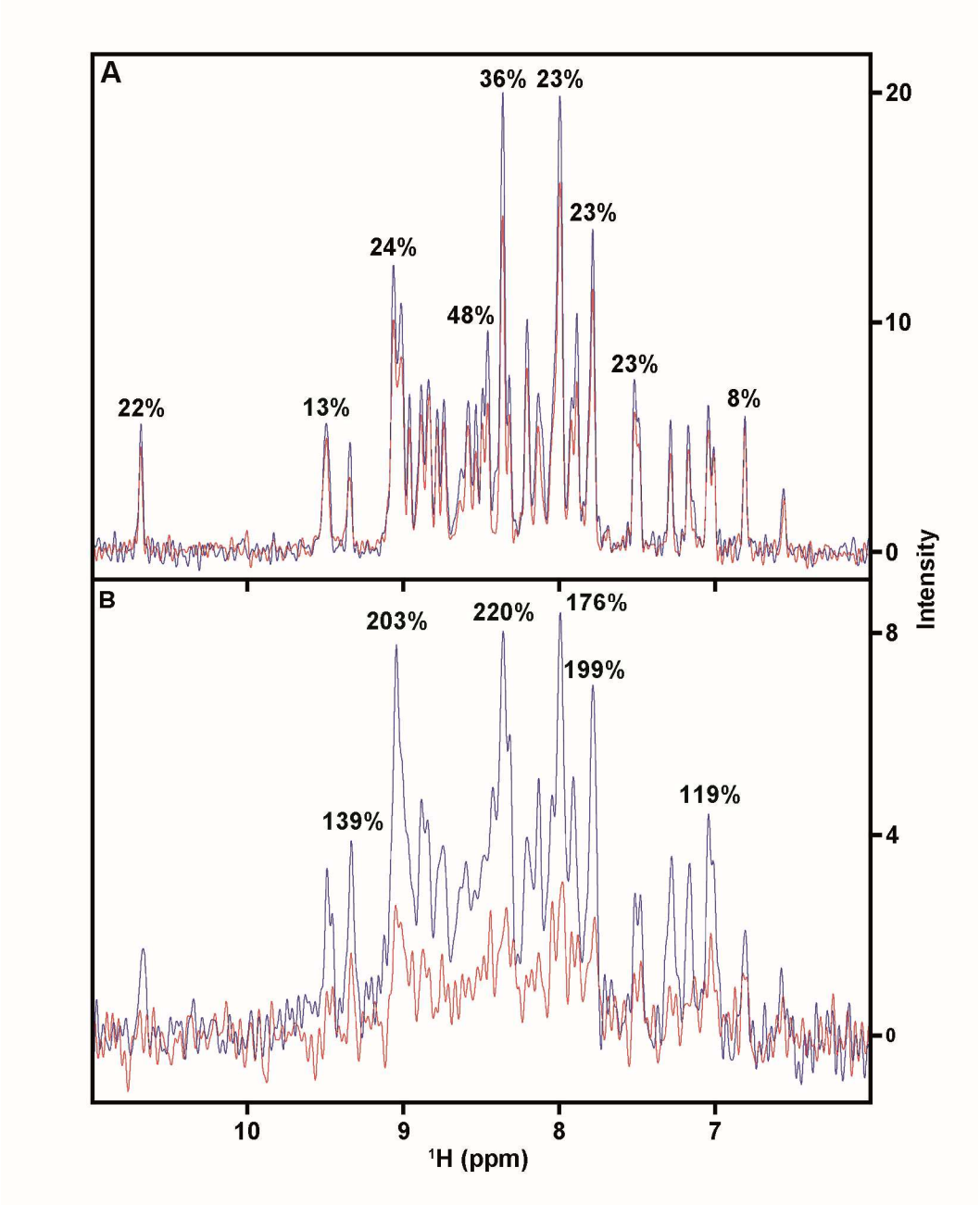

Supplementary Figure 2.1. Increase in signal from removing the sign-coding portion of the SOLEXSY pulse sequence. Sign-coded spectra are shown in red. Spectra without coding are shown in blue. Spectra are the first increment of the respective SOLEXSY experiments acquired with 24 scans and processed in Topspin using the first 1024 points of the FID, a cosine squared window function and zero-filling to 8192 points. Signal to noise ratios were measured using the built-in .sino module with a noise region of 3 to -1 ppm. A) A mean signal to noise increase of 24% is seen for the 250 ms plane in dilute solution. B) A mean signal to noise increase of 176% is seen in 100 gL^{-1} lysate for the 0 ms plane.

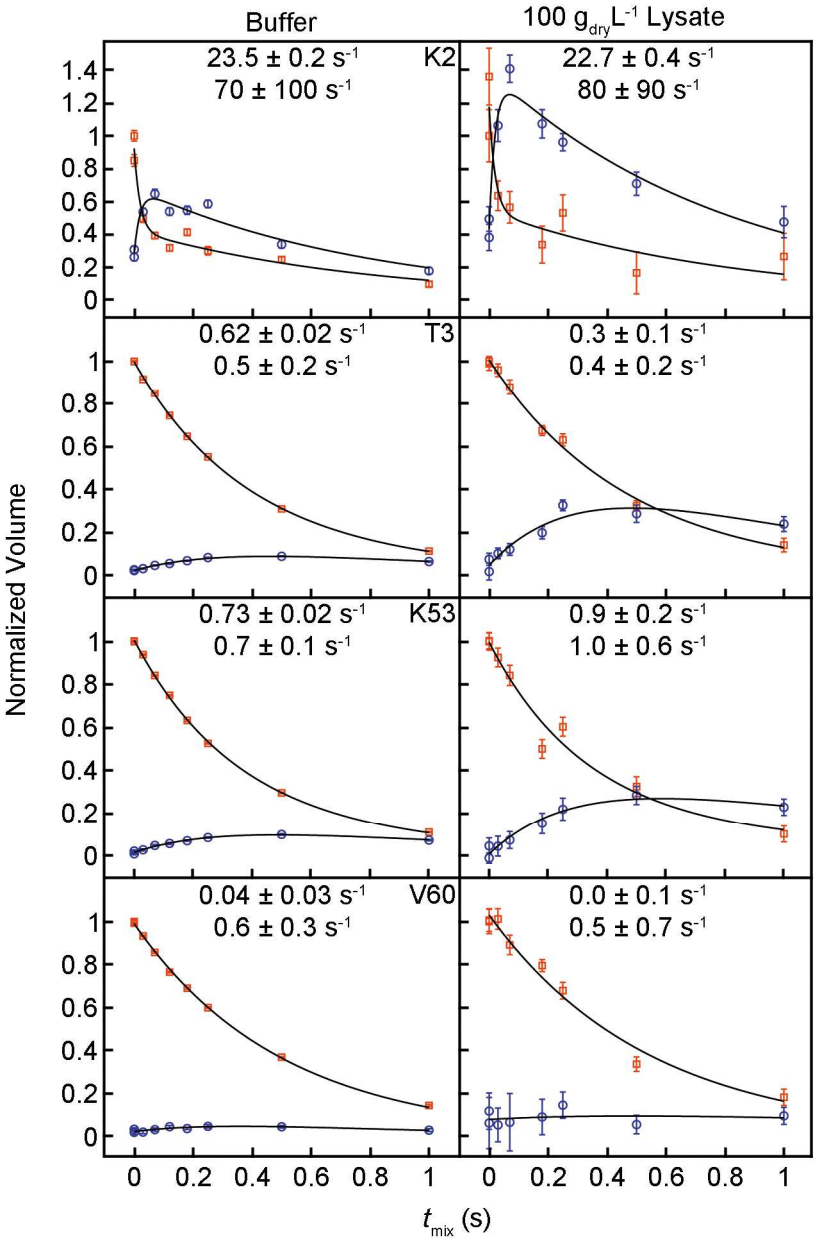

Supplementary Figure 2.2. Buildup and decay curves for N- and C-terminal regions of CI2. Crosspeak volume is plotted against time for $N^{D}H$ (blue circles) and $N^{H}H$ (red squares) resonances, creating buildup and decay curves, respectively. Data for each residue are fitted[99] to yield its rate of amide proton exchange. Error bars are the standard deviation of peak volumes in 20 spectra with representative amounts of added noise. The upper value in each panel is the fitted rate along with its uncertainty. The lower value is the average rate from the Monte Carlo analysis along with its uncertainty. The modified SOLEXSY pulse sequence (see Methods) was used.

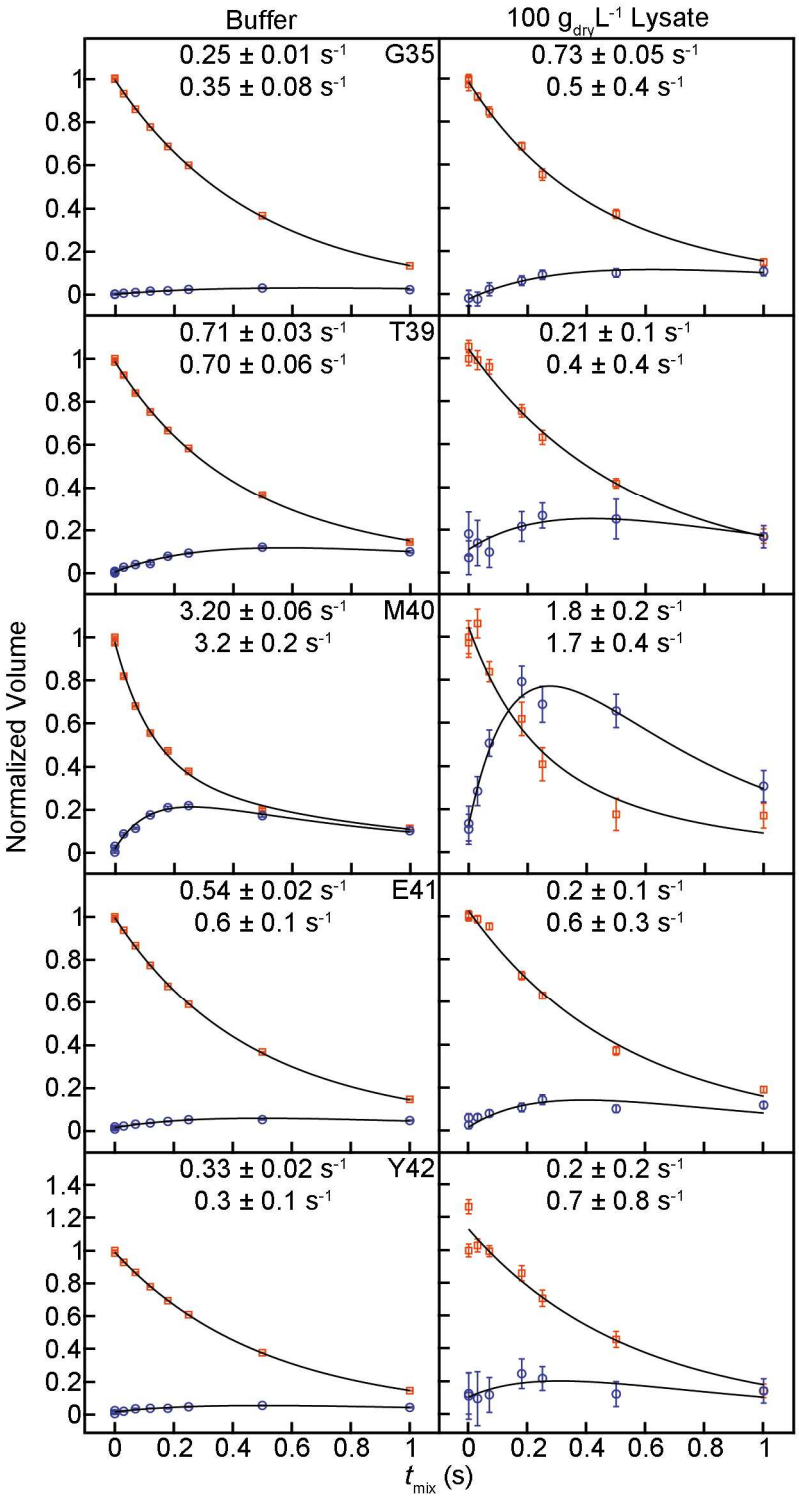

Supplementary Figure 2.3. Buildup and decay curves for the loop region of CI2. See caption to Supplementary Figure 2.2 for details.

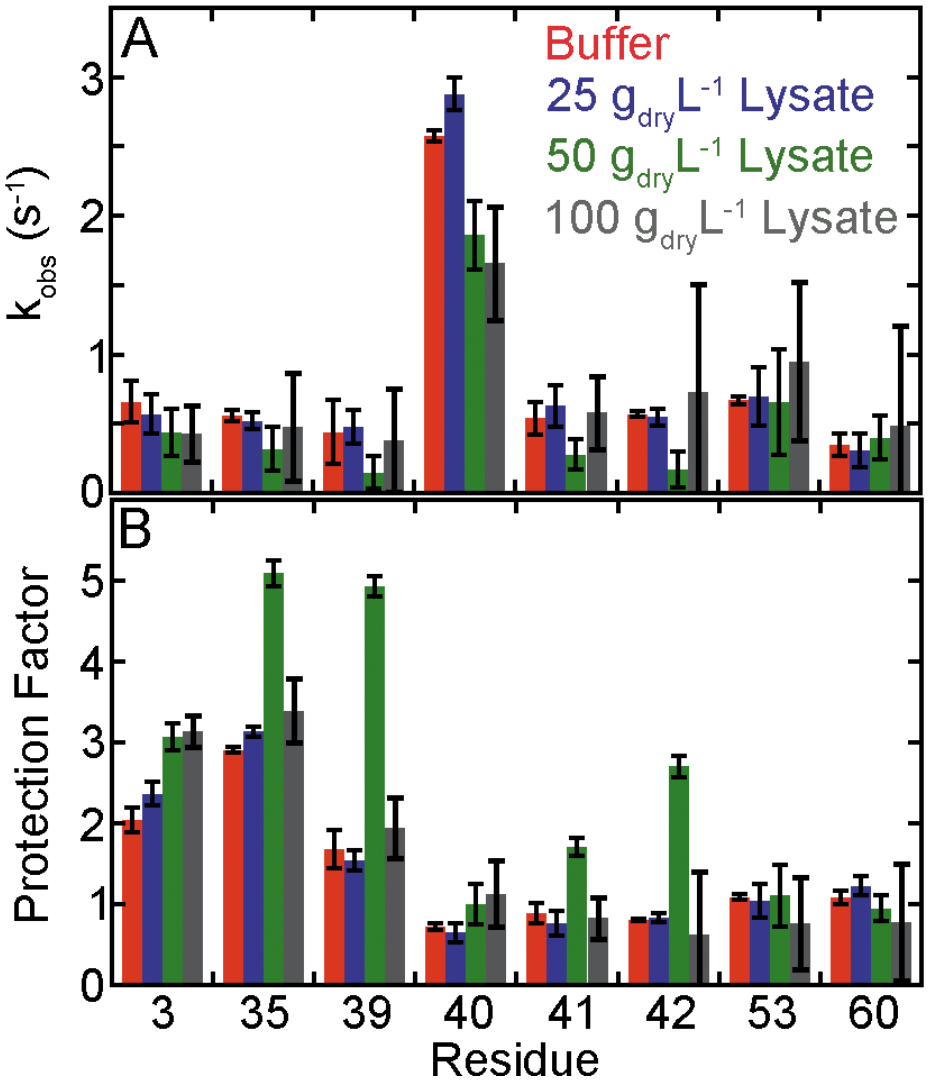

Supplementary Figure 2.4. To ensure the data in Figure 2.4 of were unaffected by our use of the modified experiment for the 'Buffer' sample, we reacquired those data using the full sequence (the remainder of the data is copied from Figure 2.4). The change does not affect our conclusions. A) Values from SOLEXSY data are the average of 20 Monte Carlo noise simulations. Error bars represent the standard deviation of the mean. B) Protection factors ($k_{int,predicted}/k_{obs,SOLEXSY}$). Predicted values were calculated as described in the footnote to Supplementary Table 2.1. Error bars are the same as in Panel A. Protection factors of less than 5 are not a reliable predictor of structure.[102]

CHAPTER 3: HYDROGEN EXCHANGE OF DISORDERED PROTEINS IN *ESCHERICHIA COLI*

Original citation: Smith AE, Zhou Z, Pielak GJ. *Protein Science.* **24**, 706-713 (2015)

Abstract

A truly disordered protein lacks a stable fold and its backbone amide protons exchange with solvent at rates predicted from studies of unstructured peptides. We have measured the exchange rates of two model disordered proteins, FlgM and α-synuclein, in buffer and in *Escherichia coli* using the NMR experiment, SOLEXSY. The rates are similar in buffer and cells and are close to the rates predicted from data on small, unstructured peptides. This result indicates that true disorder can persist inside the crowded cellular interior and that weak interactions between proteins and macromolecules in cells do not necessarily affect intrinsic rates of exchange.

Introduction

Cellular processes occur at macromolecule concentrations of 300-400 g/L.[1,73] The resulting weak, nonspecific interactions between macromolecules in the cytoplasm alter globular protein dynamics and stability.[40,57,61,74] Disordered proteins are fundamentally different. Unlike many model, single domain, globular proteins, whose structures do not change until they denature,[18] the properties of disordered proteins depend on solution conditions.[2] Thus, the crowded nature of the cell could have large effects on protein disorder. Studies show that the cellular interior can promote structure formation in proteins that are only transiently structured in buffer.[106] On the other hand, there is a growing realization from studies of globular proteins that attractive interactions favor less structure.[57,88,89,107-110]

To date, knowledge of the atomic-level structure of disordered proteins inside cells comes from a crude measure: the presence or absence of crosspeaks in ^{15}N-^{1}H HSQC NMR spectra.[5,106] Absence of peaks is caused by chemical exchange and is explained in contrasting ways: 1) intramolecular exchange involving the stabilization of particular conformations (i.e., folded species) and 2) weak, transient chemical interactions between the test protein and cellular components.[23,28,106,111] Here, we take a new approach by quantifying hydrogen exchange rates for two proteins possessing different degrees of disorder.

Structure protects backbone amide protons from solvent exchange.[48] Therefore, measuring their exchange rates inside cells and comparing the values to those measured in buffer and calculated from unstructured peptides provides

information about structure. Protection is quantified as the rate in an unstructured peptide (~0.1 - 10 s^{-1})[83] divided by the observed rate, k_{int}/k_{obs}. These protection factors range from >10^5 for backbone amide protons in the core of globular proteins to <5 for denatured proteins.[57,61,102] Intrinsic rates in buffer are estimated by using the online program, SPHERE,[86] which calculates k_{int} based on data from unstructured peptides and information about the system (i.e., primary structure, pH, deuterium content, and temperature).[83,84] These calculated rates remain valid in buffers containing physiologically relevant concentrations of globular proteins and cell lysates.[52,88]

Direct measurement of exchange in cells, however, is challenging. We investigated the disordered proteins α-synuclein and FlgM, both of which give in-cell NMR spectra,[106,111-113] using the SOLEXSY experiment[52,99] to quantify k_{obs} in *Escherichia coli* and buffer. SOLEXSY uses a variable mixing time (t_{mix}) to monitor hydrogen exchange (Supplementary Figure 3.1). Short times do not result in a buildup crosspeak. Longer times allow amide deuterons to exchange for protons and buildup of the initially deuterated amide crosspeak occurs. Likewise, a decay is observed from the initially protonated species. Rates are obtained from fits of peak volume versus mixing time.

α-Synuclein is a 140-residue protein found at the presynaptic terminals of neurons.[114] Its exact role is controversial, but the protein is *N*-terminally acetylated and thought to play a part in dopamine trafficking.[2] α-Synuclein retains the majority of its ^{15}N-^{1}H correlation crosspeaks inside *E. coli*, suggesting that the protein remains disordered in cells.[5,112,113,115]

FlgM is a 97-residue protein from *Salmonella typhimurium* that inhibits σ^{28}, a transcription factor responsible for regulating downstream flagellar and chemotaxis genes.[116,117] The protein shows characteristics of both a globular and a disordered protein. The *C*-terminus (residues 41-97) forms transient helices in buffer (between residues 60-73 and 83-90).[118] These helices are stabilized upon binding σ^{28}.[119] The absence of crosspeaks from the ^{15}N-^{1}H correlation spectrum for the *C*-terminal region in *E. coli* has been interpreted as evidence that this region gains structure in cells.[106] The *N*-terminus (residues 1-40) appears to remain disordered even in cells.[106,118]

Results

Amide proton exchange is base catalyzed at physiological pH.[48,83] In-cell NMR in *E. coli* is usually performed in dense cell slurries that are inherently low in nutrients and O_2.[11,120] These anaerobic conditions cause acidification of the cellular interior.[5,121,122] Thus, the interior pH must be known to compare data obtained in cells to data obtained in buffer. α-Synuclein has a single histidine, H50, whose $^{13}C\varepsilon1$ proton chemical shift depends on pH.[123] The C14 protons of HEPES, which is not cell permeable, were used as an external pH probe.[80,124] ^{13}C-^{1}H HSQC spectra were acquired before and after the SOLEXSY experiment.

The proton chemical shifts were compared to those from a standard curve in buffer (Supplementary Figures 3.2, 3.3). The cytoplasm and the extracellular medium acidified over the ~16 h required to acquire a SOLEXSY dataset (Supplementary Table 3.1), and the internal pH was ~0.4 units lower than the

external pH (Supplementary Figure 3.4). The average internal pH of all α-synuclein datasets is pH 6.7. We corrected the in-cell rates to pH 6.7 by using the second-order rate constant for base-catalyzed exchange (Supplementary Table 3.2, footnotes c-e).[79] We used this corrected rate to compare intracellular hydrogen exchange rates to those measured in buffer and to drive SPHERE. Since FlgM does not have a pH sensitive probe, we measured the HEPES C14 proton chemical shift before and after the SOLEXSY experiment, and applied the 0.4 pH unit correction to determine the internal pH.

During the course of an in-cell experiment the intercellular pH typically drops below 6.5 (Supplementary Table 3.1). Below this pH (at 288 K) the signal to noise ratio of buildup peaks are typically too small to allow exchange rates to be quantified, because hydrogen exchange drops below 0.1 s^{-1} for many residues. This problem is exacerbated in-cells, where peaks are inherently broad. To estimate exchange rates from crosspeaks with weak buildup curves we used a standard curve of the ratio of buildup to decay peak volumes at a t_{mix} of 0.3 s versus the k_{obs} values from the fit obtained in buffer (Supplementary Figure 3.5). This procedure allows an exchange rate to be estimated by a SOLEXSY experiment with one t_{mix}, 0.3 s. The uncertainty in this measurement was estimated as the maximum and minimum rates within 0.1 a unit of the ratio.

Hydrogen exchange rates for α-synuclein and FlgM are compiled in Supplementary Tables 3.3-3.7. SPHERE-predicted k_{int} values match k_{obs} values in buffer for both α-synuclein, acetylated α-synuclein, and FlgM. In addition, rates and protection factors for α-synuclein in buffer closely match those measured with

CLEANEX (Supplementary Table 3.3).[112] The differences likely reflect differences in buffer composition and extrapolation to pH 6.7.

In buffer, 26 α-synuclein residues give quantifiable exchange rates and seven more rates can be estimated (Figure 3.1A, 3.2A, Supplementary Table 3.3). The residues are distributed throughout the primary structure. Their protection factors are all similar and less than two. The same is observed for α-synuclein in buffer supplemented with 150 mM NaCl (Supplementary Table 3.3). Protection factors this small indicate a lack of structure.[102]

In cells, nine α-synuclein residues give quantifiable rates, eight more rates can be estimated, and an additional six qualitatively show exchange (Figures 3.1B, 3.2A, Supplementary Tables 3.2, 3.3). Rates in cells and in buffer are in reasonable agreement with the values predicted by SPHERE. No protection factor is greater than three (Figure 3.2B). There is no significant difference between the protection factors, both measured and estimated, in cells and in buffer (two-tailed t-test with unequal variance[125], $\rho > 0.07$). The same is observed for acetylated α-synuclein. There is no significant difference between protection factors in cells and buffer (Supplementary Figure 3.6, Supplementary Tables 3.4, 3.5, two-tailed t-test with unequal variance, $\rho > 0.5$). These observations indicate that α-synuclein, with or without acetylation, remains disordered in the crowded bacterial cytoplasm.

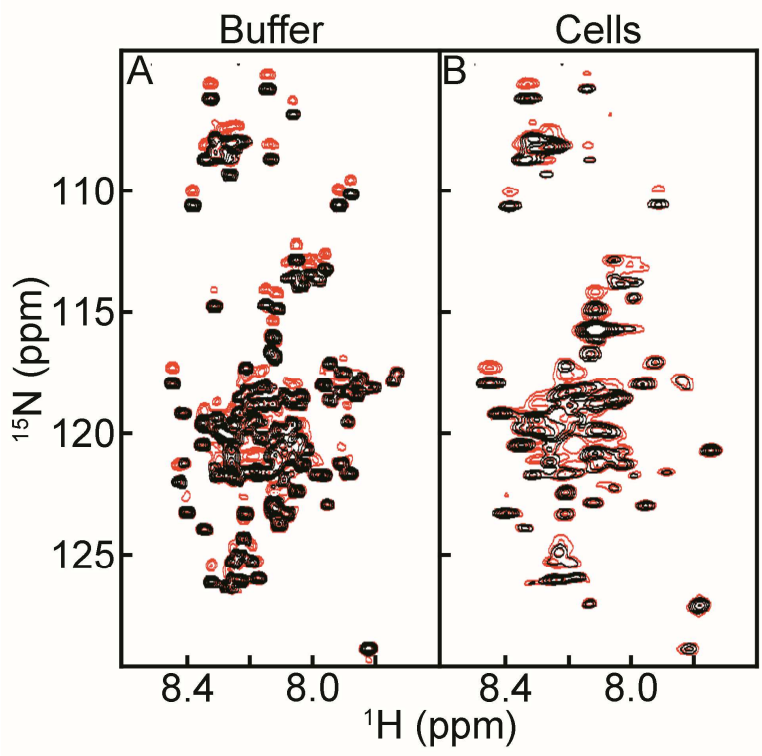

Figure 3.1. $^{15}N^{H/D}$-SOLEXSY spectra of α-synuclein in A) buffer and B) *E. coli*. Each panel is an overlay of the 0 ms (black) and 300 ms (red) mixing times. The contour levels in panels A and B are the same.

The activation energy of amide proton exchange was also measured (Supplementary Table 3.8). The means and their standard deviations are 15 ± 3 kcal/mol in buffer and 17 ± 1 kcal/mol in cells. The activation energy used in SPHERE is 17 kcal/mol.[83,86] These observations lend further support our to conclusion that α-synuclein has the properties of a disordered peptide in the *E. coli* cytoplasm.

Turning to FlgM, 24 residues give quantifiable exchange rates in buffer (Figure 3.3A, 3.4A, Supplementary Table 3.7). Significantly larger protection factors ($\rho < 0.002$, two-tailed t-test with unequal variance) are observed for the 13 *C*-terminal residues compared to the 11 *N*-terminal residues (means and their standard deviations of 1.6 ± 0.3 and 0.5 ± 0.1, respectively). This observation suggests the existence of some structure in the *C*-terminal region, consistent with chemical shift data showing that the *C*-terminus forms transient α-helices in buffer.[118,119] However,

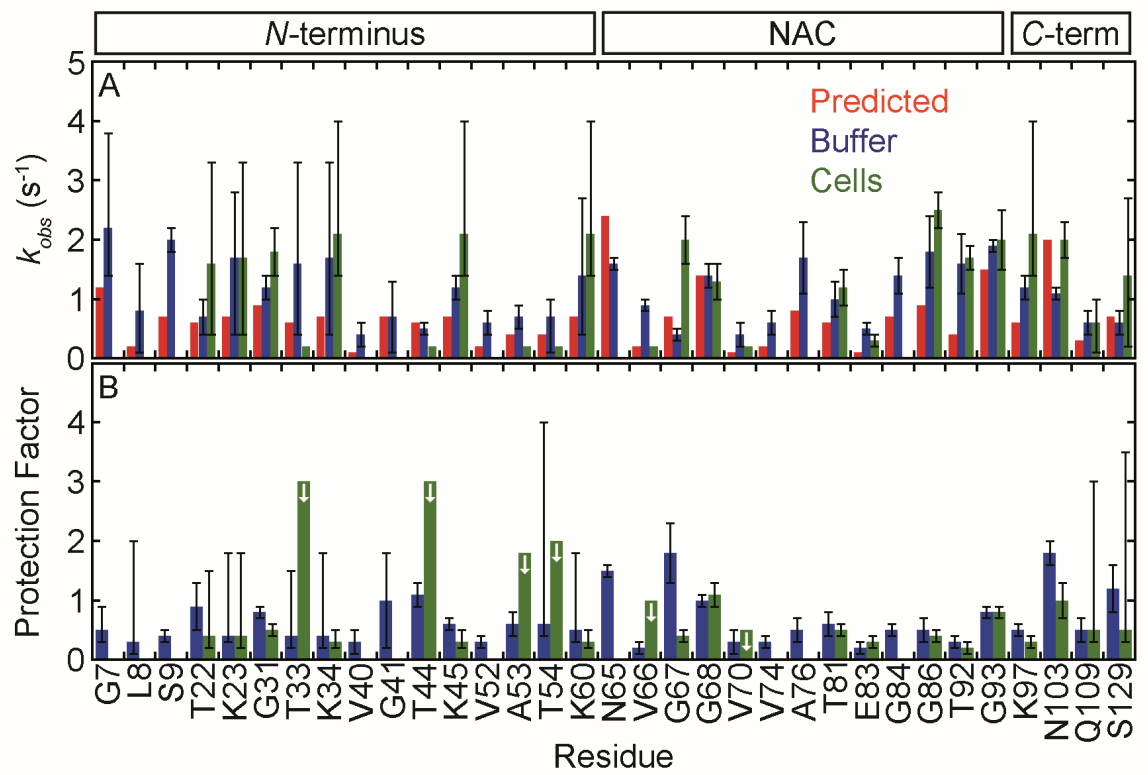

Figure 3.2. α-Synuclein exhibits similar backbone amide hydrogen exchange rates in cells and in buffer (pH 6.7, 288 K). A) Rates from prediction (red),[83,84,86] and from SOLEXSY data (blue, buffer; green, cells). Uncertainties in buffer are the standard deviation of 20 Monte Carlo noise simulations.[99] Uncertainties for the in-cell data are the standard deviation of the mean from three or more trials (For T81 ad G93, the uncertainties are the range of two experiments.). Asymmetric error bars are shown for rates derived from the data in Supplementary Figure 3.5, as described in the text. In-cell rates without error bars are for residues that that exchange too slowly for reliable fits, or have overlapped decay peaks, and were assigned a rate of ≥ 0.2 s^{-1}, the lower limit of SOLXESY. B) Protection factors ($k_{int,\ predicted}/k_{obs,\ buffer}$ and $k_{int,\ predicted}/k_{obs,\ cells}$). Uncertainties are from propagation of the uncertainties shown in panel A unless the rate was derived from Supplementary Figure 3.5. For those residues, the uncertainty reflects a range, as described in the text. The arrows denote residues for which only a maximum value can be assigned.

the protection factors from the *C*-terminal region were all <5, indicating an absence of persistent structure.[102] In summary, the agreement between the chemical shift data and the hydrogen exchange data show that protection factors are a sensitive measure of sparsely populated secondary structure.

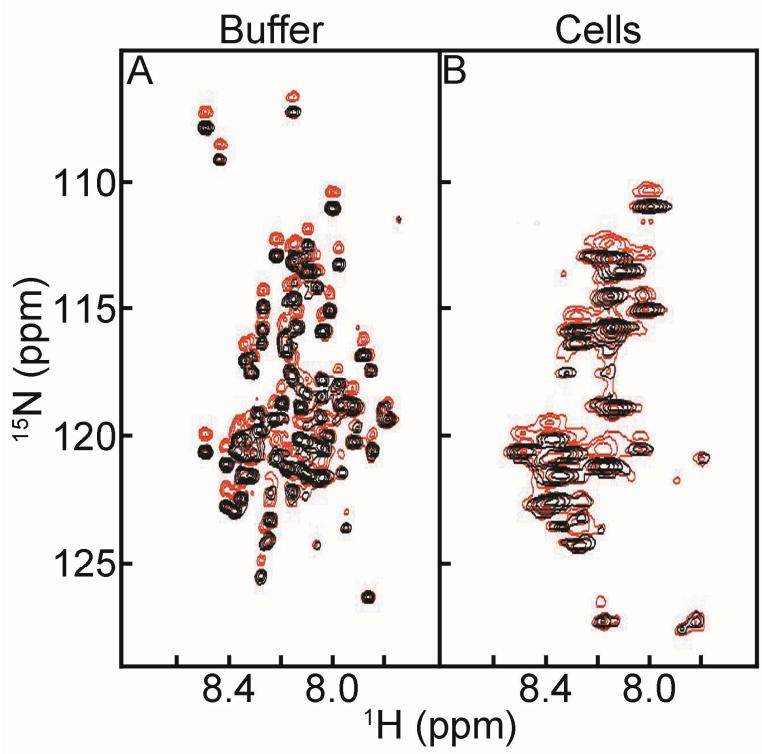

Figure 3.3. $^{15}N^{H/D}$-SOLEXSY spectra of FlgM in A) buffer and B) *E. coli*. Each panel is an overlay of the 0 ms (black) and 300 ms (red) mixing times. The contour levels in panels A and B are the same.

In cells, seven FlgM residues give quantifiable rates and four more qualitatively show exchange (Figure 3.3B, 3.4A, Supplementary Tables 3.6, 3.7). The rates in cells are similar to those in buffer. For the N-terminus seven residues can be quantified in cells and 11 in buffer. Protection factors for these residues (Figure 3.4B) are the same in cells as they are in buffer (two-tailed t-test with unequal variance, $\rho > 0.1$).

Discussion

Unfortunately, we cannot directly compare cell and buffer data from the *C*-terminus of FlgM because *C*-terminal crosspeaks disappear in cells.[106] However, the smaller exchange rates in buffer and the absence of crosspeaks are both consistent with the existence of a nascent *C*-terminal structure. Likewise, for both acetylated and non-acetylated α-synuclein, crosspeaks from the first 12 residues and residues 37-41 show peak broadening inside cells (Supplementary Figure 3.7). This broadening is likely due to conformational exchange involving a helical form that is

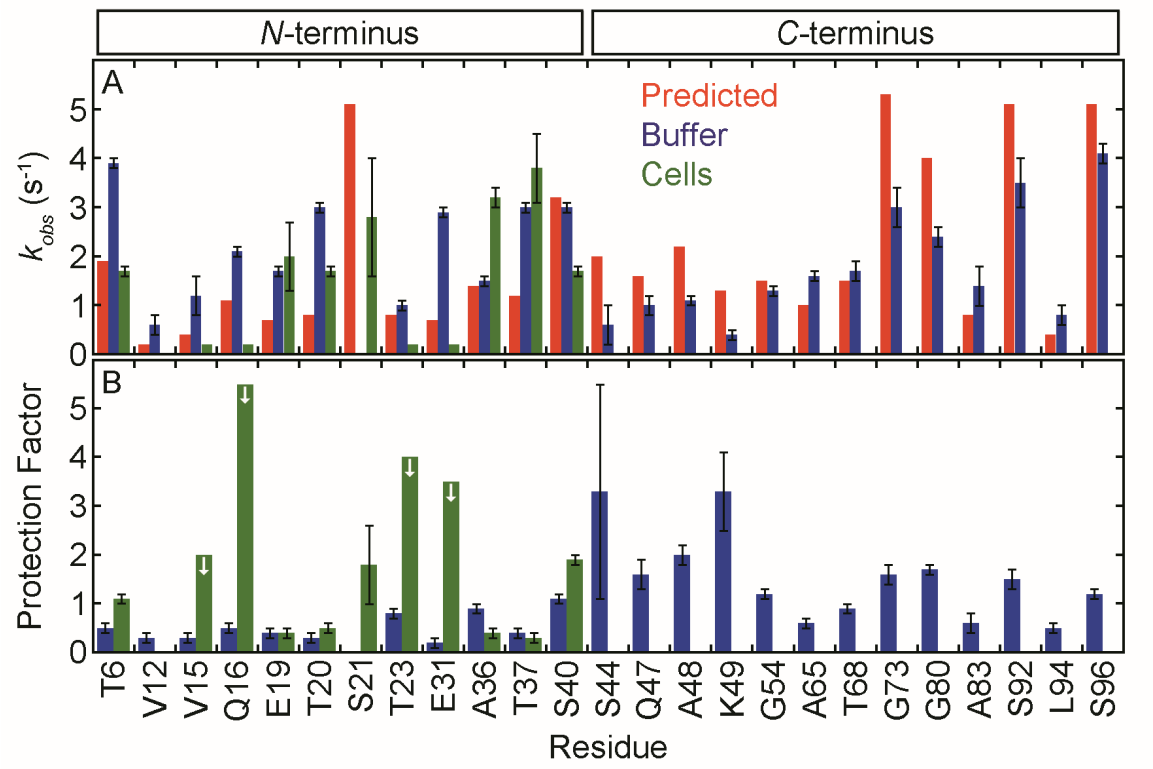

Figure 3.4. FlgM exhibits similar backbone amide hydrogen exchange rates in cells and in buffer (pH 6.7, 298 K). See the caption to Figure 3.1 for further information.

populated in buffer to ~17% for acetylated α-synuclein and slightly less for the non-acetylated form.[126,127] This conformational exchange is likely slowed in cells causing broadening. A similar observation has been made for a folding intermediate of the FF domain in cell lysates.[40]

Our data for α-synuclein and the *N*-terminal region of FlgM indicate that disorder can persist in *E. coli* irrespective of the existence of hard-core repulsions, i.e. macromolecular crowding.[74,128] We have shown that measured exchange rates in *E. coli* agree with both those obtained in buffer and those calculated based on exchange rates of small, unstructured peptides. Data for the *C*-terminal region of FlgM in buffer show that even small protection factors can be useful indicators of sparsely populated structured states in disordered proteins. This work also has

implications for determining the stability of globular proteins in living cells. Specifically, the data indicate that predicted rates from model peptides can be applied to hydrogen exchange studies of globular proteins inside *E. coli*.[61] Most importantly, we have shown that protein disorder can persist under physiological conditions and that the crowded cellular interior need not affect the structure of disordered proteins.

Methods

Protein expression for in-cell NMR

Plasmids harboring the gene encoding FlgM (PMC64, ampicillin resistance) or α-synuclein (pT7-7, ampicillin resistance) were transformed into Agilent BL21 DE3 Gold cells by heat-shock. For acetylated α-synuclein, plasmids harboring pNatB (chloramphenicol resistance) and α-synuclein were co-transformed into Agilent BL21 DE3 Gold cells by electroporation. A single colony was used to inoculate a 5 mL culture of Luria-Bertani media supplemented with 100 μg/mL ampicillin (FlgM or α-synuclein) or 100 μg/mL ampicillin and 25 μg/mL chloramphenicol (pNatB/α-synuclein). The culture was grown 37 °C. After 8 h, 50 μL of the saturated culture was used to inoculate 50 mL of supplemented M9 media as described next.

For uniform labeling, M9 media (50 mM Na_2HPO_4, 20 mM KH_2PO_4, 9 mM NaCl) was supplemented with 2 mg/mL ^{13}C-glucose, 1 mg/mL $^{15}NH_4Cl$, 100 μM $CaCl_2$, 2 mM $MgSO_4$, 10 μg/mL thiamine and 10 μg/mL biotin, and 150 μg/mL ampicillin (100 μg/mL ampicillin and 25 μg/mL chloramphenicol for pNatB/α-synuclein). For glycine or threonine “unlabeling,” the media described above was

also supplemented with 1 mg/mL natural abundance glycine or 1.5 mg/mL natural abundance threonine.[129,130]

For selective lysine/threonine enrichment, natural abundance glucose and NH_4Cl were used in the M9 media, which was also supplemented with 0.1 mg/mL uniformly enriched $^{13}C/^{15}N$ threonine, 0.2 mg/mL uniformly $^{13}C/^{15}N$ enriched lysine and 0.2 mg/mL natural abundance glycine were added.[131,132]

The 50 mL cultures were shaken (New Brunswick Scientific Innova I26, 225 rpm) at 37 °C overnight. The culture was diluted to 100 mL with supplemented M9 media and shaken until the optical density at 600 nm was at least 0.8. Isopropyl β-D-1-thiogalactopyranoside (1 mM) was used to induce expression. After 4 h cells were pelleted at 1000*g* and washed 3 times with 30 mL NMR buffer (100 mM HEPES, 35 mM bis-tris propane,[133] 50 μg/mL chloramphenicol, 100 μg/mL ampicillin, 50% D_2O). For pNatB/α-synuclein the buffer contained half the amount of chloramphenicol and 15 μg/mL rifampin. Chloramphenicol or rifampin is required to halt protein expression prior to NMR. (Rifampin is required because the pNatB plasmid harbors a gene for chloramphenicol resistance.) Cell pellets were resuspended in 100-200 μL of NMR buffer and loaded into a standard 5 mm NMR tube. Typical cell slurries were 70% wet cells by volume.

Protein purification

Cell pellets were frozen after in-cell NMR experiments. For α-synuclein (with or without acetylation) cells were lysed by boiling. Cell debris was removed by centrifugation at 16000*g*. Using a GE AKTA FPLC, anion exchange (GE Q column,

50 mM Tris-HCl wash buffer, 50 mM Tris-HCl/1 M NaCl elute buffer, pH 7.5, 10-90% gradient) and subsequent size exclusion chromatography (GE Superdex 75 column eluted with non-supplemented M9, 0.5 ml/min flow rate) were used. SDS-PAGE was used to assess purity. Purified protein was dialyzed against 17 MΩ cm^{-1} H_2O for 4 h at room temperature or overnight at 5 °C. After dialysis, the sample was flash frozen in a dry-ice/ethanol bath and lyophilized.

FlgM was purified in a similar fashion except the cells were sonicated (Fisher Scientific Sonic Dismembrator Model 500, 15% amplitude, 20 s, 67% duty cycle). FlgM does not bind to anion exchange media.

LC-ESI-MS

Purified samples of α-synuclein were resuspended in 17 MΩ cm^{-1} H_2O and subjected to LC-ESI-MS using a Restek Viva C4 column (linear gradient from 0.1% aqueous formic acid, 5% acetonitrile to 0.1% aqueous formic acid, 95% acetonitrile over 15 m, followed by 5 m in the 95% eluant) coupled to an Agilent 6520 Accurate-Mass Q-TOF running in positive ion mode. Deconvoluted masses of 15240 Da and 15280 Da were found for $^{13}C/^{15}N$ α-synuclein and $^{13}C/^{15}N$ acetylated α-synuclein, respectively. This mass difference corresponds to the addition of an acetyl group (~40 Da). No unmodified α-synuclein was observed when the protein was co-expressed with pNatB, indicating 100% acetylation, consistent with previous work.[134]

pH determination

Purified α-synuclein (0.5 mM) was suspended in 50 mM citrate, 50 mM bis-tris propane, 50 mM HEPES, 50 mM borate, 5% D_2O, containing 0.1% DSS at various

pH values (adjusted by addition NaOH or HCl). Data were acquired at 288 K (pH: 3.0, 4.2, 5.3, 5.7, 6.0, 6.4, 6.6, 6.8, 7.0, 7.5, 7.8, 8.9) and 298 K (pH: 5.3, 6.1, 6.6, 7.0, 7.4, 7.9, 8.9) on either a 600 or 700 MHz Bruker Avance III HD spectrometer equipped with a Bruker TCI cryoprobe. ^{13}C-HSQC spectra were acquired using sweep widths of 12 ppm in the ^{1}H dimension and 200 ppm in the ^{13}C dimension. Four transients were collected using 512 complex points in t_2 and 64 complex increments in t_1. Spectra were referenced to DSS at 0 ppm. Data were processed with Topspin 3.2. The ^{1}H chemical shifts of H50 $^{13}C^{\varepsilon 1}$-^{1}H and $^{13}C^{\delta 2}$-^{1}H of α-synuclein and HEPES were followed as a function of pH. The data were fit to a modified Henderson-Hasselbach equation, $\delta = \delta_{low} - \frac{\delta_{low} - \delta_{high}}{1+10^{n(pK_a - pH)}}$, where δ_{low} is the low pH chemical-shift plateau and δ_{high} is the high plateau, n is the number of protons, and pK_a is the negative logarithm of the dissociation constant.[135-137] Our pK_a values (6.7 for H50 and 7.5 for HEPES) are similar to literature values (6.8 and 7.6, respectively).[123,124]

Using a glass electrode (AgCl reference), buffers containing 5% and 50% D_2O and α-synuclein (0.5 mM) were adjusted to a pH reading of 6.9. The solutions gave nearly identical proton chemical shifts for ε1 (7.984 ppm and 7.983 ppm) and δ2 (7.074 ppm and 7.073 ppm), for 5 and 50% D_2O. Thus, the H50 $^{13}C^{\varepsilon 1}$ and $^{13}C^{\delta 1}$ protons are insensitive to the H/D isotope effect and 0.2 pH units were added to the value obtained from the standard curve in solutions containing a 1:1 H_2O:D_2O mixture to account for the H/D isotope effect on the electrode for a 50% D_2O solution.[138,139] The C14 protons of HEPES, however, exhibit an isotope effect. In 5% D_2O the proton chemical shift is 3.117 ppm while in 50% D_2O the chemical shift is

3.134 ppm. For this reason, a correction of -0.017 ppm was applied to values obtained in 50% D_2O to account for the deviation from the conditions used to acquire the standard curve, then the 0.2 pH unit correction was added to the value obtained from the standard curve.

NMR

In-cell samples were prepared as described above. For the buffer experiments purified ^{13}C-, ^{15}N-enriched protein (final protein concentration of ~500 μM as judged by a Lowry assay using bovine serum albumin as the standard) was added to NMR buffer (pH 6.7, minus antibiotics). One buffer experiment with α-synuclein used NMR buffer plus 150 mM NaCl, to ensure minimal salt dependence of exchange. In-cell data were acquired at 288 K (α-synuclein, acetylated α-synuclein), and 298 K (FlgM, α-synuclein) with a 700 MHz Bruker Avance III HD spectrometer running Topspin Version 3.2 and equipped with a Bruker TCI cryoprobe. Buffer data were acquired at 288 K (α-synuclein, acetylated α-synuclein), 293 K (α-synuclein) and 298 K (FlgM, α-synuclein). An interleaved, modified[52] SOLEXSY[99] (Appendix 1) experiment with mixing times (t_{mix}) of 0, 70, 140, 210, 300, 500, and 800 ms was used to measure hydrogen exchange rates. One in-cell exchange experiment with α-synuclein used t_{mix} of 0, 70, 150, 300, 700 ms in an attempt to shorten the acquisition time and minimize pH changes. Sweep widths were 7000 Hz and 2500 Hz in the ^1H and ^{15}N dimensions, respectively. 512 complex points were collected in t_2 with 128 TPPI points in t_1 at each t_{mix}. In buffer, 32 transients were acquired per increment. Forty transients were acquired for the in-cell NMR experiments. Data acquisition required ~16 h per sample.

^{15}N-^{1}H and ^{13}C-^{1}H HSQC spectra were acquired before and after the SOLEXSY experiment to assess sample integrity and pH. Four or eight transients were collected using 512 complex points in t_2 with 64 complex points in t_1 for each experiment. The sweep widths were 8500 Hz in ^{1}H and either 2500 Hz or 34500 Hz in the ^{15}N or ^{13}C dimension, respectively. For the in-cell samples, the cell slurry was removed after the experiment and gently pelleted. The supernatant was removed, diluted two- to three-fold, and placed in the spectrometer. A ^{15}N-^{1}H HSQC was acquired to assess protein leakage.[24] No leakage was observed (~μM detection limit).

To ensure the pH associated with an in-cell SOLEXSY experiment was the average of the values obtained from the bracketed ^{13}C-^{1}H HSQC spectra, an experiment using α-synuclein was performed where ^{13}C-^{1}H HSQC spectra were acquired as a function of time. These HSQC spectra bracketed a short SOLEXSY (only t_{mix} 0.3 s) experiment and an ^{15}N-^{1}H TROSY-HSQC experiment. This regimen not only allowed us to determine that the pH drop was linear but also allowed collection of single-plane SOLEXSY experiments where the pH drop was only averaged over ~2.5 h instead of the ~16 h required for a complete SOLEXSY experiment. This protocol allowed us to assess hydrogen exchange at discreet pH values, instead of exchange averaged over a ~0.5 pH unit range.

Data processing

Data were processed with NMRPipe.[104] t_2 data were subjected to a cosine squared bell function (512 complex points for buffer solutions and 256 complex

points for in-cell experiments) before zero-filling to 2048 points and Fourier transformation. t_1 data were linear predicted to 256 points before application of a cosine squared bell function. Subsequent zero-filling to 1024 points and Fourier transform yielded the final spectra. Spectra were peak picked and integrated using the built-in nlinLS routine. Peak volumes were fitted as described.[99] Published assignments were used.[118,119,140,141]

Supplementary Information for Chapter 3

Supplementary Table 3.1. pH.

				pH range		
				Interior		Exterior
Protein	Enrichment[a]	Temperature (K)	Time (h)[b]	H50 ε1[c]	H50 δ2[c]	HEPES[c]
α-synuclein	$^{13}C/^{15}N$	288	11	7.1 – 6.8	7.0 – 6.9	7.6 – 7.1
	$^{13}C/^{15}N$	288	16	7.1 – 6.3	7.0 – 6.2	7.6 – 6.7
	$^{13}C/^{15}N$	288	16	6.9 – 6.2	6.8 – 6.1	7.3 – 6.6
	$^{13}C/^{15}N$	298	16	6.5 – 5.3	6.5 – ND	6.5 – 6.2
	$^{13}C/^{15}N$, -G	288	16	ND	6.7 – 5.7	6.9 – 6.3
	$^{13}C/^{15}N$, -T	288	16	6.8 – 6.1	6.7 – 5.9	6.9 – 6.4
	+T/K	288	16	7.0 – 6.5	ND	7.6 – 6.9
Acetylated	$^{13}C/^{15}N$	288	16	6.8 – 6.3	6.7 – 6.1	7.2 – 6.6
α-synuclein	$^{13}C/^{15}N$	288	17	7.1 – 6.7	7.0 – 6.5	7.6 – 7.2
	$^{13}C/^{15}N$	288	17	7.0 – 6.6	7.0 – 6.6	7.6 – 7.2
FlgM	$^{13}C/^{15}N$	298	16	NA	NA	6.9 – 6.3
	$^{13}C/^{15}N$	298	16	NA	NA	6.9 – 6.3
	$^{13}C/^{15}N$	298	16	NA	NA	6.8 – 6.3

Footnotes

[a] Media
$^{13}C/^{15}N$: ^{13}C-glucose and $^{15}NH_4Cl$.
$^{13}C/^{15}N$, -G: ^{13}C-glucose and $^{15}NH_4Cl$ plus natural abundance glycine.
$^{13}C/^{15}N$, -T: ^{13}C-glucose and $^{15}NH_4Cl$ plus natural abundance threonine.
+T/K: natural abundance glucose and NH_4Cl plus $^{13}C/^{15}N$ enriched threonine and lysine.

[b] Duration of SOLEXSY experiment.

[c] pH before SOLEXSY experiment and pH after SOLEXSY experiment. pH values were obtained from ^{13}C-^{1}H HSQC spectra and the standard curves shown in Supplementary Figure 3.2. ND; not determined. NA; not applicable.

Supplementary Table 3.2. Triplicate α-synuclein in-cell data extrapolated to pH 6.7.

Residue	k_{obs} (s^{-1})[a]	In-cell pH[b]	logk_{obs}	pOH[-c]	logk_{OH^-}[d]	k_{obs} at pH 6.7 (s^{-1})[e]
G31	1.2	6.6	0.1	8.2	8.3	1.7
	2.7	6.7	0.4	8.1	8.5	2.7
	2.0	7.0	0.3	7.8	8.1	1.1
G67	1.5	6.6	0.2	8.2	8.4	2.1
	2.8	6.7	0.4	8.1	8.5	2.8
	2.2	7.0	0.3	7.8	8.2	1.2
G68	1.2	6.6	0.1	8.2	8.3	1.6
	1.4	6.7	0.2	8.1	8.2	1.4
	1.4	7.0	0.1	7.8	8.0	0.8
T81	1.5	6.8	0.2	8.0	8.2	1.3
	0.3	6.2	-0.5	8.6	8.1	1.0
E83	0.3	6.6	-0.5	8.2	7.8	0.5
	0.1	6.7	-0.9	8.1	7.2	0.1
	0.7	7.0	-0.2	7.8	7.7	0.4
G86	1.7	6.6	0.2	8.2	8.5	2.4
	3.0	6.7	0.5	8.1	8.6	3.0
	3.6	7.0	0.6	7.8	8.4	2.0
T92	0.9	6.6	-0.04	8.2	8.2	1.3
	1.6	6.7	0.2	8.1	8.3	1.6
	3.3	7.0	0.5	7.8	8.4	1.9
	0.7	6.2	-0.2	8.6	8.4	2.1
G93	1.6	6.6	0.2	8.2	8.4	2.2
	3.0	7.0	0.5	7.8	8.3	1.7
N103	1.4	6.6	0.1	8.2	8.4	1.9
	1.9	6.7	0.3	8.1	8.4	1.9
	2.9	7.0	0.5	7.8	8.3	1.6
	1.0	6.2	-0.02	8.6	8.6	3.0
	0.9	6.6	-0.04	8.2	8.2	1.3

Footnotes

[a] From fitting SOLEXSY exchange curves. Cells were resuspended in 100 mM HEPES, 35 mM bis-tris propane, 50 µg/mL chloramphenicol, 100 µg/mL ampicillin, 288 K, 50% D_2O.

[b] Average pH from the chemical shift of H50 ε1 or δ2 proton before and after the SOLEXSY experiment (Supplementary Figures 3.2 and 3.3).

[c] $pOH^- = pK_W - pH$; $pK_W = 14.79$ (to account for 50% D_2O, 288 K).

[d] Logarithm of the second-order rate constant for base-catalyzed exchange ($k_{OH^-} = k_{obs}/[OH^-]$).

[e] k_{obs} extrapolated to pH 6.7: $10^{(\log kOH - pOH)} = 10^{(\log kOH - pKW + pH)} = 10^{(\log kOH - 14.79 + 6.7)} = 10^{(\log kOH - 8.09)}$.

Supplementary Table 3.3. α-Synuclein exchange rates (s^{-1}) and protection factors (PF).

Residue	SPHERE[a]	Buffer[b]	Croke[c]	Cells[d]	Buff PF[e]	Cell PF[e]
G7	1.2	2.2 (1.4 - 3.8)[f]	NR	ND[g]	0.5 (0.3 - 0.9)	ND
L8	0.2	0.8 (0.1 - 1.6)	0.7 ± 0.1	ND	0.3 (0.1 - 2.0)	ND
S9	0.7	2.0 [2.2] ± 0.2	1.4 ± 0.4	ND	0.4 [0.3] ± 0.1	ND
T22	0.6	0.7 [1.1] ± 0.3	0.9 ± 0.1	1.6 (0.4 - 3.3)[f]	0.9 [0.5] ± 0.4	0.4 (0.2 - 1.5)
K23	0.7	1.7 (0.4 - 2.8)	NR	1.7 (0.4 - 3.3)	0.4 (0.3 - 1.8)	0.4 (0.2 - 1.8)
G31	0.9	1.2 [2.3] ± 0.2	NR	1.8 ± 0.4	0.8 [0.4] ± 0.1	0.5 ± 0.1
T33	0.6	1.6 (0.4 - 3.3)	NR	≥ 0.2	0.4 (0.2 - 1.5)	≤ 3.0
K34	0.7	1.7 (0.4 - 3.3)	NR	2.1 (1.4 - 4.0)[h]	0.4 (0.2 - 1.8)	0.3 (0.2 - 0.5)
V40	0.1	0.4 [0.2] ± 0.2	0.3 ± 0.1	ND	0.3 [0.5] ± 0.2	ND
G41	0.7	0.7 [0.6] ± 0.6	1.2 ± 0.2	ND	1.0 [1.2] ± 0.8	ND
T44	0.6	0.5 [1.2] ± 0.1	1.1 ± 0.3	≥ 0.2	1.1 [0.5] ± 0.2	≤ 3.0
K45	0.7	1.2 ± 0.2[i]	NR	2.1 (1.4 - 4.0)	0.6 ± 0.1	0.3 (0.2 - 0.5)
V52	0.2	0.6 ± 0.2[j]	NR	ND	0.3 ± 0.1	ND
A53	0.4	0.7 [0.7] ± 0.2	0.5 ± 0.1	≥ 0.2	0.6 [0.6] ± 0.2	≤ 1.8
T54	0.4	0.7 (0.1 - 1.0)	0.6 ± 0.1	≥ 0.2	0.6 (0.4 - 4.0)	≤ 2.0
K60	0.7	1.4 (0.4 - 2.7)	0.7 ± 0.1	2.1 (1.4 - 4.0)	0.5 (0.3 - 1.8)	0.3 (0.2 - 0.5)
N65	2.4	1.6 [1.4] ± 0.1	NR	ND	1.5 [1.7] ± 0.1	ND
V66	0.2	0.9 ± 0.1	NR	≥ 0.2	0.2 ± 0.1	≤ 1.0
G67	0.7	0.4 [1.8] ± 0.1	0.8 ± 0.2	2.0 ± 0.4	1.8 [0.4] ± 0.5	0.4 ± 0.1
G68	1.4	1.4 ± 0.2	0.8 ± 0.2	1.3 ± 0.3	1.0 ± 0.1	1.1 ± 0.2
V70	0.1	0.4 ± 0.2	NR	≥ 0.2	0.3 ± 0.2	≤ 0.5
V74	0.2	0.6 ± 0.2	0.7 ± 0.1	ND	0.3 ± 0.1	ND
A76	0.8	1.7 ± 0.6	0.9 ± 0.2	ND	0.5 ± 0.2	ND
T81	0.6	1.0 [1.2] ± 0.3	1.1 ± 0.2	1.2 ± 0.3	0.6 [0.5] ± 0.2	0.5 ± 0.1
E83	0.1	0.5 [0.7] ± 0.1	NR	0.3 ± 0.1	0.2 [0.1] ± 0.1	0.3 ± 0.1
G84	0.7	1.4 ± 0.3	0.8 ± 0.2	ND	0.5 ± 0.1	ND
G86	0.9	1.8 [2.1] ± 0.6	0.7 ± 0.2	2.5 ± 0.3	0.5 [0.4] ± 0.2	0.4 ± 0.1
T92	0.4	1.6 [1.1] ± 0.5	0.7 ± 0.2	1.7 ± 0.2	0.3 [0.4] ± 0.1	0.2 ± 0.1
G93	1.5	1.9 ± 0.1	1.2 ± 0.4	2.0 ± 0.5	0.8 ± 0.1	0.8 ± 0.1
K97	0.6	1.2 ± 0.2	NR	2.1 (1.4 - 4.0)	0.5 ± 0.1	0.3 (0.2 - 0.4)
N103	2.0	1.1 [2.4] ± 0.1	0.8 ± 0.3	2.0 ± 0.3	1.8 [0.8] ± 0.2	1.0 ± 0.2
Q109	0.3	0.6 ± 0.2	0.5 ± 0.1	0.6 (0.1 - 1.0)	0.5 ± 0.2	0.5 (0.3 - 3.0)
S129	0.7	0.6 ± 0.2	0.4 ± 0.1	1.4 (0.2 - 2.7)	1.2 ± 0.4	0.5 (0.3 - 3.5)

Footnotes

[a] Calculated with the online server SPHERE[86] using the PDLA rate basis, pH_{meter} 6.3, 100% D_2O and the amino acid sequence of α-synuclein.[83,84,86] Rates from SPHERE match hand-calculated rates for 1:1 H_2O:D_2O buffer.[52]

[b] From fitting SOLEXSY exchange curves (pH 6.7, 100 mM HEPES, 35 mM bis-tris propane, 288 K, 50% D_2O). Uncertainties are from Monte Carlo noise estimation. Values in brackets are from the same buffer plus 0.15 M NaCl (uncertainties ≤0.6 s^{-1}).

[c] CLEANEX data from Croke, *et al.* (pH 7.4, 20 mM phosphate, 288 K).[112] Converted to base-catalyzed rates using pK_W of 14.44 (pOH 7.04, to account for 10% D_2O) followed by extrapolation to pH 6.7 using a pK_W of 14.79 (pOH 8.09, to account for 50% D_2O).[101] Uncertainties <0.1 were set to 0.1. NR; not reported.

[d] From fitting SOLEXSY exchange curves and subsequent extrapolation to pH 6.7 using a pK_W of 14.79 (pOH 8.09, to account for 50% D_2O).[101] Uncertainties are the standard deviations of the mean. Uncertainty for T81 and G93 are the range from two experiments. Cells were resuspended in 100 mM HEPES, 35 mM bis-tris propane, 50 µg/mL chloramphenicol, 100 µg/mL ampicillin, 50% D_2O, 288 K. Rates of ≥0.2 s^{-1} were assumed for residues that exhibit a buildup peak at t_{mix} 0.3 s whose decay peak overlapped another crosspeak.

[e] Calculated by dividing the rates from SPHERE by the rates in buffer or in cells. Uncertainties are from error propagation. Uncertainties <0.1 were set to 0.1. Protection factors in brackets are from the same buffer plus 0.15 M NaCl.

[f] Values estimated from the linear fit shown in Supplementary Figure 3.5 using the ratio of the volumes of buildup to decay peaks at a t_{mix} of 0.3 s. Uncertainty (in parentheses) are the maximum and minimum rates within 0.1 units of this ratio as shown in the figure.

[g] ND: not determined due to crosspeak overlap or broadening.

[h] K34 overlaps with K45 and K97 in cells, yielding one exchange rate.

[i] In buffer K45 and K97 overlap, yielding one exchange rate.

[j] In buffer V52 and V74 overlap, yielding one exchange rate.

Supplementary Table 3.4. Triplicate acetylated α-synuclein in-cell data extrapolated to pH 6.7.

Residue	k_{obs} (s^{-1})[a]	In-cell pH[b]	logk_{obs}	pOH^-[c]	logk_{OH^-}[d]	k_{obs} at pH 6.7 (s^{-1})[e]
G67	2.8	6.9	0.4	7.9	8.3	1.8
	3.3	6.8	0.5	8.0	8.5	2.6
	1.3	6.6	0.1	8.2	8.3	1.6
E83	0.8	6.9	-0.1	7.9	7.8	0.5
	0.9	6.8	-0.05	8.0	7.9	0.7
	0.8	6.6	-0.1	8.2	8.1	1.0
G86	3.6	6.9	0.6	7.9	8.4	2.3
	3	6.8	0.5	8.0	8.5	2.4
	1.8	6.6	0.3	8.2	8.4	2.3
T92	0.9	6.9	-0.05	7.9	7.8	0.6
	1.6	6.8	0.2	8.0	8.2	1.3
	1.1	6.6	0.04	8.2	8.2	1.4
	3.2	6.9	0.5	7.9	8.4	2.0
N103	2.6	6.8	0.4	8.0	8.4	2.1
	1.5	6.6	0.2	8.2	8.4	1.9
	2.8	6.9	0.4	7.9	8.3	1.8

Footnotes

[a] From fitting SOLEXSY exchange curves. Cells were resuspended in 100 mM HEPES, 35 mM bis-tris propane, 25 µg/mL chloramphenicol, 100 µg/mL ampicillin, 15 µg/mL rifampin, 288 K, 50% D_2O.

[b] Average pH from the chemical shift of H50 ε1 or δ2 proton before and after the SOLEXSY experiment (Supplementary Figures 3.2 and 3.3).

[c] $pOH^- = pK_W - pH$; pK_W of 14.79 (to account for 50% D_2O, 288 K).

[d] Logarithm of the second-order rate constant for base-catalyzed exchange ($k_{OH^-} = k_{obs}/[OH^-]$).

[e] k_{obs} extrapolated to pH 6.7: $10^{(\log kOH - pOH)} = 10^{(\log kOH - pKW + pH)} = 10^{(\log kOH - 14.79 + 6.7)} = 10^{(\log kOH - 8.09)}$.

Supplementary Table 3.5. Acetylated α-synuclein exchange rates (s^{-1}) and protection factors (PF).

Residue	SPHERE[a]	Buffer[b]	Cells[c]	Buffer PF[d]	Cell PF[d]
D2	0.3	0.8 ± 0.2	ND[e]	0.4 ± 0.1	ND
G7	1.2	1.9 ± 0.4	ND	0.6 ± 0.1	ND
S9	0.7	2.4 ± 0.1	ND	0.3 ± 0.1	ND
T22	0.6	1.5 ± 0.3	ND	0.4 ± 0.1	ND
G31	0.9	1.1 ± 0.1	1.1 (0.3 - 2.7)[f]	0.8 ± 0.1	0.8 (0.3 - 3.0)
T33	0.6	2.4 (0.5 - 5.0)	ND	0.3 (0.1 - 1.2)	ND
K34[g]	0.7	1.2 ± 0.3	≥ 0.2	0.6 ± 0.2	≤ 3.5
V40	0.1	0.6 ± 0.3	ND	0.2 ± 0.1	ND
G41	0.7	0.9 ± 0.1	ND	0.8 ± 0.1	ND
T44	0.6	1.1 ± 0.3	ND	0.5 ± 0.1	ND
K45	0.7	1.2 ± 0.3	≥ 0.2	0.6 ± 0.2	≤ 3.5
A53	0.4	0.9 ± 0.2	ND	0.4 ± 0.1	ND
T54	0.4	0.9 (0.1 - 1.8)	ND	0.4 (0.2 - 4.0)	ND
V66	0.2	0.8 ± 0.1	ND	0.3 ± 0.1	ND
G67	0.7	0.3 ± 0.1	2.0 ± 0.3	0.4 ± 0.1	0.4 ± 0.1
T81	0.6	1.2 (0.3 - 2.7)	0.7 (0.1 - 1.6)	0.5 (0.2 - 2.0)	0.9 (0.4 - 6.0)
E83	0.1	0.1 ± 0.1	0.7 ± 0.2	1.0 ± 1.0	0.1 ± 0.1
G84	0.7	1.3 ± 0.3	ND	0.5 ± 0.1	ND
G86	0.9	1.7 ± 0.1	2.3 ± 0.1	0.5 ± 0.1	0.4 ± 0.1
T92	0.4	0.3 ± 0.1	1.1 ± 0.3	1.3 ± 0.4	0.4 ± 0.1
G93	1.5	2.7 ± 0.3	3.2 (3.0 - 4.0)[h]	0.6 ± 0.1	0.5 (0.4 - 0.5)
K97	0.6	1.2 ± 0.3	≥ 0.2	0.5 ± 0.1	≤ 3.0
N103	2.0	0.7 ± 0.1	2.0 ± 0.1	2.9 ± 0.4	1.0 ± 0.1
Q109	0.3	0.6 ± 0.3	0.7 (0.1 - 1.0)	0.5 ± 0.3	0.4 (0.3 - 3.0)
S129	0.7	0.2 ± 0.2	0.5 (0.1 - 1.0)	3.5 ± 3.5	1.4 (0.7 - 7.0)

Footnotes

[a] Calculated with the online server SPHERE[86] using the PDLA rate basis, pH_{meter} 6.3, 100% D_2O, a blocked *N*-terminus and the amino acid sequence of α-synuclein.[83,84,86]

[b] From fitting SOLEXSY exchange curves (pH 6.7, 100 mM HEPES, 35 mM bis-tris propane, 288 K, 50% D_2O). Uncertainties are from Monte Carlo noise estimation.

[c] From fitting SOLEXSY exchange curves and subsequent extrapolation to pH 6.7 using a pK_W of 14.79 (pOH 8.09, to account for 50% D_2O).[101] Uncertainties are the standard deviations of the mean. Cells were resuspended in 100 mM HEPES, 35 mM bis-tris propane, 25 μg/mL chloramphenicol, 100 μg/mL ampicillin, 15 μg/mL rifampin, 50% D_2O, 288 K. A rate of ≥0.2 s^{-1} were assumed for residues that exhibit a buildup peak at t_{mix} 0.3 s whose decay peak overlapped another crosspeak.

[d] Calculated by dividing the rates from SPHERE by the rates in buffer or in cells. Uncertainties are from error propagation. Uncertainties <0.1 were set to 0.1.

[e] ND: not determined due to crosspeak overlap or broadening.

[f] Values estimated from the linear fit shown in Supplementary Figure 3.5 using the ratio of the volumes of buildup to decay peaks at a t_{mix} of 0.3 s. Uncertainty (in parentheses) is the maximum and minimum rates within 0.1 units of this ratio as shown in the figure.

[g] K34 overlaps with K45 and K97 in cells and buffer, yielding one exchange rate.

[h] Values estimated from the linear fit shown in Supplementary Figure 3.5 using the ratio of the volumes of buildup to decay peaks at a t_{mix} of 0.3 s. Uncertainty (in parentheses) is the closest rates to ratio.

Supplementary Table 3.6. Triplicate FlgM in-cell data extrapolated to pH 6.7.

Residue	k_{obs} (s^{-1})[a]	In-cell pH[b]	logk_{obs}	pOH[-c]	logk_{OH^-}[d]	k_{obs} at pH 6.7 (s^{-1})[e]
E19	0.2	6.2	-0.7	8.2	7.5	0.7
	0.9	6.2	-0.1	8.2	8.2	2.8
	0.9	6.2	-0.1	8.2	8.2	2.7
S21	1.6	6.2	0.2	8.2	8.4	5.1
	0.6	6.2	-0.2	8.2	8.0	1.9
	0.5	6.2	-0.3	8.2	7.9	1.5
T23	0.4	6.2	-0.4	8.2	7.8	1.3
	1.0	6.2	0.0	8.2	8.2	3.1
	0.8	6.2	-0.1	8.2	8.1	2.5
A36	1.1	6.2	0.03	8.2	8.3	3.4
	1.1	6.2	0.04	8.2	8.3	3.4
	0.9	6.2	-0.05	8.2	8.2	2.8
T37	1.6	6.2	0.2	8.2	8.4	5.1
	1.1	6.2	0.05	8.2	8.3	3.5
	0.9	6.2	-0.1	8.2	8.2	2.8
T6/T20/S40[f]	0.5	6.2	-0.3	8.2	8.0	1.7
	0.6	6.2	-0.2	8.2	8.0	1.8
	0.5	6.2	-0.3	8.2	7.9	1.6

Footnotes

[a] From fitting SOLEXSY exchange curves. Cells were resuspended in 100 mM HEPES, 35 mM bis-tris propane, 50 µg/mL chloramphenicol, 100 µg/mL ampicillin, 298 K, 50% D_2O.

[b] Average pH from chemical shift of HEPES C14 protons (minus 0.4 pH units, see Supplementary figures 3.2 and 3.4) from ^{13}C-^{1}H HSQCs before and after the SOLEXSY experiment.

[c] $pOH^- = pK_W - pH$; pK_W of 14.43 (to account for 50% D_2O, 298 K).

[d] Logarithm of the second-order rate constant for base-catalyzed exchange ($k_{OH^-} = k_{obs}/[OH^-]$).

[e] k_{obs} extrapolated to pH 6.7: $10^{(\log kOH - pOH^-)} = 10^{(\log kOH - pKW + pH)} = 10^{(\log kOH - 14.43 + 6.7)} = 10^{(\log kOH - 7.73)}$.

[f] T6, T20 and S40 crosspeaks are overlapped.

Supplementary Table 3.7. FlgM exchange rates (s^{-1}) and protection factors (PF).

Residue	SPHERE[a]	Buffer[b]	Cells[c]	Buffer PF[d]	Cell PF[d]
T6	1.9	3.9 ± 0.1	1.7 ± 0.1[e]	0.5 ± 0.1	1.1 ± 0.1
V12	0.2	0.6 ± 0.2	ND[f]	0.3 ± 0.1	ND
V15	0.4	1.2 ± 0.4	≥ 0.2	0.3 ± 0.1	≤ 2.0
Q16	1.1	2.1 ± 0.1	≥ 0.2	0.5 ± 0.1	≤ 5.5
E19	0.7	1.7 ± 0.1	2.0 ± 0.7	0.4 ± 0.1	0.4 ± 0.1
T20	0.8	3.0 ± 0.1[g]	1.7 ± 0.1	0.3 ± 0.1	0.5 ± 0.1
S21	5.1	ND	2.8 ± 1.2	ND	1.8 ± 0.8
T23	0.8	1.0 ± 0.1	≥ 0.2	0.8 ± 0.1	≤ 4.0
E31	0.7	2.9 ± 0.1	≥ 0.2	0.2 ± 0.1	≤ 3.5
A36	1.4	1.5 ± 0.1	3.2 ± 0.2	0.9 ± 0.1	0.4 ± 0.1
T37	1.2	3.0 ± 0.1	3.8 ± 0.7	0.4 ± 0.1	0.3 ± 0.1
S40	3.2	3.0 ± 0.1	1.7 ± 0.1	1.1 ± 0.1	1.9 ± 0.1
S44	2.0	0.6 ± 0.4	ND	3.3 ± 2.2	ND
Q47	1.6	1.0 ± 0.2	ND	1.6 ± 0.3	ND
A48	2.2	1.1 ± 0.1	ND	2.0 ± 0.2	ND
K49	1.3	0.4 ± 0.1	ND	3.3 ± 0.8	ND
G54	1.5	1.3 ± 0.1	ND	1.2 ± 0.1	ND
A65	1.0	1.6 ± 0.1	ND	0.6 ± 0.1	ND
T68	1.5	1.7 ± 0.2	ND	0.9 ± 0.1	ND
G73	5.3	3.0 ± 0.4	ND	1.8 ± 0.2	ND
G80	4.0	2.4 ± 0.2	ND	1.7 ± 0.1	ND
A83	0.8	1.4 ± 0.4	ND	0.6 ± 0.2	ND
S92	5.1	3.5 ± 0.5	ND	1.5 ± 0.2	ND
L94	0.4	0.8 ± 0.2	ND	0.5 ± 0.1	ND
S96	5.1	4.1 ± 0.2	ND	1.2 ± 0.1	ND

Footnotes

[a] Calculated with the online server SPHERE[86] using the poly-DL-alanine rate basis (PDLA) at pH_{meter} 6.3 in 100% D_2O and the amino acid sequence of FlgM.[83,84,86]

[b] From fitting SOLEXSY exchange curves (pH 6.7, 100 mM HEPES, 35 mM bis-tris propane, 298 K, 50% D_2O). Uncertainties are from Monte Carlo noise estimation. The exchange rate for S21 cannot be measured in buffer because its buildup crosspeak overlaps the decay crosspeak of S44.

[c] From fitting SOLEXSY exchange curves and subsequent extrapolation to pH 6.7 using a pK_W of 14.43 (pOH 7.73, to account for 50% D_2O).[101]. Uncertainties are the standard deviations of the mean from three trials. Cells were resuspended in 100 mM HEPES, 35 mM bis-tris propane, 50 µg/mL chloramphenicol, 100 µg/mL ampicillin, 50% D_2O, 298 K. Rates of ≥0.2 s^{-1} were assumed for residues that exhibit a buildup peak whose decay peak overlapped another crosspeak.

[d] Calculated by dividing the rates from SPHERE by the rates in buffer or in cells. Uncertainties are from error propagation. Uncertainties <0.1 were set to 0.1.

[e] T6, T20 and S40 overlap in cells and yield one exchange rate.

[f] ND: not determined due to crosspeak overlap or broadening.

[g] T20 and S40 overlap in buffer and yield one exchange rate.

Supplementary Table 3.8. Activation energy of amide proton exchange from α-synuclein data.

	In buffer				In cells		
Residue	k_{obs} (s^{-1}) 288 K[a]	k_{obs} (s^{-1}) 293 K[b]	k_{obs} (s^{-1}) 298 K[c]	E_a (kcal/mol)	k_{obs} (s^{-1}) 288 K[a]	k_{obs} (s^{-1}) 298 K[d]	E_a (kcal/mol)
G31	1.2 ± 0.2	1.8 ± 0.4	2.1 ± 0.1	10	1.8 ± 0.4	5.7 ± 0.6	20
G67	0.4 ± 0.1	0.5 ± 0.2	1.9 ± 0.1	26	2.0 ± 0.4	5.0 ± 0.6	16
G68	1.4 ± 0.2	1.4 ± 0.3	2.6 ± 0.2	11	1.3 ± 0.3	4.4 ± 1.9	21
G86	1.8 ± 0.6	2.6 ± 0.1	3.4 ± 0.1	11	2.5 ± 0.3	5.0 ± 0.6	12
N103	1.1 ± 0.1	1.3 ± 0.1	2.6 ± 0.1	15	2.0 ± 0.5	5.0 ± 1.3	16
Average				15 ± 3[e]			17 ± 1[e]

Footnotes

[a] From Supplementary Table 3.3.

[b] From fitting SOLEXSY exchange curves (pH 6.7, 100 mM HEPES, 35 mM bis-tris propane, 293 K, 50% D_2O). Uncertainties are from Monte Carlo noise estimation.

[c] From fitting SOLEXSY exchange curves (pH 6.7, 100 mM HEPES, 35 mM bis-tris propane, 293 K, 50% D_2O). Uncertainties are from Monte Carlo noise estimation.

[d] From fitting SOLEXSY exchange curves and subsequent extrapolation to pH 6.7 using a pK_W of 14.43 (pOH 7.73, to account for 50% D_2O).[101] Uncertainties are from Monte Carlo noise estimation. Cells were resuspended in 100 mM HEPES, 35 mM bis-tris propane, 50 µg/mL chloramphenicol, 100 µg/mL ampicillin, 50% D_2O, 298 K.

[e] Uncertainty is the standard deviation of the mean.

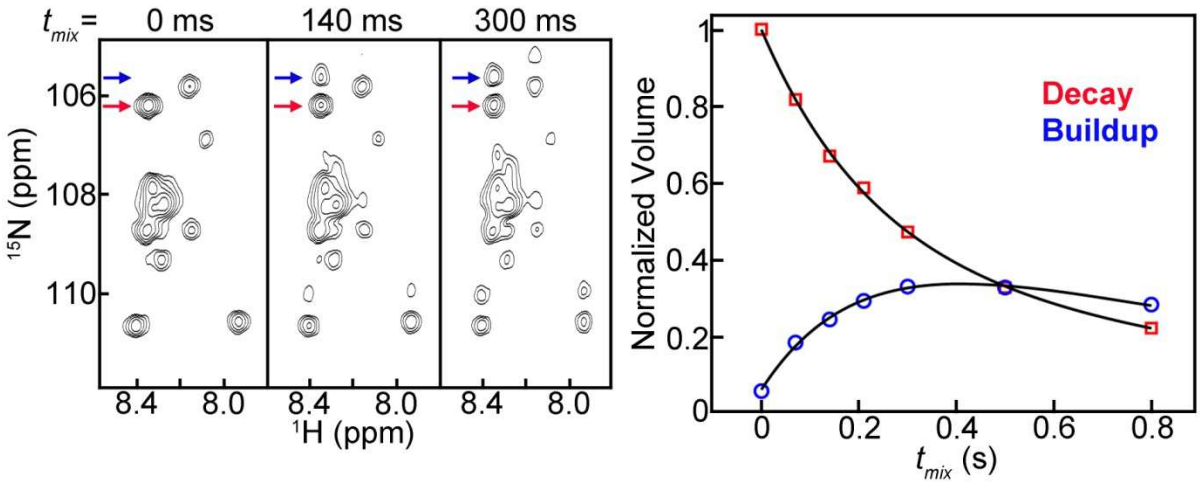

Supplementary Figure 3.1. In-cell $^{15}N^{H/D}$-^{1}H SOLEXSY spectra showing the glycine region of α-synuclein and exchange curves for G86. As t_{mix} increases, the crosspeak volume from the initially deuterated ($^{15}N^{D}$-H) amide increases, while that from the initially protonated ($^{15}N^{H}$-H) crosspeak decreases.

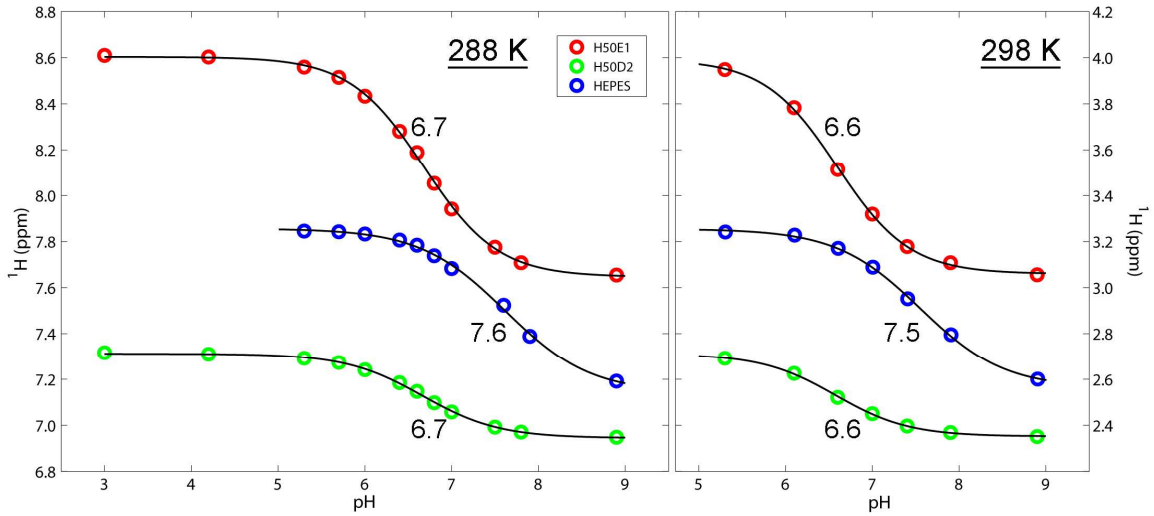

Supplementary Figure 3.2. Titration curves in buffer. The chemical shift of the $^{13}C^{\varepsilon 1}$ (○) and $^{13}C^{\delta 2}$ (○) protons from H50 of α-synuclein and the C14 protons of HEPES[80] (○) are plotted versus pH. The fitted pK_a values are shown next to the curves.

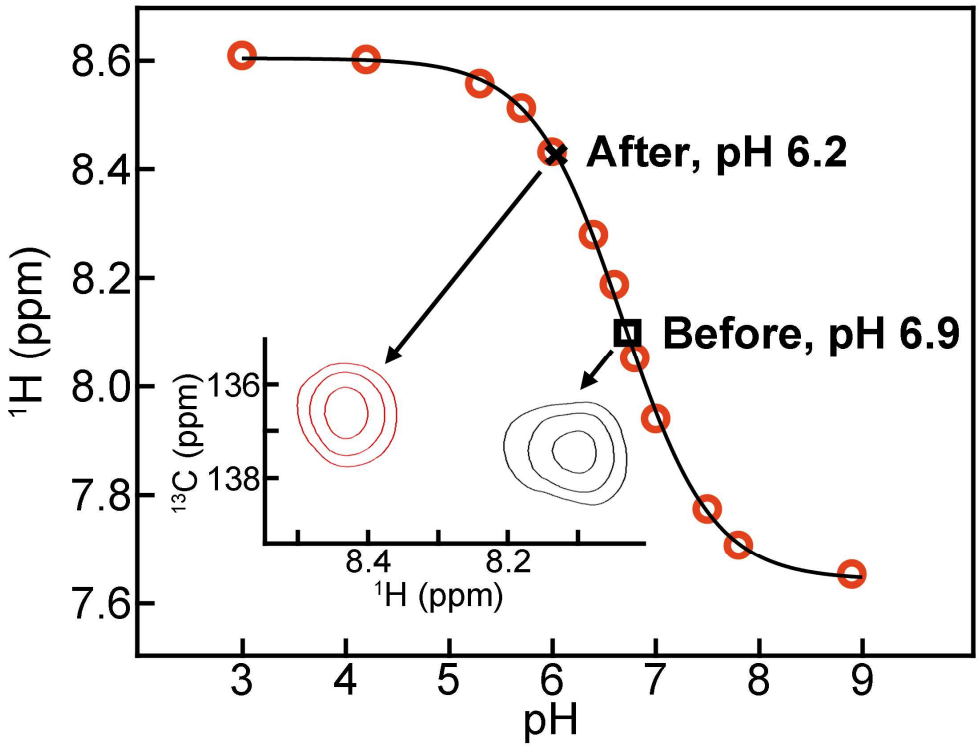

Supplementary Figure 3.3. Acidification of the cytoplasm over the ~16 h time course of the SOLEXSY experiment. Titration curve is based on the proton chemical shift from α-synuclein H50 $^{13}C^{\varepsilon 1}$ (○) at 288 K (Supplementary Figure 3.2). The chemical shift in cells was measured before (□) and after (x) each in-cell experiment. The inset shows the $^{13}C^{\varepsilon 1}$ proton crosspeaks from ^{13}C-^1H HSQC spectra before (black) and after (red) the SOLEXSY experiment.

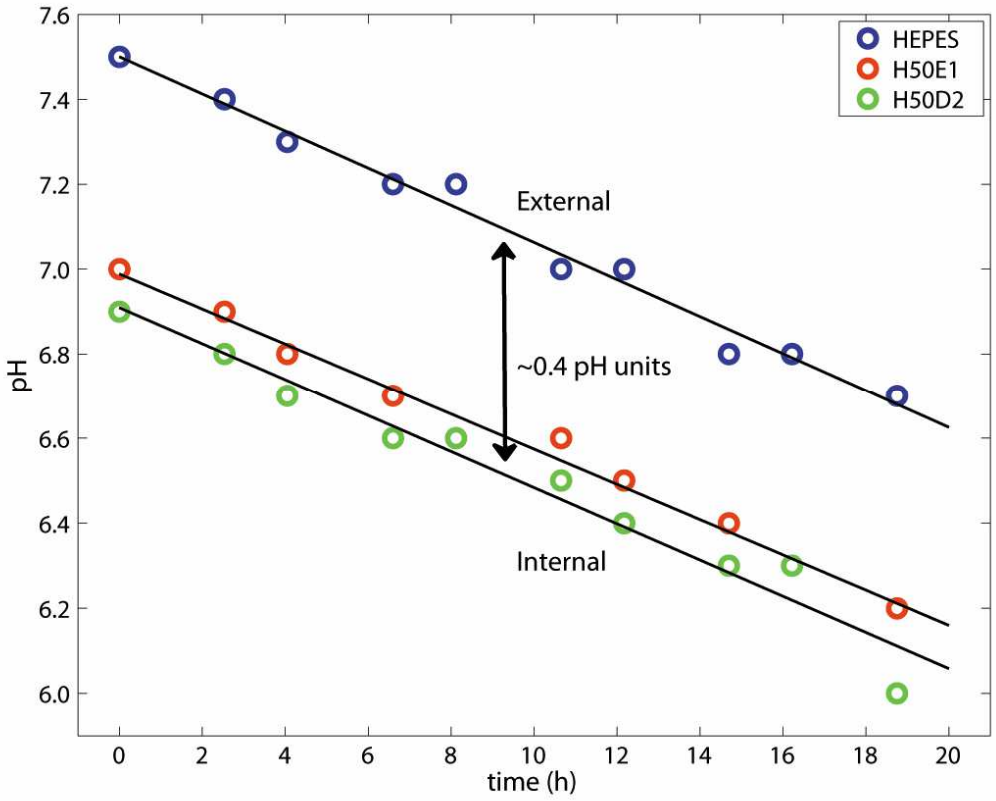

Supplementary Figure 3.4. Acidification of the cytoplasm during the SOLEXSY experiment ($pH_{external}$ - $pH_{internal}$ = ~0.4 units). The chemical shifts from HEPES and H50 of α-synuclein were measured as a function of time. The C14 protons of HEPES (○) assess external pH,[124] while the ε1 (○) and δ2 (○) protons of H50 assess internal pH.

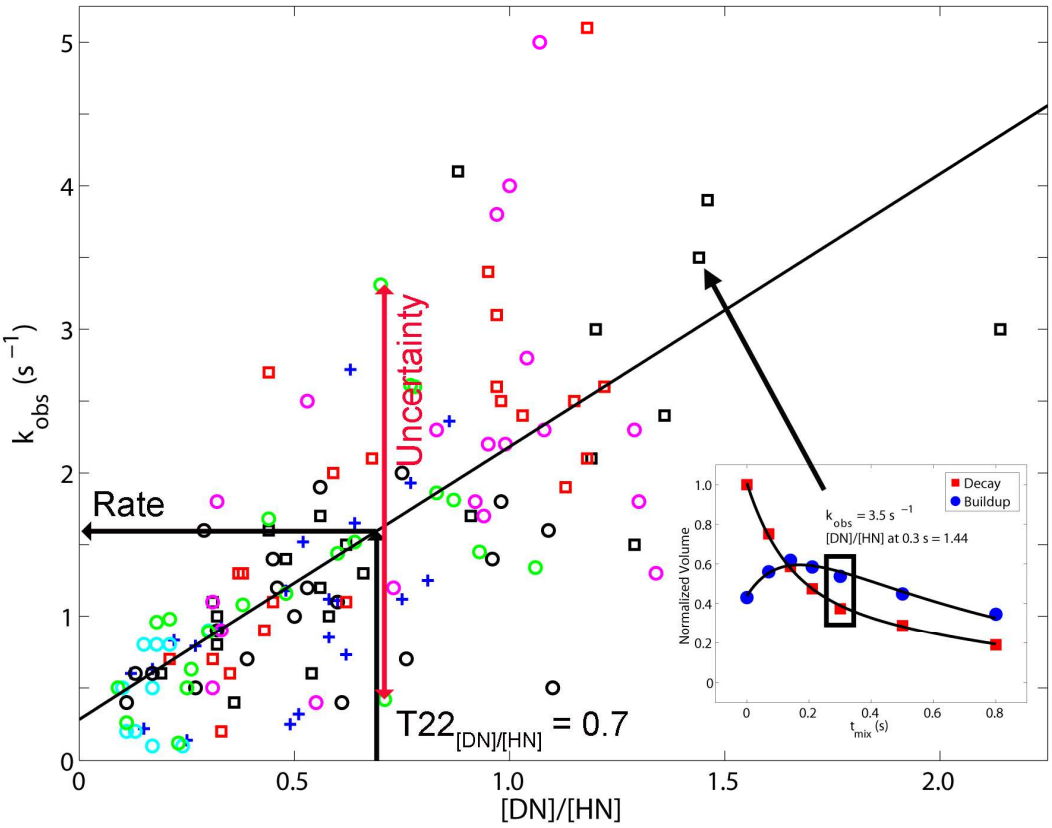

Supplementary Figure 3.5. Plot of rates versus volume ratio of buildup and decay peaks at a t_{mix} of 0.3 s used to estimate some in-cell rates. Purified α-synulcein (**o**, pH 6.7, 288 K; o, pH 6.2, 288 K; o, pH 7.1, 288 K; o, pH 6.7, 293 K; □, pH 6.7, 298 K), acetylated α-synuclein (+, pH 6.7, 288K) and FlgM (□, pH 6.7, 298 K) were dissolved in 100 mM HEPES, 35 mM bis-tris propane, 50% D_2O. A typical curve in buffer (S92 of FlgM) is shown in the inset; the rate (3.5 s^{-1}) is from curve fitting, while the box indicates data used to obtain the ratio. Rates for in-cell data that do not yield full buildup and decay curves were estimated by using a linear fit ($k_{obs} = 1.9\frac{[DN]}{[HN]} + 0.28$, R=0.71, N=138, <0.05% probability that R arises from uncorrelated data[142]). The method for T22 of α-synuclein is shown. This experiment takes 150 min, affording nearly constant pH. The uncertainty was estimated as the range of maximum and minimum rates within 0.1 units of this ratio.

_N_-terminus (pI 9.5)

B -Ac [1]MDVFMKGLSKAKEGVVAAAEKTKQGVAEAA[30]
C -Ac MDVFMKGLSKAKEGVVAAAEKTKQGVAEAA
B +Ac MDVFMKGLSKAKEGVVAAAEKTKQGVAEAA
C +Ac MDVFMKGLSKAKEGVVAAAEKTKQGVAEAA

B -Ac [31]GKTKEGVLYVGSKTKEGVVHGVATVAEKTK[60]
C -Ac GKTKEGVLYVGSKTKEGVVHGVATVAEKTK
B +Ac GKTKEGVLYVGSKTKEGVVHGVATVAEKTK
C +Ac GKTKEGVLYVGSKTKEGVVHGVATVAEKTK

NAC (pI 4.5)

B -Ac [61]EQVTNVGGAVVTGVTAVAQKTVEGAGSIAAATGFV[95]
C -Ac EQVTNVGGAVVTGVTAVAQKTVEGAGSIAAATGFV
B +Ac EQVTNVGGAVVTGVTAVAQKTVEGAGSIAAATGFV
C +Ac EQVTNVGGAVVTGVTAVAQKTVEGAGSIAAATGFV

_C_-terminus (pI 3.8)

B -Ac [96]KKDQLGKNEEGAPQEGILEDMPVDPDNEAYEMPSEEGYQDYEPEA[140]
C -Ac KKDQLGKNEEGAPQEGILEDMPVDPDNEAYEMPSEEGYQDYEPEA
B +Ac KKDQLGKNEEGAPQEGILEDMPVDPDNEAYEMPSEEGYQDYEPEA
C +Ac KKDQLGKNEEGAPQEGILEDMPVDPDNEAYEMPSEEGYQDYEPEA

Supplementary Figure 3.6. Hydrogen exchange in α-synuclein (pI 4.7) in cells (C) and in buffer (B) with (+) and without (-) acetylation. Residues whose crosspeaks show hydrogen exchange are in red. Underlined residues are quantifiable (i.e., give complete SOLEXSY buildup and decay curves). Residues whose crosspeaks are broadened (likely due to chemical exchange) are in blue. Residues that show hydrogen exchange at high pH, and probable chemical exchange as the cellular pH decreases are shown in green. Residues that are overlapped or broadened such that exchange cannot be observed are in black.

CHAPTER 4: IN-CELL THERMODYNAMICS ESTABILISHES NEW ROLES FOR PROTEIN SURFACES

Original citation: Smith AE, Zhou LZ, Gorensek AH, Senske M, Pielak GJ. *submitted*

Abstract

There is abundant, physiologically-relevant knowledge about protein cores; they are hydrophobic,[143] exquisitely well packed,[144] and nearly all hydrogen bonds are satisfied.[145] With rare exceptions,[19,21,63] however, physiological understanding of protein surfaces, which expose charged and polar groups to the environment, remains elusive because proteins are almost exclusively studied *in vitro* in the simple conditions of water and buffer. Here, we establish the essential physiological roles played by protein surfaces by measuring the equilibrium thermodynamics and kinetics of protein folding in the complex environment of living cells, where the concentration of macromolecules exceeds 200 g/L.[1] ^{19}F NMR data on the globular 7-kDa *N*-terminal SH3 domain of *Drosophila* signal transduction protein drk (SH3) acquired inside *E. coli* show that charge-charge interactions are fundamental to protein stability and folding kinetics. Our results contradict predictions from accepted theories of macromolecular crowding[146,147] and show that cosolutes commonly used

to mimic the cellular interior do not yield physiologically relevant information. As such, we provide the foundation for a complete picture of protein chemistry in cells.

Introduction

Classic theories about the effects of complex environments consider only hard-core repulsions and so predict purely entropically-driven protein stabilization.[128,146] Here, we test this idea in living cells. SH3 exists in a dynamic equilibrium between the folded state and the unfolded ensemble.[148] This two-state behavior is ideal for NMR-based studies of folding.[18] 5-Fluorotryptophan labeled[29] SH3 exhibits only two ^{19}F resonances: one from the folded state, the other from the unfolded ensemble (Figure 4.1a).[149] The area under each resonance is proportional to its population, p_f and p_u, respectively. These populations are used to quantify protein stability *via* the modified standard state free energy of unfolding, $\Delta G_U^{\circ\prime} = -RTln\frac{p_U}{p_F}$, where R is the gas constant and T is the absolute temperature. Furthermore, the width at half height of each resonance is proportional to the transverse relaxation rate, which is an approximate measure of intermolecular interactions.[98,100,150] Thus, this simple system yields both quantitative thermodynamic knowledge and information about interactions involving surfaces of the folded state and the unfolded ensemble.

Results and Discussion

To assess the enthalpic ($\Delta H_U^{\circ\prime}$) and entropic ($\Delta S_U^{\circ\prime}$) components of stability we measured the temperature dependence of $\Delta G_U^{\circ\prime}$. The data were fitted to the integrated Gibbs-Helmholtz equation,[151] assuming a constant heat capacity of unfolding, $\Delta C_{p,U}^{\circ}$:

$$\Delta G_U^\circ = \Delta H_{U,ref}^\circ - T\Delta S_{U,ref}^\circ + \Delta C_{p,U}^\circ \left[T - T_{ref} - T \ln \frac{T}{T_{ref}}\right],$$

where, T_{ref}, is the melting temperature, T_m (where $p_f = p_u$), or the temperature of maximum stability, T_s (where $\Delta S_U^{\circ\prime} = 0$).[151] In buffer at pH 7.2 and 298 K, $\Delta G_U^{\circ\prime}$ is 0.52 ± 0.03 kcal/mol, $\Delta H_U^{\circ\prime}$ is 10 ± 1 kcal/mol and a $T\Delta S_U^{\circ\prime}$ is 10 ± 1 kcal/mol (Figure 4.1c, Supplementary Tables 4.1 and 4.2).

Spectra were then acquired in *E. coli* (Figure 4.1b). Both T_m and $\Delta G_U^{\circ\prime}$ decreased relative to buffer (Figure 4.1c, Supplementary Tables 4.1 and 4.2), consistent with other studies,[58,63,152,153] but inconsistent with theory.[146,147] Furthermore, the stability decrease (0.50 ± 0.06 kcal/mol at 298 K) arises from a 2 ± 1 kcal/mol decrease to $\Delta H_U^{\circ\prime}$ (Supplementary Table 4.3), which is also inconsistent with theory.

The source of the inconsistency can be seen from the width of the resonances. The resonance from both the folded state and the unfolded ensemble are broader in cells than in buffer (Figure 4.1a, b, Supplementary Table 4.2), suggesting the presence of weak, attractive intermolecular interactions of SH3 with other cytoplasmic components.[150] This finding is consistent with the existence of nonspecific, attractive surface interactions, which are absent from simple theory.[128] The key observation is that the resonance from the unfolded ensemble is twelve-fold broader compared to buffer, while the folded state resonance is broadened only four-fold. The unfolded ensemble is more affected because it exposes more surface than the folded state,[154]

suggesting that the enthalpic destabilization arises from attractive interactions between the unfolded ensemble and the cytoplasm.

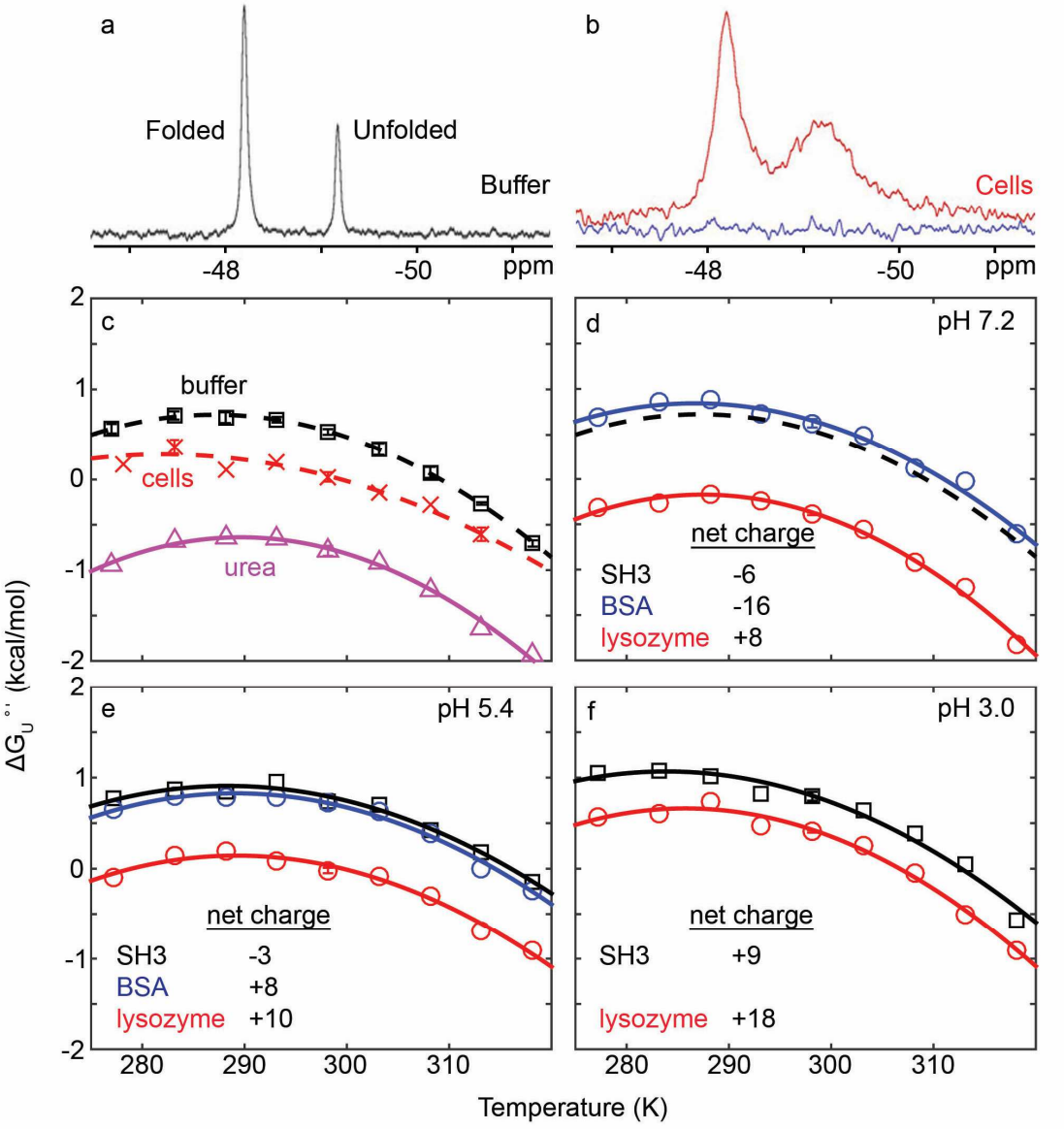

Figure 4.1. The intracellular environment destabilizes SH3 relative to buffer. ^{19}F spectra acquired at 298 K, in buffer (a) and in cells (b). The blue trace is from the post-experiment supernatant and shows that the red spectrum arises from protein inside cells. c) Stability curves in buffer (black), in cells (red) and in 100 g/L urea (magenta). Error bars in buffer are smaller than the labels and represent the standard deviation of three independent trials. Error bars for the in-cell data at 273 K, 298 K and 313 K represent the standard deviation of three independent trials. d-f) Stability in buffer (black) and solutions of 100 g/L BSA (blue) and

lysozyme (red). The curve for buffer from panel c is reproduced in d. The net charges on SH3, BSA and lysozyme (based on sequence) are shown. Error bars for the *in vitro* crowded 298 K data represent the standard deviation from three trials. Analysis of uncertainties are discussed in Methods. Appearance of new resonances in the pH 3 BSA sample prevented extraction of thermodynamic parameters.

To explore the enthalpic component, we performed *in vitro* experiments at pH 7.2, 5.4 and 3.0 in 100 g/L solutions of protein cosolutes with different net charges (Figure 4.1d-f). SH3 (pI_{calc} 5) and bovine serum albumin (BSA, 66 kDa, pI_{calc} 6) change from polyanions to polycations over this pH range, but lysozyme (14 kDa, pI_{calc} 9) remains a polycation.

At pH 7.2, lysozyme destabilized SH3 ($\Delta\Delta G^{\circ\prime}_{U,298\ K}$= -0.92 ± 0.03; Figure 4.1d) and broadened its resonances (Figure 4.2a, Supplementary Table 4.2). We attribute both effects primarily to attractive charge-charge interactions between the protein surfaces. Consistent with this idea, adding 0.15 M NaCl to screen the charge-charge interaction, diminished both the destabilization ($\Delta\Delta G^{\circ\prime}_{U,298\ K}$= -0.70 ± 0.03) and line width (Supplementary Table 4.2). BSA, which has the same net charge as SH3 at this pH, was slightly stabilizing ($\Delta\Delta G^{\circ\prime}_{U,298\ K}$= 0.09 ± 0.06) and accompanied by weak broadening, as expected for proteins having the same net charge.[128] An explanation for the modest stabilization is that BSA exposes a distribution of positive and negative charges, partially offsetting the net charge-charge repulsion.

At pH 5.4 (Figure 4.1e), SH3 is a polyanion, but both BSA and lysozyme are polycations. Under these conditions, both BSA ($\Delta\Delta G^{\circ\prime}_{U,298\ K}$= -0.02 ± 0.11) and lysozyme ($\Delta\Delta G^{\circ\prime}_{U,298\ K}$= -0.76 ± 0.09) are destabilizing, and BSA-induced

broadening is more severe (Supplementary Table 4.2). The crossover in stability for BSA from pH 7.2 to 5.4 and the observation that lysozyme is less destabilizing and causes less broadening reinforce the idea that charge-charge attractions play a key role in modulating stability. At pH 3.0 (Figure 4.1f), lysozyme and SH3 have the same net charge, yet SH3 is destabilized ($\Delta\Delta G^{\circ\prime}_{U,298\ K}$= -0.39 ± 0.05). These results suggest that hydrogen-bonds, weakly polar interactions, and hydrophobicity[32] also contribute to attractive intermolecular interactions in cells.

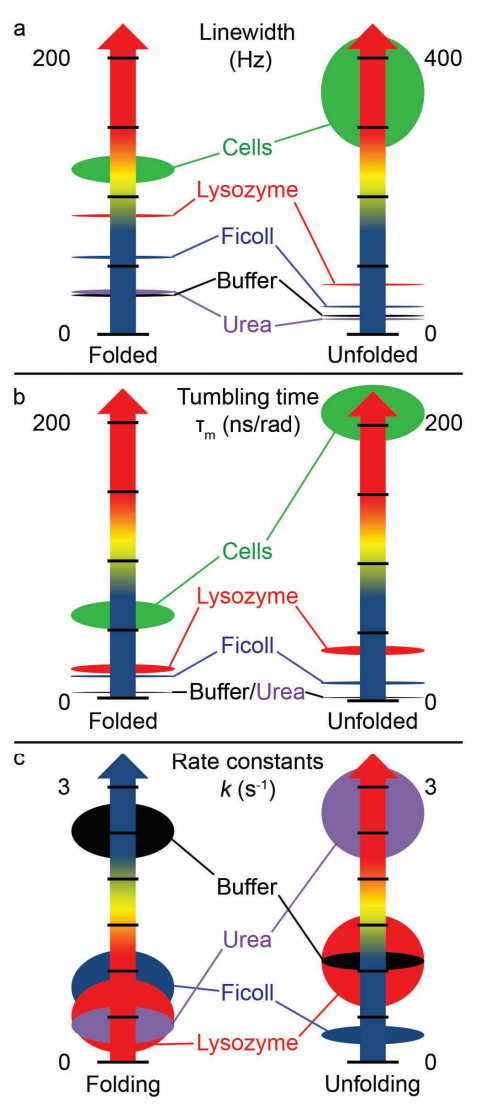

Figure 4.2. Effects on the unfolded ensemble are key to understanding how the cytoplasm affects folding. For each "thermometer", red indicates attractive interactions or destabilization and blue indicates stabilization or lack of interactions, and the size of the symbol reflects the uncertainty (data acquired at pH 7.2). a) More resonance broadening is observed for the unfolded ensemble in cells. b) The cytoplasm increases the tumbling time of the unfolded ensemble. c) Folding rates decrease in crowded solutions but there is a differential effect on unfolding; Ficoll slows unfolding, urea increases unfolding, and lysozyme has an insignificant effect.

Sucrose-, glucose-, and ethylene glycol-based polymers, Ficoll, dextran, and PEG, respectively, have been used for decades to mimic the cellular interior.[147] Contrary to what is observed in cells (Figure 4.1c), both monomers and their polymers stabilize SH3 relative to buffer (Figure 4.3,

Supplementary Tables 4.1-4.3). Furthermore, the monomers are more stabilizing than the polymers; the opposite of what is usually implied by the term macromolecular crowding. In addition, theory predicts the stabilization arises from entropic effects, yet ethylene glycol and PEG stabilize SH3 enthalpically, while the sugar-induced stabilization is entropic. Clearly, synthetic polymers are poor mimics of the cellular interior.

Surprisingly, urea is the most accurate mimic of the thermodynamics observed in cells (Figure 4.1c). This cosolute destabilizes proteins by interacting favorably with the backbone,[155] which is more exposed in the unfolded ensemble.[154] Urea shows a strong enthalpic destabilization that overcomes a stabilizing entropic term at 298 K ($\Delta\Delta G_U^{\circ\prime}$= -1.32 ± 0.07, $\Delta\Delta H_U^{\circ\prime}$= -3 ± 1, $\mathrm{T}\Delta\Delta S_U^{\circ\prime}$= -2 ± 1 kcal/mol at 100 g/L). This is the same pattern seen in cells. These data strengthen our conclusion that the destabilization arises by attractive interactions with the unfolded ensemble.

Resonance broadening (Figure 4.2a) is only an approximate measure of attractive intermolecular interactions. Attractive interactions with larger proteins slow tumbling. Therefore, to obtain more detailed knowledge, we used ^{19}F relaxation to estimate tumbling times (τ_m) of SH3.[150] In buffer, τ_m is 4 ns for the folded state and 3 ns for the unfolded ensemble (Figure 4.3b, Supplementary Table 4.4), similar to published values.[156] In cells, the τ_m increases to 60 ns for the folded state and 210 ns for the unfolded ensemble, 15- and 70-fold increases, respectively. Increases may arise from higher viscosity (η), but the viscosity in cells is only about twice that in water.[150] The larger effect on the

unfolded ensemble bolsters our conclusion that the interior of the cell interacts more strongly with the unfolded ensemble, which explains the observed destabilization.

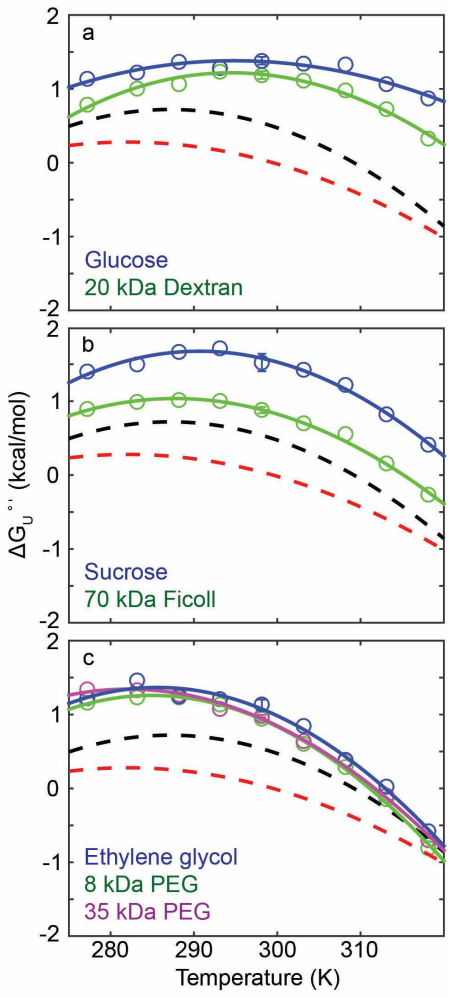

Figure 4.3. Synthetic polymers do not replicate the cytoplasm. Buffer (black) and in-cell (red) curves are reproduced from Figure 4.1c. Error bars for the 298 K data are the standard deviation of three independent trials at 298 K. a) Glucose and 20 kDa dextran, b) sucrose and 70 kDa Ficoll (all at 300 g/L), c) ethylene glycol, 8 kDa PEG and 35 kDa PEG (all at 200 g/L) stabilize the SH3 domain.

To lend further support to our conclusion, we examined the effects of Ficoll and lysozyme on τ_m. Ficoll increased τ_m to 15 ns and 13 ns for the folded state and unfolded ensemble, respectively. These increases likely arise from the large increase in viscosity.[42] The viscosity of the 100 g/L lysozyme solution is only 1.3 times that of water,[42] yet the apparent τ_m increased to 21 ns for the folded state and 37 ns for the unfolded ensemble. These data strongly support the idea that effects on the unfolded ensemble are the cause of the stability decrease in cells.

We also quantified the effects of cosolutes on folding and unfolding rates. We were unable to asses the rates in cells because, although SH3 is stable for one hour in cells, it is degraded during the >12 h needed for these experiments (all other in-cell experiments require a few minutes). Rate data were acquired in

lysozyme, urea and Ficoll (Figure 4.3c, Supplementary Table 4.5). Ficoll (70 kDa, 300 g/L) decreased the folding rate 2.5-fold, but decreased the unfolding rate 2.8-fold. The slower folding is consistent with the viscosity increase and slower unfolding consistent with both viscosity and the idea of an entropic pressure for the protein to adopt a compact form.[157,158] In contrast, lysozyme (100 g/L) slowed folding 5-fold, but had no effect on unfolding. Like lysozyme, urea (100 g/L) slowed folding 5-fold, but increased unfolding only 2.5 fold. We speculate that urea's small size allows it to penetrate the folded state to speed unfolding and its interaction with the backbone in the unfolded ensemble slowed folding, whereas lysozyme is too large to affect unfolding, but slows folding *via* interactions with the unfolded ensemble. These observations reinforce the idea that biologically relevant conditions can destabilize proteins by facilitating favorably interactions with the unfolded ensemble.

In summary, physiologically relevant information about proteins exteriors have been hidden because proteins are most often studied in buffer instead of in cells. This limitation does not matter for protein cores; they yield relevant information even in buffer because interior atoms experience the same environment in cells as they do in buffer -- they are surrounded by other protein atoms. Exteriors, however, are fundamentally different. In buffer, the surface is exposed to mostly water, but the cytoplasm is dramatically complex and crowded. Our data indicate that the cellular matrix interacts strongly with protein surfaces, and these interactions affect both the equilibrium thermodynamics and kinetics of folding. Although synthetic polymers are important in industrial

applications, these cosolutes are poor models of the cellular interior. These data also show that theories to explain protein behavior in cells must consider both the folded state and unfolded ensemble and must include terms for both hard-core repulsions and charge-charge interactions, but also hydrogen bonds, weakly polar interactions and hydrophobics. Recent modifications to theory,[159] as well as simulations of intracellular dynamics are pointing the way.[73] Most importantly, our data show that studying protein folding in living cells is key to gaining information needed to understand the role of proteins in biology.

Methods

Protein expression for in-cell NMR

Plasmids harboring the gene encoding the *N*-terminal SH3 domain of *drk* (SH3) were transformed into Agilent BL21 DE3 Gold cells by heat-shock. A single colony was used to inoculate a 5 mL culture of Lennox broth (LB, 10 g/L tryptone, 5 g/L yeast extract, 5 g/L NaCl) supplemented with 100 µg/mL ampicillin. The culture was incubated with shaking at 37 °C (New Brunswick Scientific Innova I26, 225 rpm). After 8 h, 50 µL of the saturated culture was used to inoculate 50 mL of supplemented M9 media (50 mM Na_2HPO_4, 20 mM KH_2PO_4, 9 mM NaCl, 4 g/L glucose, 1 g/L NH_4Cl, 0.1 mM $CaCl_2$, 2 mM $MgSO_4$, 10 mg/L thiamine, 10 mg/L biotin, and 150 mg/L ampicillin, pH 7.4).

The 50 mL culture was shaken at 37 °C overnight. The culture was then diluted to 100 mL with supplemented M9 media. 5-Fluoroindole (in dimethylsulfoxide) was added to a final concentration of 0.1 g/L, and the culture

was shaken for 30 min. Isopropyl β-D-1-thiogalactopyranoside (IPTG, 1 mM final concentration) was used to induce expression. After 45 min, cells were pelleted at 1000*g* and resuspended in M9 media without 5-fluoroindole, and expression was again induced to ensure efficient incorporation of the label. After 45 min, the cells were pelleted at 1000*g* and washed three times with in-cell NMR buffer (200 mM HEPES, 100 mM bis-tris propane, 50 µg/mL chloramphenicol, 150 µg/mL ampicillin, pH ~7.6. Chloramphenicol was used to halt protein expression prior to NMR. Cell pellets were resuspended in 300 µL of in-cell NMR buffer and loaded into a standard 5 mm NMR tube. Typical cell slurries were 50% wet cells by volume.

Protein expression for purification

Transformation and growth were performed as described in the first paragraph of the previous section.

The 50 mL cultures were shaken at 37 °C overnight, diluted to 1 L with supplemented M9 media and shaken until the optical density at 600 nm reached 0.6. 5-Fluoroindole was added (0.1 g/L final concentration) and the culture shaken for an additional 30 min. IPTG (1 mM final concentration) was used to induce expression. After 1 h, cells were pelleted at 1000*g* at 10 ^{o}C for 30 min, resuspended in 50 mM Tris-HCl (pH 7.5) and frozen at -80 °C.

Protease inhibitors (Sigma-Aldrich P-2714, containing AEBSF, aprotinin, bestatin, E-64, EDTA and leupeptin, refer to Methods Chapter 2 for concentrations) were added before lysis. Cells were lysed by sonication (Fisher

Scientific Sonic Dismembrator Model 500, 15% amplitude, 15 min, 67% duty cycle) on ice. Cell debris was removed by centrifugation at 16000*g* at 10 ^{o}C for 30 min, and the sample was passed through a 0.45 µm filter. Purification involved two chromatography steps using a GE AKTA FPLC. The first step was anion exchange (20 mL GE Q column, 5-45% gradient over 4 column volumes, 50 mM Tris-HCl wash buffer, 50 mM Tris-HCl/1 M NaCl eluant buffer, pH 7.5). SH3 binds weakly to anion exchange media. Protease inhibitors were added to the SH3-containing fractions, and the sample was passed through a 0.22 µm filter. The second step was size exclusion chromatography (GE Superdex 75 column eluted with 50 mM K_2HPO_4, 150 mM NaCl, 1 mM EDTA, pH 7.2, 0.5 ml/min flow rate). Purified protein was dialyzed against 4 L, 17 MΩ cm^{-1} H_2O for 4 h at room temperature and/or overnight at 5 °C. Buffer was changed every 1.5 to 2 h. After dialysis and filtration through a 0.22 µm filter, the sample was flash frozen in a dry-ice/ethanol bath and lyophilized for 12 h (Labconco FreeZone). Purity was asses via SDS-PAGE.

NMR

In-cell samples were prepared as described above. For *in vitro* experiments, purified ^{19}F-labeled protein was added to NMR buffer (50 mM acetic acid/sodium acetate, HEPES, bis-tris propane, pH 7.2). One experiment used NMR buffer plus 150 mM NaCl, to assess salt dependence. ^{19}F-spectra were acquired at 4 °C (5 °C for in-cell experiments), 10 °C, 15 °C, 20 °C, 25 °C, 30 °C, 35 °C, 40 °C, and 45 °C with a Bruker Avance III HD spectrometer operating at a ^{19}F Larmor frequency of 470 MHz running Topspin Version 3.2 and equipped

with a Bruker QCI cryoprobe. The temperature was calibrated with a two point standard curve using deuterated methanol. The total relaxation delay for one-dimensional experiments was 5 s. The sweep width was 70 ppm. The number of scans depended on cosolute and ranged from 32 to 256.

Carr-Purcell-Meiboom-Gill (CPMG)-based spin-spin relaxation time (T_2) measurements used mixing times (t_{mix}) of 1.0, 2.1,4.2, 6.3, 8.4, 16.8, 33.5, and 67.0 ms. A 955 Hz effective field was used to negate effects of chemical exchange. The transmitter was placed on-resonance to prevent ineffective refocusing. Spin-lattice relaxation times (T_1) were measured using an inversion recovery sequence (t_{mix}: 0, 0.05, 0.10, 0.25, 0.50, 0.80, 1.00 and 1.50 s). A Bruker library NOESY experiment (t_{mix}: 1.5, 50, 90, 150, 225, 300, 600 and 1000 ms for buffer and 1.5, 70, 140, 210, 300, 500, and 800 ms for crowded samples) with a 2 s relaxation delay was used to measure folding/unfolding rates. Sweep widths were 70 ppm in both dimensions. 1024 complex points were collected during t_2 with 64 complex points in t_1 at each t_{mix}. Sixteen transients were acquired per increment.

The SH3 domain is degraded in cells in a few hours, but T_1 and T_2 measurements require ~5 h. Therefore, T_2 measured in cells used a 0.002 s constant time period and a 1000 Hz effective field.

^{19}F-spectra were acquired before and after the relaxation and exchange experiments to assess sample integrity and reversibility. Populations of the folded and unfolded states remained constant, or the dataset was discarded. For

the in-cell samples, the cell slurry was removed after the experiment and gently pelleted. The supernatant was diluted two-fold. The cells were resuspended in 0.4 mL of in-cell NMR buffer plus protease inhibitors, lysed by sonication and clarified at 16000*g*. ^{19}F spectra were acquired on the supernatant to assess protein leakage and on the lysates to assess the effect of lysates on stability. No leakage was observed. A labeled metabolite that leaks from the cells overlaps with the peak corresponding to the unfolded ensemble. Integrals from the ^{19}F spectrum of the supernatant were subtracted from the in-cell integrals.

Resonances were referenced to trifluoroacetic acid (0.1%) in D_2O placed in a coaxial insert inside the NMR tube. The D_2O also served to lock the spectrometer.

Data processing

Data were processed with Topspin 3.2. For temperature variation experiments, free induction decays (fids, 50k points each) were subjected to a 10 to 15 Hz broadening function before zero filling (to 131,000 points) and Fourier transformation. For T_1 and T_2 experiments, fids (50k points) were subjected to a 10- to 15-Hz broadening function before zero-filling to 131k points. For exchange spectroscopy, t_2 data (1024 complex points) were subjected to a cosine squared bell function before zero filling to 4096 points. t_1 data were linear predicted to 256 points before application of a cosine squared bell function. Subsequent zero filling to 512 points and Fourier transform yielded the final spectra.

Resonance intensities were extracted for relaxation experiments. For temperature variation experiments, peaks were integrated. Peak volumes were fitted as described. Published assignments were used.[149]

^{19}F T_1 ($1/R_1$) and T_2 ($1/R_2$) data were fit using Model Free formalism to calculate rotational correlation times (τ_m).[160,161] The internal correlation time (τ_e) and the order parameter (S^2) were set to 20 ps and 0.82 for the folded state and 1200 ps and 0.34 for the unfolded state.[156] Chemical shift anisotropy and asymmetry terms were set to -93.5 ppm and 0.24.[162] No µs-ms motion was observed in buffer, and a 950 Hz effective field was used for the R_2 measurements. Therefore, chemical exchange was not included in fitting. The average ^{19}F-^{1}H distances (r) and τ_m were then minimized based on fitting the R_1 and R_2 data.

Analysis of uncertainties

Triplicate datasets, using three different batches of purified protein, were acquired for the pH 7.2 buffer dataset. The sample standard deviations depended on temperature (±52 cal/mol, ±45 cal/mol, ±59 cal/mol, ±31 cal/mol, ±31 cal/mol, ±66 cal/mol, ±61 cal/mol, ±14 cal/mol, ±35 cal/mol at 4 °C, 10 °C, 15 °C, 20 °C, 25 °C, 30 °C, 35 °C, 40 °C, and 45 °C, respectively). For buffer, we used these standard deviations to drive Monte Carlo error analysis. One-thousand randomly-generated datasets were fitted to the integrated Gibbs-Helmholtz equation at T_{ref} (Appendix 2). To extrapolate $\Delta H^{\circ}_{U,T_{ref}}$ and $\Delta S^{\circ}_{U,T_{ref}}$, and their uncertainties, to 298 K, the average and sample standard deviations of

$\Delta H^{\circ\prime}_{U,T_{ref}}$, T_{ref} and $\Delta C^{\circ}_{p,U}$ from this analysis were used to drive another Monte Carlo analysis (N=10^6) using Kirchoff's relations (Appendix 3). The uncertainties in $\Delta H^{\circ}_{U,298\ K}$ and $\Delta S^{\circ}_{U,298\ K}$ are larger than the uncertainty in $\Delta G^{\circ\prime}_{U,298\ K}$ because the enthalpy and entropy changes are derived from for three variables ($\Delta H^{\circ\prime}_{U,T_{ref}}$, T_{ref} and $\Delta C^{\circ}_{p,U}$) and their uncertainties.

For the in-cell data, a similar method was used. Triplicate data were obtained for the 10 °C, 25 °C and 40 °C datasets. For the other datasets uncertainties from the nearest-neighbor triplicate dataset were used to drive the analysis. For example, the 5 °C and 15 °C used the uncertainty associated with the 10 °C dataset.

For *in-vitro* experiments in the presence of crowders, triplicate 25 °C data were acquired on the same sample. This uncertainty was scaled as described in the first paragraph of this section and used to drive the Monte Carlo analysis.

For *in vitro* relaxation-rates, one mixing time was acquired three times. The sample standard deviation was used to drive Monte Carlo analysis (N=1000) to obtain R_1 and R_2 (Appendix 4, 5). The mean and standard deviations from this analysis were used to drive another Monte Carlo (N=1000) using the Model Free approach to obtain r, τ_m and their uncertainties (Appendix 6). Fitted r values varied from 1.8 to 2.1 Å for the folded state and 2.0 to 2.4 Å for the unfolded state. For fitting in-cell R_2, r was varied between these ranges, and τ_m was then fitted using only R_2. The uncertainty in τ_m is the range of values from these fits.

Folding rate data in buffer were acquired in triplicate and fitted as described (Appendix 7).[163] The uncertainty is the sample standard deviation. For *in vitro* folding-rates, one mixing time was acquired three times. The sample standard deviation was used to drive Monte Carlo analysis (N=100). For folding rates, R_1 was fixed to the value acquired from inversion recovery experiments for *in vitro* crowded conditions.

In-cell pH

Purified protein was resuspended in 50 mM citrate, 50 mM bis-tris propane, 50 mM HEPES, 50 mM borate, 5% D_2O, 0.1% DSS (pH values: 5.0, 5.8, 6.5, 6.9, and 7.5). Data were acquired from 10 to 40 °C in 5 °C increments. The difference in the ^{19}F chemical shifts between the two states is sensitive to pH (Supplementary Figure 4.1). These experiments were combined with two NMR buffer experiments [50 mM acetate, 50 mM HEPES, 50 mM bis-tris at pH 7.2 (with and without 0.15 M NaCl)] to assess salt effects, which were minimal. Shift change as a function pH was fitted to a second order polynomial to produce a standard curve. Shift differences from in-cell data sets were then compared to this standard curve to obtain the pH in cells. The values in cells, pH 7.2, compare favorably to the external meter reading minus 0.4 pH units, as previously described by us and others.[5,54]

Supplementary Information for Chapter 4

Supplementary Table 4.1. Equilibrium thermodynamic parameters.

Condition[a]	From Monte Carlo analysis[b]			
	$\Delta H^{\circ\prime}_{U,T_m \text{ or } T_s}$ (kcal/mol)[c]	$\Delta C^{\circ\prime}_{p,U}$ (kcal/mol/K)	T_m (K)	T_s (K)
pH 7.2 ± 0.1				
Buffer	20.0 ± 0.8	0.87 ± 0.06	309.2 ± 0.3	NA[d]
Cells (-Supernatant)	9 ± 1	0.6 ± 0.1	299 ± 1	NA
100 g/L urea	-0.640 ± 0.03	1.00 ± 0.09	No T_m	290 ± 1
50 g/L TMAO	23 ± 1	0.70 ± 0.06	316.3 ± 0.4	NA
200 g/L ethylene glycol	31 ± 2	1.1 ± 0.1	313.0 ± 0.4	NA
200 g/L 8K PEG	29.4 ± 0.7	1.07 ± 0.05	311.1 ± 0.2	NA
200 g/L 35K PEG	27.8 ± 0.5	0.89 ± 0.04	311.7 ± 0.2	NA
300 g/L glucose	1.39 ± 0.09	0.5 ± 0.2	>320	294 ± 10
300 g/L 20K dextran	1.22 ± 0.03	0.91 ± 0.09	>320	294 ± 1
300 g/L sucrose	1.68 ± 0.07	1.0 ± 0.2	>320	291 ± 2
300 g/L 70K Ficoll	24 ± 1	0.83 ± 0.07	315.3 ± 0.3	NA
100 g/L BSA	21 ± 1	0.83 ± 0.08	311.0 ± 0.4	NA
200 g/L BSA	21 ± 2	0.8 ± 0.1	310.0 ± 0.6	NA
100 g/L lysozyme[e]	-0.170 ± 0.01	0.99 ± 0.04	No T_m	NA
pH 5.4 ± 0.1				
Buffer	20 ± 2	0.7 ± 0.1	316.2 ± 0.9	NA
100 g/L BSA[e]	20 ± 2	0.8 ± 0.1	314.4 ± 0.7	NA
100 g/L lysozyme	8.2 ± 0.6	0.77 ± 0.05	299.6 ± 0.7	NA
pH 3.0 ± 0.1				
Buffer	23 ± 2	0.7 ± 0.1	312.9 ± 0.8	NA
100 g/L lysozyme	19.1 ± 0.3	0.88 ± 0.02	306.7 ± 0.1	NA

Footnotes

[a] Abbreviations: TMAO, trimethylamine-N-oxide; PEG, polyethylene glycol; BSA, bovine serum albumin.

[b] See “Analysis of uncertainty”.

[c] Enthalpy of unfolding at T_m or T_s. T_s is used when T_m cannot be defined. T_s is used for sugars and sugar based polymers because T_m is outside the range of temperatures where data could be acquired.

[d] NA, not applicable.

[e] Uncertainty used to drive the Monte Carlo analysis is the range from two independent trials.

Supplementary Table 4.2. Thermodynamic parameters and linewidths at 298K.

Condition[a]	Raw Data			Error Propagation[c] (kcal/mol)	
	$\Delta G^{\circ\prime}_{U.298\ K}$ (kcal/mol)	Linewidth[b] (Hz)			
		Folded	Unfolded	$\Delta H^{\circ\prime}_{U,298\ K}$	$T\Delta S^{\circ\prime}_{U,298\ K}$
pH 7.2 ± 0.1					
Buffer	0.53 ± 0.03	29 (34)[d] ± 1	29 (30)[d] ± 1	10 ± 1	10 ± 1
Cells (-Supernatant)	0.03 ± 0.05	120 ± 10	350 ± 80	8 ± 1	8 ± 1
100 g/L urea	-0.79 ± 0.06	31 ± 2	24 ± 1	7 ± 1	8 ± 1
50 g/L TMAO	0.92 ± 0.04	30 ± 1	28 ± 2	10 ± 2	9 ± 1
200 g/L ethylene glycol	1.14 ± 0.07	34 ± 1	29 ± 1	14 ± 3	13 ± 2
200 g/L 8K PEG	0.94 ± 0.02	44 ± 1	31 ± 1	15 ± 1	14 ± 1
200 g/L 35K PEG	0.98 ± 0.02	46 ± 1	36 ± 2	16 ± 1	15 ± 3
300 g/L glucose	1.38 ± 0.18	49 ± 1	NA[e]	4 ± 5	2 ± 6
300 g/L 20K dextran	1.19 ± 0.05	66 ± 2	56 ± 3	5 ± 1	4 ± 1
300 g/L sucrose	1.52 ± 0.12	45 ± 1	NA	9 ± 2	7 ± 3
300 g/L 70K Ficoll	0.88 ± 0.04	56 ± 1	40 ± 1	10 ± 2	9 ± 2
100 g/L BSA	0.62 ± 0.05	34 ± 1	39 ± 1	10 ± 1	10 ± 1
200 g/L BSA	0.55 ± 0.07	59 ± 1	117 ± 15	11 ± 2	11 ± 2
100 g/L lysozyme[f]	-0.39 ± 0.01	86 (66)[d] ± 1	71 (63)[d] ± 1	11 ± 1	11 ± 1
pH 5.4 ± 0.1					
Buffer	0.74 ± 0.08	30 ± 1	27 ± 1	7 ± 3	6 ± 3
100 g/L BSA[f]	0.72 ± 0.07	36 ± 1	50 ± 4	7 ± 3	6 ± 3
100 g/L lysozyme	-0.02 ± 0.03	55 ± 3	49 ± 1	7 ± 1	7 ± 1
pH 3.0 ± 0.1					
Buffer	0.80 ± 0.05	31 ± 1	31 ± 2	13 ± 3	12 ± 2
100 g/L lysozyme	0.41 ± 0.01	33 ± 1	34 ± 2	11 ± 1	11 ± 1

Footnotes

[a] See Footnote in Supplementary Table 4.1 for abbreviations.

[b] Errors less than 1 Hz were set to 1 Hz.

[c] See “Analysis of uncertainty”.

[d] Plus 0.15 M NaCl. Uncertainties were less than 5 Hz.

[e] NA, not applicable. Unfolded peak is too small for simulation to converge.

[f] The uncertainly is the range of two trials.

Supplementary Table 4.3. Change in thermodynamic parameters at 298 K. Green shading indicates significant stabilization (i.e., >0 uncertainty). Red shading indicates significant destabilization. For other entries, the uncertainties are too large to permit classification.

Condition[a]	$\Delta\Delta G^{\circ\prime}_{U,298\ K}$ (kcal/mol)	$\Delta\Delta H^{\circ\prime}_{U,298\ K}$ (kcal/mol)	$T\Delta\Delta S^{\circ\prime}_{U,298\ K}$ (kcal/mol)
pH 7.2 ± 0.1			
Cells (- Supernatant)	-0.50 ± 0.06	-2 ± 1	-2 ± 1
100 g/L urea	-1.32 ± 0.07	-3 ± 1	-2 ± 1
50 g/L TMAO	0.39 ± 0.05	0 ± 2	-1 ± 1
200 g/L ethylene glycol	0.61 ± 0.08	4 ± 3	3 ± 2
200 g/L 8K PEG	0.41 ± 0.04	5 ± 1	4 ± 1
200 g/L 35K PEG	0.45 ± 0.04	6 ± 1	5 ± 3
300 g/L glucose	0.85 ± 0.18	-6 ± 5	-8 ± 6
300 g/L 20K dextran	0.66 ± 0.06	-5 ± 1	-6 ± 1
300 g/L sucrose	0.99 ± 0.12	-1 ± 2	-3 ± 3
300 g/L 70K Ficoll	0.35 ± 0.05	0 ± 2	-1 ± 2
100 g/L BSA	0.09 ± 0.06	0 ± 1	0 ± 1
100 g/L lysozyme[b]	-0.92 ± 0.03	1 ± 1	1 ± 1
pH 5.4 ± 0.1			
100 g/L BSA[b]	-0.02 ± 0.11	0 ± 3	0 ± 4
100 g/L lysozyme	-0.76 ± 0.09	0 ± 3	1 ± 3
pH 3.0 ± 0.1			
100 g/L lysozyme	-0.39 ± 0.05	-2 ± 3	-1 ± 2

Footnotes

[a] See Footnote in Supplementary Table 4.1 for abbreviations.

[b] The uncertainly is the range of two trials.

Supplementary Table 4.4. Relaxation rates and correlation times (298 K, pH 7.2 ± 0.1).

	Folded				Unfolded			
Condition[a]	R_1 (s^{-1})	R_2 (s^{-1})	r (Å)	τ_m (ns)	R_1 (s^{-1})	R_2 (s^{-1})	r (Å)	τ_m (ns)
Buffer	2.5 ± 0.1	30 ± 2	1.93 ± 0.02	3.9 ± 0.2	2.0 ± 0.2	13.6 ± 0.3	2.09 ± 0.07	2.9 ± 0.2
Cells	NA[b]	440	set	60 ± 10	NA	560	set	210 ± 20
300 g/L 70K Ficoll	1.53 ± 0.09	113 ± 4	1.93 ± 0.02	15.3 ± 0.5	1.4 ± 0.2	42 ± 2	2.2 ± 0.1	13.4 ± 0.8
100 g/L urea	1.8 ± 0.2	28 ± 2	2.06 ± 0.05	4.0 ± 0.3	1.49 ± 0.06	11.3 ± 0.1	2.34 ± 0.04	2.5 ± 0.1
100 g/L lysozyme	1.46 ± 0.08	165 ± 27	1.86 ± 0.04	21 ± 3	1.37 ± 0.05	110 ± 8	2.10 ± 0.02	37 ± 3

Footnotes

[a] See “Analysis of uncertainty”. The cellular viscosity is thought to be 2-4 times that of water.[150] 300 g/L Ficoll is ~24 times water and 100 g/L lysozyme is ~1.3 times water.[42]

[b] NA, not applicable. R_1 could not be obtained in cells due to degradation.

Supplementary Table 4.5. Folding rates (s^{-1}) at 298 K, pH 7.2 ± 0.1.

Condition[a]	k_f	k_u
Buffer	2.5 ± 0.3	1.1 ± 0.1
300 g/L 70K	0.8 ± 0.4	0.3 ± 0.1
100 g/L urea	0.4 ± 0.2	2.7 ± 0.5
100 g/L	0.5 ± 0.4	1.1 ± 0.5

Footnotes

[a]See “Analysis of uncertainty”.

Supplementary Table 4.6. Chemical shift upfield from trifluoroacetic acid at 298 K.

Condition[a]	Folded (ppm)	Unfolded (ppm)	Δω (Hz)
pH 7.2 ± 0.1			
Buffer	48.23 (48.17)[b]	49.21 (49.24)[b]	461 (489)
Cells	48.21	49.18	456
100 g/L urea	48.14	49.21	503
50 g/L TMAO	48.20	49.19	465
200 g/L ethylene glycol	48.53	49.37	395
200 g/L 8K PEG	48.33	49.26	437
200 g/L 35K PEG	48.32	49.26	442
300 g/L glucose	48.53	49.18	306
300 g/L 20K dextran	48.42	49.23	381
300 g/L sucrose	48.48	49.25	362
300 g/L 70K Ficoll	48.38	49.22	395
100 g/L BSA	48.24	49.23	465
200 g/L BSA	48.23	49.26	484
100 g/L lysozyme	48.21 (48.19)	49.14 (49.14)	437
pH 5.4 ± 0.1			
Buffer	48.78	49.20	197
100 g/L BSA	48.74	49.21	221
100 g/L lysozyme	48.68	49.13	212
pH 3.0 ± 0.1			
Buffer	48.81	49.37	263
100 g/L lysozyme	48.80	49.35	259

Footnotes

[a] See Footnote in Supplementary Table 4.1 for abbreviations.

[b] Plus 0.15 M NaCl

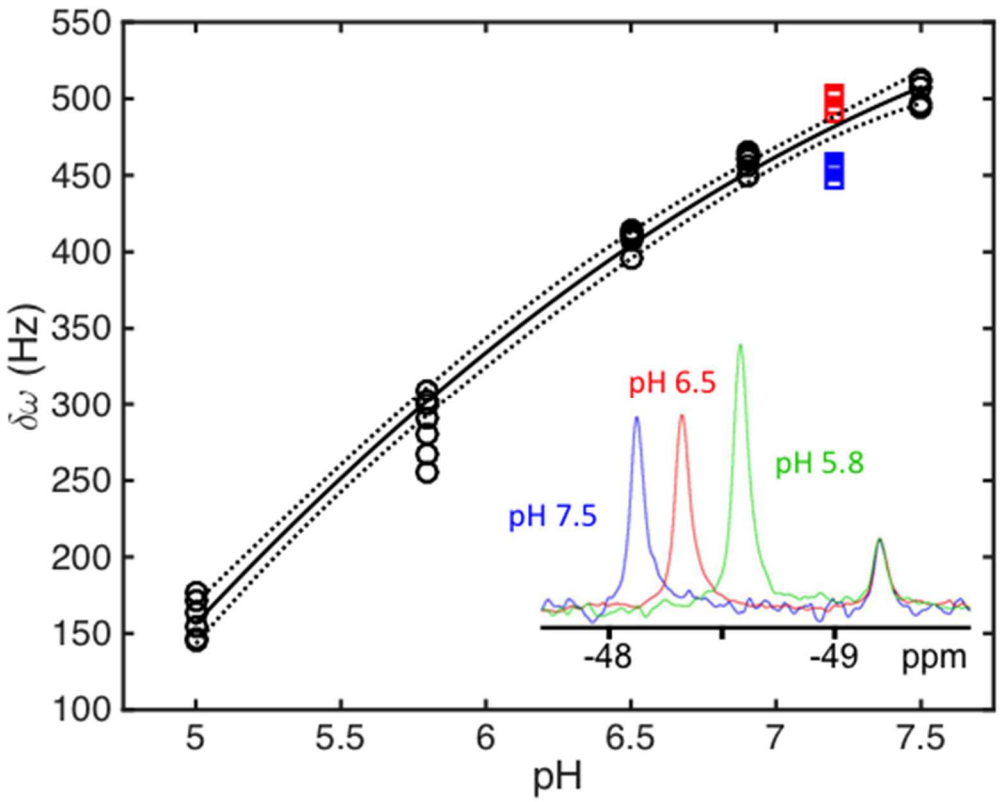

Supplementary Figure 4.1. Chemical shift between the folded and unfolded peaks (δω) is pH dependent. Black circles, δω in buffer at various pH values (see Methods). Squares, δω in NMR buffer with (red) and without (blue) 150 mM NaCl. Data were fitted to a second-order polynomial ($\delta\omega=-24.77\times pH^2+449.9\times pH-1474$). The 95% confidence interval is shown by the dotted curve. The inset shows ^{19}F spectra at pH 7.5, 6.5 and 5.8 at 298 K. The spectra were normalized to the position and intensity of the unfolded ensemble at pH 7.5.

APPENDIX 1. INTERLEAVED SOLEXSY PULSE CODE WITH SIGN CODING REMOVED.

```
;SOLEXSY
;Bruker pp to measure 1H/2H exchange as described in
;Chevelkov, et. al., JBNMR, 2010
;based on H(CACO)NH
;F1(H) -> F2(Ca) -> F2(C=O) -> F3(N,t1) ->  F1(H,t2)
;on/off resonance Ca and C=O pulses using shaped pulse
;phase sensitive (t1)
;phase sensitive using TPPI (t2)
;$CLASS=HighRes
;$DIM=3D

;edits made by Austin E. Smith, UNC Chapel Hill
;Avance-III HD, Topspin 3.2, prosol compliant
;Removed sign coding for proteins with good peak dispersion or short T2
;INTERLEAVED, set td1 = # in VDLIST

prosol relations=<triple>

#include <Avance.incl>
#include <Grad.incl>
#include <Delay.incl>

;; AES Pulse Linkages, just set p21 and p1
;; unlink if necessary
"p22=p21*2"    ;;15N 180 links to 90
"p2=p1*2"      ;;1H 180 links to 90
"p27=p1"       ;;watergate pulses
"p0=p1"        ;;watergate final pulse
"p19=800u"     ;;purge grad in mix

;;AES linkages for 15N incrementation
"in0=(inf2/4)/(1+cnst0)"
"in29=(in0*cnst0)"
"in30=(in0*cnst0)"

"cnst5=d30/in30"          ;; Max number of increments
"cnst6=d30-(td2*in30)"  ;;Time remaining in constant time period

;;Delays
"d0=4u"
"d4=1/(4*cnst1)"  ;;1/(4*JCaH) ~1.8 ms
"d11=30m"
"d12=20u"
```

```
"d16=183u"
"d21=d4*2"          ;; CA-H 2*inept time exact
"d22=1/(4*cnst2)"  ;;1/(4*JCaCO) ~4.5 ms
"d23=1/(4*cnst3)"  ;;1/(4*JCON) ~16.7 ms
"d24=1/(4*cnst4)"  ;;1/(4*JNH) ~2.5ms
"d25=d22*2"         ;; CA-CO 2*inept time exact
"d27=d23-d25"
"d29=4u"
"d30=d23"

"DELTA1=d22-d21-p14-4u"
"DELTA2=d22-p14-4u"
"DELTA6=d24-p16-d16-p27*3-d19*5"
"DELTA7=d19-p22/2"
"DELTA8=d24-p16-d16-p27*2-p0-d19*5-4u"

define list<delay> exchange=<$VDLIST>

;;Offsets
"spoff2=0"    ;; p90 on CA to XY
"spoff3=0"
"spoff5=bf2*((cnst21-cnst22)/1000000)"  ;; to move bf2 from CA to CO
"spoff8=0"
"spoff9=0"
"spoff13=bf2*((cnst26-cnst21)/1000000)" ;; move bf2 to midle when on CO
"spoff7=-bf2*((cnst21-cnst22)/1000000)"  ;; bf2 on CA from CO

aqseq 312

1 d11 ze
  d11 LOCKDEC_ON
  d11 LOCKH_ON
  d11 H2_PULSE
  d11 pl17:f4
  d11 pl16:f3

2 d11 do:f3
  5u pl3:f3
  2u pl2:f2

  "DELTA=exchange"

3 d11 H2_LOCK
  10m LOCKH_OFF
  d1 pl1:f1 fq=cnst22(bf ppm):f2
  50u LOCKH_ON
```

```
  d12 H2_PULSE
  d11 UNBLKGRAMP
  d11

  (p3 ph11):f2
  p19:gp2
  d16

;; Ha to Ca

  (p1 ph11)
  d4
  (center (p2 ph2) (p14:sp3 ph1):f2 )
  d4
  (p1 ph2)
  p16:gp3
  d16

;; transfer from Ca to 15N

  (p13:sp2 ph12):f2          ;; CA p90 to Y
  d21 pl19:f1
  DELTA1 cpds1:f1 ph2
  (p14:sp5 ph1):f2           ;; CO p180 of res.
  4u
  (p24:sp9 ph4):f2           ;; CA p180 on res.
  DELTA2
  (p14:sp5 ph1):f2           ;; CO p180 of res.  refocuss
  4u
  (p13:sp8 ph1):f2           ;; CA p90
  15u fq=cnst21(bf ppm):f2   ;; CO chemshift
  15u
  (p13:sp2 ph13):f2          ;; CO p90
  4u
  (p14:sp7 ph1):f2           ;; CA p180 refocus
  d25                        ;; CA-CO transfer
  d27                        ;; CA-CO transfer
  (center (p14:sp3 ph1):f2 (p22 ph1):f3 )
  d27
  d22
  (p14:sp7 ph1):f2           ;; CA p180 of res.
  d22
  (p13:sp8 ph3):f2           ;; CO p90 to Z
  4u do:f1

;; t1 encode using semiconstant time evolution
```

```
  4u cpds4:f4
  (p21 ph5):f3                ;; N p90 to Y: COzNy
  4u
  d30 pl1:f1                  ;; td - kappa*t1/2
  (center (p14:sp3 ph1):f2 (p22 ph1):f3 )
  4u
  d23                         ;; td
  (center (p14:sp7 ph1):f2 (p2 ph10):f1 )   ;; CA p180 refocus
  d29                         ;; kappa*t1/2
  d0                          ;; t1/2
  (center (p8:sp13 ph4):f2 (p2 ph1):f1 )
  d0                          ;; t1/2
  (p22 ph1):f3
  4u
  (center (p8:sp13 ph4):f2 (p2 ph1):f1  )
  4u
  (center (p14:sp7 ph1):f2 (p2 ph10):f1 )
  4u

  (p21 ph18):f3               ;; 15N to Z from Nx
  4u do:f4

;; EXCHANGE (tmix)

  DELTA
  (p1 ph1):f1                 ;; H2O saturation/purge
  4u
  p19:gp3
  d16

;; Rev INEPT

  (p21 ph15):f3               ;; 15N to Y for Inept
  d24
  (center (p2 ph1) (p22 ph1):f3 )
  d24
  (p21 ph2):f3                ;; 15N along Z
  4u
  p16:gp3
  d16

;; WATERGATE

  (p1 ph2)
  DELTA6  ;;;; d24-p16-d16-p27*3-d19*5
```

```
  p16:gp4
  d16 pl18:f1
  p27*0.231 ph16
  d19*2
  p27*0.692 ph16
  d19*2
  p27*1.462 ph16
  DELTA7   ;;d19-p22
  (p22 ph1):f3
  DELTA7
  p27*1.462 ph17
  d19*2
  p27*0.692 ph17
  d19*2
  p0*0.231 ph17
  4u
  p16:gp4
  d16
  DELTA8   ;; d24-p16-d16-p27*2-p0-d19*5-4u
  4u pl16:f3 BLKGRAMP

  go=2 ph31 cpd3:f3
  20u do:f3
  10m wr #0  if #0 zd

  20u exchange.inc
  lo to 2 times td1
  20u exchange.res

  20u ip18
  20u dd30
  20u id29
  20u id0
  lo to 2 times td2

  d11
  d11 H2_LOCK
  d11 LOCKH_OFF
  d11 LOCKDEC_OFF

exit

ph1=0
ph2=1
ph3=0
ph4=0
```

```
ph5=0
ph10=2
ph15=0 2          ;; 15N to Y for t1 and HN inept
ph11=0 0 2 2      ;; 1H excite
ph12=0 0 0 0  2 2 2 2  ;; CA to Y before  d21 - HzCAy refocusing
ph13=0 0 0 0  0 0 0 0  2 2 2 2  2 2 2 2  ;; CO to Y before  d25 - CAzCOy refocusing
ph16=2            ;; in wg 1st cycle
ph17=0            ;; in wg 2nd cycle
ph18=1            ;; for tppi p90 on 15N after t1


ph31=0 2 2 0  2 0 0 2  2 0 0 2  0 2 2 0


;pl1 : 1H, f1 hard pulse (default)
;pl2 : 13C, f2 hard pulse (default)
;pl3 : 15N, f3 hard pulse (default)
;pl16: 15N, CPD/BB decoupling
;pl17: 2H, CPD/BB decoupling
;pl19: 1H, f1 DIPSI for CPD/BB decoupling

;sp2 : 13C, f2 sel. p90=p13, on resonance
;sp3 : 13C, f2 sel. p180=p14, on resonance
;sp7 : 13C, f2 sel. p180=p14, for CA when its off resonance.
;sp5 : 13C, f2 sel. p180=p14, for C=O when its off resonance.
;sp8 : 13C, f2 sel. p90=p13, on resonance, time reversed CA
;     sp8 for time reversed Calpha pulses
;sp9 : 13C, f2 sel. p180=p24, on CA, CO and CB off resonance,
;     sp9 requires higher selectivity than sp3 (Ca only)
;sp13: 13C, f2 sel. p180, on Ca and C=O, adiabatic

;p0 : last p90 in Watergate
;p1 : 1H p90 degree high power
;p2 : 1H p180 degree high power
;p3 : 13C hard p90 for refocusing in beginning
;p8 : 13C sp180 Ca & CO, adiabatic for N Jdecoupling
;p13: f2 channel -  90 degree shaped pulse
;p14: f2 channel - 180 degree shaped pulse
;p16: homospoil/gradient pulse                    [1 msec]
;p19: short gradient
;p21: 15N p90 degree high power pulse
;p22: 15N p180 degree high power pulse
;p24: f2 channel - 180 degree shaped pulse (sp9)
;p27: Watergate 1H p90 pulse
;p28: weak H2O saturation pulse
```

```
;d0 : incremented delay (F1 in 2D)                    [3 usec]
;d1 : relaxation delay; 1-5 * T1
;d11: delay for disk I/O                              [30 msec]
;d12: delay for power switching
;d16: delay for homospoil/gradient recovery
;d19: delay for binomial water suppression d19 = (1/(2*d)), d = distance of next null
(in Hz)
;DELTA : 1H exchange delay
;d4 : CA-H inept time
;d21: CA-H 2*inept time exact
;d22: CA-CO inept time
;d23: CO-N inept
;d24: N-H inept
;d25: CA-CO 2*inept time exact

;cnst0: kappa in Chevelkov, et al. (0.235)
;cnst1: JCaH (~140 Hz) OPT
;cnst2: JCaCO (~55 Hz) OPT
;cnst3: JCON (~15 Hz) OPT
;cnst4: JNH (~95 Hz) OPT
;cnst5: Max Increments!!
;cnst6: Time remaining for last increment of d30
;cnst21: CO chemical shift (offset, in ppm) (~180 ppm)
;cnst22: Calpha chemical shift (offset, in ppm) (~55 ppm)
;cnst26: Call chemical shift (offset, in ppm) (~100 ppm)
;o2p: Calpha chemical shift (cnst22)

;NS: 8 * n
;DS: >32
;td1: number of delays
;td2: number of 15N increments
;FnMODE: TPPI in F2
;FnMODE: echo-antiecho in F3 (DQD)
;cpds1: decoupling according to sequence defined by cpdprg1
;cpd2: decoupling according to sequence defined by cpdprg2
;pcpd1: f1 channel - 90 degree pulse for decoupling sequence
;pcpd2: f2 channel - 90 degree pulse for decoupling sequence

;for z-only gradients:
;gpz2: 60.1% 13C def. in beginning
;gpz3: 40%
;gpz4: 60%

;use gradient files:
;gpnam2: SINE.100
;gpnam3: SINE.100
```

;gpnam4: SINE.100

;$Id: hcacongp3d,v 1.4 2007/04/11 13:34:29 ber Exp $

APPENDIX 2. MONTE CARLO FOR FITTING IN-CELL DATA TO THE INTEGRATED FORM OF THE GIBBS-HELMHOLTZ EQUATION.

```
clear all
close all

tempfull = [277.15;283.15;288.15;293.15;298.15;303.15;308.15;313.15;318.15];
tempIC =[278.15;283.15;288.15;293.15;298.15;303.15;308.15;313.15];
nsamples = 1000; %number of simulations

fileID = fopen('CellDataTg.dat','w'); %naming the data file
formatSpec = '%d %d %d\n'; %this defines the format of the data file

%DATA
%Buffer:50 mM acetate, bis-tris propane, HEPES
DILUTE = [568;713;690;668;532;340;78;-265;-705]; %Average of all 5-45
DILERR = [30;26;34;18;18;38;35;8;20]; % These are the standard deviation of the
mean

Raw = [175;359;103;192;29;-151;-276;-604]; % Insert Raw data here
Err = [NaN;84;NaN;NaN;52;NaN;NaN;74]; %STD
Covar = [84^2 84^2 84^2 52^2 52^2 52^2 74^2 74^2]; %if NaN, used the closest
triplicate data. Covar is STD^2

MC = mvnrnd(Raw,Covar,nsamples); % Uses covariance... square the STD
std(MC) % You can use this as a check to make sure the sigma generated by the
MC is correct

%FIT DATA
Ts = fittype('dH+dCp*((x-Ts)-
(x*log(x/Ts)))','independent',{'x'},'coefficients',{'dH','dCp','Ts'}); % Declaring the fit: a
is dH (1000), b is dCp (900), t is Ts (290)
TsCp = fittype('dH+920*((x-Ts)-
(x*log(x/Ts)))','independent',{'x'},'coefficients',{'dH','Ts'}); % Holding dCp constant
Tg = fittype('dH-(T*(dH/Tg))+dCp*(T-(Tg)-
(T*log(T/(Tg))))','independent',{'T'},'coefficients',{'dH','dCp','Tg'}); % Declaring the fit:
a is dH (20000), b is dCp (900), t is Ts (50)

[fit1,gof1] = fit(tempfull,DILUTE,Tg,'startpoint',[20000,900,300],'algorithm','Trust-
Region','Robust','on'); % This does the fitting
[fit2,gof2] = fit(tempIC,Raw,Tg,'startpoint',[20000,900,300],'algorithm','Trust-
Region','Robust','on');

for i=[1:nsamples] % This will fit the data for however many simulations you choose
    DataMC = MC(i,:)'; % This reads the matrix row-by-row
    [fitx]=fit(tempIC,DataMC,Tg,'startpoint',[fit2.dH,fit2.dCp,fit2.Tg],'algorithm','Trust-
```

```
Region','Robust','on'); %Fits each row
    F= {fitx.dH,fitx.dCp,fitx.Tg}; %This pulls the data into a new 1 line file for writing.
fprintf(fileID,formatSpec,F{1,:}); %This writes the data to whatever you set the fileID
fprintf('%d ', i);
end %Then we loop back till i=nsamples
fclose(fileID);

errorbar(tempIC,Raw,Err,'ks','MarkerSize',12,'LineWidth',2);
hold on
o = plot(fit1,'black','predfunc');
set(o,'LineWidth',2);
v = plot(fit2,'red','predfunc');
set(v,'LineWidth',2);
xlabel('Temp (K)','fontsize', 20);
ylabel('\DeltaG_D\circ'' (kcal/mol)','fontsize',20);

fit1 % this gives the fits to the raw data
fit2

load CellDataTg.dat
mean(CellDataTg) % This gives the mean of the Monte Carlo simulation
std(CellDataTg) % and the error in the dataset
mean(CellDataTg([1:100],:))
std(CellDataTg([1:100],:))
```

APPENDIX 3. MONTE CARLO FOR EXTRAPOLATING DATA FROM THE GIBBS-HELMHOLTZ EQUATION TO ANY TEMPERATURE USING KIRCHOFF'S RELATIONS.

```
clear all
close all

temp = 298
nsamples=1e6

%random following gaussian, DILUTE
dH=normrnd(19.1,0.3,nsamples,1);
dCp=normrnd(0.88,0.02,nsamples,1);
T=normrnd(306.7,0.1,nsamples,1);

%generate data
H=dH+dCp.*(temp-T);
TdS= temp.*((dH./T)+dCp.*log(temp./T));
Ts1=exp(log(T)-((dH./T)./dCp));

%mean and STD of data
Enthalpy = mean(H)
STD = std(H)

Entropy = mean(TdS)
STD = std(TdS)

Ts = mean(Ts1)
STD = std(Ts1)
```

APPENDIX 4. T2 FITTING SCRIPT.

```
clear all
close all

%Script to Measure 19F T2 Rates
%Uses a Monte Carlo for error if you take one plane 3 times
% AES, 2015

%-----ENTER INFORMATION-----
d20 = 0.00025; %Insert echo time
p1 = 0.00001275; %Insert pulse length
cycles = [2;8;128;4;64;32;16;12]; % # of cycles

%Folded State
A=[89934,91251,90215]; %Insert 3 repeated delays
B=mean(A);
Folded = [102385;B;16083;96622;38777;61369;80235;85086];
sigmaF=std(A);
covarF=sigmaF^2; %MC uses covariance, which is standard deviation squared
CovarF = [covarF covarF covarF covarF covarF covarF covarF covarF]; % Make
sure this is the same size as cycles

%Unfolded State
C=[89841,89795,89109];
D=mean(C);
Unfolded = [94371;D;42550;94781;64204;78122;84680;89287];
sigmaU=std(C);
covarU=sigmaU^2;
CovarU = [covarU covarU covarU covarU covarU covarU covarU covarU];

%MC stuff, can name files whatever, but need to change below if you do
nsamples = 10;
fileIDF = fopen('Folded.dat','w');
fileIDU = fopen('Unfolded.dat','w');
formatSpec = '%d %d\n';

%Finds Field and Relaxation times
tCP = (d20*2) + (p1*2);
vCPMG = 1 / (2 * tCP)
time = tCP * cycles

%-----STARTS DATA ANALYSIS-----
T2fit = fittype('(A*exp(-x/T))','independent',{'x'},'coefficients',{'A','T'}); % Declaring the
fit: a is overall height, b is T1
T2cfit = fittype('(A*exp(-x/T)+C)','independent',{'x'},'coefficients',{'A','T','C'}); %
```

```
Declaring the fit: a is overall height, b is T1, c is variable

[fit1,gof1] = fit(time,Folded,T2fit,'startpoint',[max(Folded),0.005],'algorithm','Trust-
Region');
[fit2,gof2] =
fit(time,Unfolded,T2fit,'startpoint',[max(Unfolded),0.005],'algorithm','Trust-Region');
[fit3,gof3] = fit(time,Folded,T2cfit,'startpoint',[max(Folded),0.005,0],'algorithm','Trust-
Region');
[fit4,gof4] =
fit(time,Unfolded,T2cfit,'startpoint',[max(Unfolded),0.005,0],'algorithm','Trust-
Region');

%Values
%T2 = fit1.T;
R2F = 1/fit1.T
%gof1.rsquare;
%T2 = fit2.T;
R2U = 1/fit2.T
%gof2.rsquare;

%Plotting
plot(time,Folded,'rs','MarkerSize',10,'LineWidth',2);
hold on
plot(time,Unfolded,'bo','MarkerSize',10,'LineWidth',2);
plot(fit1,'black','predfunc');
hold on
plot(fit2,'black','predfunc');
hold on
plot(fit3,'green');
hold on
plot(fit4,'green');
legend('Folded','Unfolded','Location','Best');
hold off
title(['19F drkN SH3'],'fontsize',10);
xlabel('Time (s)','fontsize', 10);
ylabel('Intensity','fontsize',10);
hold off

%-----MONTE CARLO-----
%MC FOLDED State
fprintf('FOLDED\n');
MC = mvnrnd(Folded,CovarF,nsamples); %This generates the cycles*nsamples
matrix
sigmaF
std(MC) %Make sure this is equal to the std you put in
for i=[1:nsamples] % Loops and fits
```

```
    DataMC = MC(i,:)'; % reads row by row
    [fitx]=fit(time,DataMC,T2fit,'startpoint',[fit1.A,fit1.T],'algorithm','Trust-
Region','Robust','on');
    F= {fitx.A,1/fitx.T};
fprintf(fileIDF,formatSpec,F{1,:}); %prints to file
fprintf('%d ', i);
end
fclose(fileIDF);
fprintf('\n');
fprintf('\nFOLDED\n');
load Folded.dat
mean(Folded(:,2))
std(Folded(:,2))
mean(Folded([1:100],2))
std(Folded([1:100],2))

%MC UNFOLDED STATE
fprintf('UNFOLDED\n');
MC = mvnrnd(Unfolded,CovarU,nsamples); % Uses covariance... square the STD
sigmaU
std(MC)
for i=[1:nsamples]
    DataMC = MC(i,:)';
    [fitx]=fit(time,DataMC,T2fit,'startpoint',[fit2.A,fit2.T],'algorithm','Trust-
Region','Robust','on');
    F= {fitx.A,1/fitx.T};
fprintf(fileIDU,formatSpec,F{1,:});
fprintf('%d ', i);
end
fclose(fileIDU);
fprintf('\n');
fprintf('\nUUNFOLDED\n');
load Unfolded.dat
mean(Unfolded(:,2))
std(Unfolded(:,2))
mean(Unfolded([1:100],2))
std(Unfolded([1:100],2))
```

APPENDIX 5. T1 FITTING SCRIPT.

```
clear all
close all

time = [0
    0.8
    0.05
    0.1
    1.5
    0.5
    0.25]; %Input mixing time T1

%Folded State
A=[22416,19935,22194]; %Insert 3 repeated delays
B=mean(A);
Folded = [-43866;B;-35112;-27787;37217;3135;-15520];
sigmaF=std(A);
covarF=sigmaF^2; %MC uses covariance, which is standard deviation squared
CovarF = [covarF covarF covarF covarF covarF covarF covarF]; % Make sure this is
the same size as cycles

%Unfolded State
C=[33151,38388,34403];
D=mean(C);
Unfolded = [-83758;D;-75811;-60023;71491;4188;-33815];
sigmaU=std(C);
covarU=sigmaU^2;
CovarU = [covarU covarU covarU covarU covarU covarU covarU];

%MC stuff, can name files whatever, but need to change below if you do
nsamples = 1000;
fileIDF = fopen('Folded.dat','w');
fileIDU = fopen('Unfolded.dat','w');
formatSpec = '%d %d %d\n';

%-----STARTS DATA ANALYSIS-----
T1fit =fittype('M*(1-V*exp(-x/T))','independent',{'x'},'coefficients',{'M','T','V'}); %
Declaring the fit: M is Sz, T is T1, V is fudge factor

[fit1,gof1] = fit(time,Folded,T1fit,'startpoint',[max(Folded),0.05,1],'algorithm','Trust-
Region');
[fit2,gof2] =
fit(time,Unfolded,T1fit,'startpoint',[max(Unfolded),0.05,1],'algorithm','Trust-Region');

%Values
```

```
%T1 = fit1.T
R1F = 1/fit1.T
%gof1.rsquare;
%T1 = fit2.T
R1U = 1/fit2.T
%gof2.rsquare;

plot(time,Folded,'rs','MarkerSize',10,'LineWidth',2);
hold on
plot(time,Unfolded,'bo','MarkerSize',10,'LineWidth',2);
plot(fit1,'black');
hold on
plot(fit2,'black');
legend('Folded','Unfolded','Location','Best');
hold off
title(['19F drkN SH3'],'fontsize',10);
xlabel('Time (s)','fontsize', 10);
ylabel('Volume','fontsize',10);
%axis([0 1.6 -50000 50000]); % x- axis, y-axis
hold off

%-----MONTE CARLO-----
%MC FOLDED State
fprintf('FOLDED\n');
MC = mvnrnd(Folded,CovarF,nsamples); % Uses covariance... square the STD
std(MC);
for i=[1:nsamples]
    DataMC = MC(i,:)';
    [fitx]=fit(time,DataMC,T1fit,'startpoint',[fit1.M,fit1.T,fit1.V],'algorithm','Trust-
Region','Robust','on');
    F= {fitx.M,1/fitx.T,fitx.V};
fprintf(fileIDF,formatSpec,F{1,:});
fprintf('%d ', i);
end
fclose(fileIDF);
fprintf('\n');
fprintf('\nFOLDED\n');
load Folded.dat
mean(Folded(:,2))
std(Folded(:,2))
mean(Folded([1:100],2))
std(Folded([1:100],2))

%MC UNFOLDED STATE
fprintf('UNFOLDED\n');
MC = mvnrnd(Unfolded,CovarU,nsamples); % Uses covariance... square the STD
```

```
std(MC);
for i=[1:nsamples]
    DataMC = MC(i,:)';
    [fitx]=fit(time,DataMC,T1fit,'startpoint',[fit2.M,fit2.T,fit2.V],'algorithm','Trust-
Region','Robust','on');
    F= {fitx.M,1/fitx.T,fitx.V};
fprintf(fileIDU,formatSpec,F{1,:});
fprintf('%d ', i);
end
fclose(fileIDU);
fprintf('\n');
fprintf('\nUUNFOLDED\n');
load Unfolded.dat
mean(Unfolded(:,2))
std(Unfolded(:,2))
mean(Unfolded([1:100],2))
std(Unfolded([1:100],2))
```

APPENDIX 6.1. SCRIPT FOR FITTING T1 AND T2 DATA USING A MODEL FREE APPROACH TO OBTAIN TUMBLING TIMES.

Calls on Appendix 6.2 and 6.3, ensure they are in the same folder as 6.1.

```
clear all;
close all;

global R1F R2F  R1U R2U  % experimental R1
global calc_R1F calc_R2F calc_R1U calc_R2U   % obtained by simulations of R1
global err2 err3                % error
global r tm te S
global MCR1F MCR1U MCR2F MCR2U

nsamples = 1000;
fileIDF = fopen('Foldedtm.dat','w');
fileIDU = fopen('Unfoldedtm.dat','w');
formatSpec = '%d %d %d\n'; %

R1F=normrnd(1.46,0.08,nsamples,1);  % R1 Folded
R2F=normrnd(165,27,nsamples,1);  % R2 Folded
R1U=normrnd(1.37,0.05,nsamples,1);  % R1 unfolded
R2U=normrnd(110,8,nsamples,1);  % R2 unfolded

% ---------------- END OF INPUT -----------------
% --- FIT  ---
fprintf('\nFOLDED:\n')
for i=[1:nsamples]
   MCR1F = R1F(i,:);
   MCR2F = R2F(i,:);

r = 2.0;
tm = 5e-9;
te = 50e-12;
S = 0.9;

x0 = [r,tm];

minopt = optimset('TolX',1e-14,'TolFun',1e-14,'MaxFunEvals',1e10,'MaxIter',1e10);

x=fminsearch('F19_Folded_tc_equation_MC',x0,minopt);

Ans= {x(1),x(2),err2};
fprintf(fileIDF,formatSpec,Ans{1,:}); % prints to file
%fprintf('%d ', i);
end
```

```
load Foldedtm.dat;
fprintf('\nF-H distance (A) = ');
mean(Foldedtm(:,1))
std(Foldedtm(:,1))
fprintf('\nCorrelation time (ns) = ');
mean(Foldedtm(:,2))
std(Foldedtm(:,2))

fprintf('\nInternal motion (ps) = ');
fprintf('%d\n',20);
fprintf('Order parameter = ');
fprintf('%d\n',0.82);
fprintf('Error = ');
fprintf('%d\n', err2);
fprintf('\n')

fprintf('\nUNFOLDED:\n')
for i=[1:nsamples]
    MCR1U = R1U(i,:);
    MCR2U = R2U(i,:);

r = 2.0;
tm = 5e-9;
te = 50e-12;
S = 0.9;

x0 = [r,tm];

minopt = optimset('TolX',1e-14,'TolFun',1e-14,'MaxFunEvals',1e10,'MaxIter',1e10);

x=fminsearch('F19_Unfolded_tc_equation_MC',x0,minopt);

Ans= {x(1),x(2),err3};
fprintf(fileIDU,formatSpec,Ans{1,:}); % prints to file
%fprintf('%d ', i);
end

load Unfoldedtm.dat;
fprintf('\nF-H distance (A) = ');
mean(Unfoldedtm(:,1))
std(Unfoldedtm(:,1))
fprintf('\nCorrelation time (ns) = ');
mean(Unfoldedtm(:,2))
std(Unfoldedtm(:,2))
```

```
fprintf('\nInternal motion (ps) = ');
fprintf('%d\n',1200);
fprintf('Order parameter = ');
fprintf('%d\n',0.32);
fprintf('Error = ');
fprintf('%d\n', err3);
fprintf('\n')
```

APPENDIX 6.2. SPECTRAL DENSITY FUNCTIONS FOR THE FOLDED STATE.

```
% Equations were modified from Li, Chemistry. 2013,19(38):12705-10. doi:
10.1002/chem.201301657.
% CSA (-93.5) and n (0.24) were taken from London, JBNMR 1996, 7, 261
% CSA (42.2) and n (0.27) were taken from Durr, JMR 2008, 191, 7-15
% te and S were taken from Farrow, Biochemistry 1995, 34, 868

function chi2=chi2_simple(xarg);

global MCR1F  MCR2F
global calc_R1F  calc_R2F
global err2
global r tm te S

r = xarg(1); %in Angstrom
tm = xarg(2);
te = 20e-12;
S = 0.82;

wF= 470530000 * 2*pi; %rad/s
wH= 500120000 * 2*pi; %rad/s

dO= -93.5; % CSA ppm
n= 0.24; % asymmetry, 0.2-0.4

gH= 42576000; % /s/T
gF= 40052000; % /s/T
yF= 251790000; %rad/s/T
yH= 267530000; %rad/s/T

uo= 4*pi*10^-7; % T2 * m3 * J-1
hbar = 1.054571726 * 10^-34; % J * s

C = (((uo/(4*pi))*hbar*yF*yH)/(r*10^-10)^3); % F-H dipolar coupling constant
CSA = wF^2*(dO/1000000)^2*(1+((n^2)/3)); % CSA

t=1/((1/tm)+(1/te));

%Spectral density functions
JwF = (((S*tm)/(1+((wF*tm)^2)))+((((1-S)*t)/(1+((wF*t)^2)))));
JwH = (((S*tm)/(1+((wH*tm)^2)))+((((1-S)*t)/(1+((wH*t)^2)))));
JwFmwH = (((S*tm)/(1+(((wF-wH)*tm)^2)))+((((1-S)*t)/(1+(((wF-wH)*t)^2)))));
JwFpwH = (((S*tm)/(1+(((wF+wH)*tm)^2)))+((((1-S)*t)/(1+(((wF+wH)*t)^2)))));
J0 = ((S*tm)+((1-S)*t));
```

```
%Calculate relaxation rates
calc_R1F = ((C^2/10)*[(3*JwF)+JwFmwH+(6*JwFpwH)])+((2/15)*JwF*CSA);
calc_R2F =
((C^2/20)*[(4*J0)+(3*JwF)+JwFmwH+(6*JwH)+(6*JwFpwH)])+((1/45)*CSA*[(3*JwF)
+(4*J0)]); %This had a CSA multiplier of 2/15

%Error
ChiR1=(calc_R1F-MCR1F).^2;
ChiR2=(calc_R2F-MCR2F).^2;

chi2=ChiR1+ChiR2;
err2=sqrt(chi2);
```

APPENDIX 6.3. SPECTRAL DENSITY FUNCTIONS FOR THE UNFOLDED STATE.

```
% Equations were modified from Li, Chemistry. 2013,19(38):12705-10. doi:
10.1002/chem.201301657.
% CSA (-93.5) and n (0.24) were taken from London, JBNMR 1996, 7, 261
% CSA (42.2) and n (0.27) were taken from Durr, JMR 2008, 191, 7-15
% te and S were taken from Farrow, Biochemistry 1995, 34, 868

function chi2=chi2_simple(xarg);

global MCR1U  MCR2U
global calc_R1U  calc_R2U
global err3
global r tm te S

r = xarg(1); %in Angstrom
tm = xarg(2);
te = 1200-12;
S = 0.32;

wF= 470530000 * 2*pi; %rad/s
wH= 500120000 * 2*pi; %rad/s

dO= -93.5; % CSA ppm
n= 0.24; % asymmetry, 0.2-0.4

gH= 42576000; % /s/T
gF= 40052000; % /s/T
yF= 251790000; %rad/s/T
yH= 267530000; %rad/s/T

uo= 4*pi*10^-7; % T2 * m3 * J-1
hbar = 1.054571726 * 10^-34; % J * s

C = (((uo/(4*pi))*hbar*yF*yH)/(r*10^-10)^3); % F-H dipolar coupling constant
CSA = wF^2*(dO/1000000)^2*(1+((n^2)/3)); % CSA

t=1/((1/tm)+(1/te));

%Spectral density functions
JwF = (((S*tm)/(1+((wF*tm)^2)))+((((1-S)*t)/(1+((wF*t)^2)))));
JwH = (((S*tm)/(1+((wH*tm)^2)))+((((1-S)*t)/(1+((wH*t)^2)))));
JwFmwH = (((S*tm)/(1+(((wF-wH)*tm)^2)))+((((1-S)*t)/(1+(((wF-wH)*t)^2)))));
JwFpwH = (((S*tm)/(1+(((wF+wH)*tm)^2)))+((((1-S)*t)/(1+(((wF+wH)*t)^2)))));
J0 = ((S*tm)+((1-S)*t));
```

```
%Calculate relaxation rates
calc_R1U = ((C^2/10)*[(3*JwF)+JwFmwH+(6*JwFpwH)])+((2/15)*JwF*CSA);
calc_R2U =
((C^2/20)*[(4*J0)+(3*JwF)+JwFmwH+(6*JwH)+(6*JwFpwH)])+((1/45)*CSA*[(3*JwF)
+(4*J0)]); %This had a CSA multiplier of 2/15

%Error
ChiR1=(calc_R1U-MCR1U).^2;
ChiR2=(calc_R2U-MCR2U).^2;

chi2=ChiR1+ChiR2;
err3=sqrt(chi2);
```

APPENDIX 7.1. SCRIPT FOR FITTING EXCHANGE SPECTROSCOPY DATA.

Calls on Appendix 7.2 and 7.3, ensure they are in the same folder as 7.1.

```
% Fit for Slow exchange
% drkN SH3, F19
% by AES
% Can set R1 to value attained from inversion recovery sequence if desired.

clear all
close all

global tmix                 % exchange time, in seconds
global expt_FF_pk expt_UU_pk    % experimental self peaks
global expt_FU_pk expt_UF_pk    % experimental cross peaks
global calc_FF_pk calc_UU_pk    % obtained by simulations of self peaks
global calc_FU_pk calc_UF_pk    % obtained by simulations of cross peaks
global tmix_plot              % array of exchange times used for plotting
global err2                 % error
global calc_FF_pk_plot calc_UU_pk_plot calc_FU_pk_plot calc_UF_pk_plot % plots
fits
global DataFF DataUU          % MC self peaks
global DataFU DataUF          % MC cross peaks

tmix=[0.300 0.140 0.800 0.0015 0.210 0.070 0.500];  % exchange times, in seconds

FF=[146271,144431,103987]; % insert triplicate delays
UU=[915785,928604,847891];
FU=[53659,51912,51386];
UF=[15430,14034,13400];

A=mean(FF); % calculates the average of the triplicates
B=mean(UU);
C=mean(FU);
D=mean(UF);

expt_FF_pk=[72815 A 15682 271150 109976 195355 34026]; % extracting
experimental FF points
expt_UU_pk=[698989 B 320137 1220349 831850 1052992 519585];     % extracting
experimental UU points
expt_FU_pk=[68907 C 44151 3555 60381 28220 60108];       % extracting cross
peaks
expt_UF_pk=[93498 D 50937 19080 71081 58115 69447];       % extracting cross
peaks

sigmaFF=std(FF); % calculates the standard deviation of the triplicates
```

```
sigmaUU=std(UU);
sigmaFU=std(FU);
sigmaUF=std(UF);

covarFF=sigmaFF^2; %MC uses covariance, which is standard deviation squared
covarUU=sigmaUU^2;
covarFU=sigmaFU^2;
covarUF=sigmaUF^2;

CovarFF = [covarFF covarFF covarFF covarFF covarFF covarFF covarFF]; % Make
sure this is the same size as tmix
CovarUU = [covarUU covarUU covarUU covarUU covarUU covarUU covarUU];
CovarFU = [covarFU covarFU covarFU covarFU covarFU covarFU covarFU];
CovarUF = [covarUF covarUF covarUF covarUF covarUF covarUF covarUF];

%MC stuff, can name files whatever, but need to change below if you do
nsamples = 100;
fileIDF = fopen('Exchange.dat','w');
formatSpec = '%d %d %d %d %d %d %d %d %d\n'; % This will depend on if you
allow R1 to vary or if you set it
%formatSpec = '%d %d %d %d %d %d %d\n'; % This will depend on if you allow R1
to vary or if you set it

% ---------------- END OF INPUT -----------------

% --- FIT ---
MCFF = mvnrnd(expt_FF_pk,CovarFF,nsamples); % This generates the MC matrix
sigmaFF % Actual sample standard deviation
std(MCFF) % MC standard deviation, make sure it matches the actual standard
deviation
MCUU = mvnrnd(expt_UU_pk,CovarUU,nsamples);
MCFU = mvnrnd(expt_FU_pk,CovarFU,nsamples);
MCUF = mvnrnd(expt_UF_pk,CovarUF,nsamples);

for i=[1:nsamples] % Loops and fits
    DataFF = MCFF(i,:); % reads row by row
    DataUU = MCUU(i,:);
    DataFU = MCFU(i,:);
    DataUF = MCUF(i,:);

Izf = max(DataFF);  %  Folded decay curve initial amplitude
Izu = max(DataUU);  %  Unfolded decay curve initial amplitude
kfu = 3; %  unfolding rate
kuf = 0.5; %  folding rate
R1f = 1.8;  %  R1 guess for folded
R1u = 1.5; %  R1 guess for unfolded
```

```
Efu = min(DataFU); % Leakage, if the 0ms point gives a buildup peak
Euf = min(DataUF); % Leakage, if the 0ms point gives a buildup peak

x0 = [kfu, kuf, Izf, Izu, Efu, Euf, R1f,R1u]; % declaring variables to minimize
%x0 = [kfu, kuf, Izf, Izu, Efu, Euf]; % declaring variables to minimize with R1 set

minopt = optimset('TolX',1e-6,'TolFun',1e-6,'MaxFunEvals',1e6,'MaxIter',1e6);

x=fminsearch('chi2_simple35_F19_MC',x0,minopt);

Ans= {x(1),x(2),x(3),x(4),x(5),x(6),x(7),x(8),err2}; % vary R1
%Ans= {x(1),x(2),x(3),x(4),x(5),x(6),err2}; % dont vary R1
fprintf(fileIDF,formatSpec,Ans{1,:}); %prints to file
fprintf('%d ', i);
end

load Exchange.dat;
fprintf('\nkunfold\n');
mean(Exchange(:,1))
std(Exchange(:,1))
fprintf('\nkfold\n');
mean(Exchange(:,2))
std(Exchange(:,2))
fprintf('\nR1F\n'); % comment and uncomment depending on if you vary R1
mean(Exchange(:,7))
std(Exchange(:,7))
fprintf('\nR1U\n'); % comment and uncomment depending on if you vary R1
mean(Exchange(:,8))
std(Exchange(:,8))

% Plotting

figure(1);
plot(tmix,expt_FF_pk,'rs', 'MarkerSize',14,'Linewidth',4);
hold on
plot(tmix,expt_UU_pk,'bo','MarkerSize',14,'Linewidth',4);
hold on
plot(tmix,expt_FU_pk,'rs', 'MarkerSize',14,'Linewidth',4);
hold on
plot(tmix,expt_UF_pk,'bo','MarkerSize',14,'Linewidth',4);

tmix_plot=linspace(min(tmix),max(tmix),200);

Izf = mean(Exchange(:,3));  %  Decay curve initial amplitude
Izu = mean(Exchange(:,4));  %  Buildup curve initial amplitude
kfu = mean(Exchange(:,1)); %  kfu
```

```
kuf = mean(Exchange(:,2)); %  kuf
%R1f = 1.8;  %  R1 guess for folded
%R1u = 1.5; %  R1 guess for unfolded
R1f = mean(Exchange(:,7));  %  R1 guess for folded
R1u = mean(Exchange(:,8)); %  R1 guess for unfolded
Efu = mean(Exchange(:,5)); % Leakage, if the 0ms point gives a buildup peak
Euf = mean(Exchange(:,6)); % Leakage, if the 0ms point gives a buildup peak

chi2_simple_plot35_F19(x);

plot(tmix_plot,calc_FF_pk_plot,'k-','Linewidth', 2);
plot(tmix_plot,calc_UU_pk_plot,'k-','Linewidth',2);
plot(tmix_plot,calc_FU_pk_plot,'k-','Linewidth', 2);
plot(tmix_plot,calc_UF_pk_plot,'k-','Linewidth',2);
fig_leg=legend('FF','UU','FU','UF','Location','Best');
set(fig_leg,'FontSize',18,'fontweight','bold','Box','off');
hold off

tit=[' 19F drkN SH3 ', '  error = ', num2str(err2)];
title(tit,'fontsize',20);
xlabel('Time (s)','fontsize', 20);
ylabel('Intensity','fontsize',20);
set(gca,'fontsize',18);

%fn0 = ['Dilute_EXSY_022315.eps'];
%print( gcf, '-depsc2', fn0 )

hold off
```

APPENDIX 7.2. EVOLUTION EQUATIONS FOR EXCHANGE SPECTROSCOPY.

```
% Equations were taken from Farrow, J. Bio. NMR, 4 (1994) 727-734

function chi2=chi2_simple(xarg);

global tmix
global DataFF DataUU    % MC self peaks
global DataFU DataUF    % MC cross peaks
global calc_FF_pk calc_UU_pk calc_FU_pk calc_UF_pk
global err2

kfu=xarg(1);
kuf=xarg(2);
Izf=xarg(3);
Izu=xarg(4);
Efu=xarg(5);
Euf=xarg(6);

%R1f=1.8; % Set to value if desired, ie R1f=[2.4];
%R1u=1.5; % Set to value if desired.
R1f=xarg(7); % Set to value if desired, ie R1f=[2.4];
R1u=xarg(8);

a11 = R1f + kfu;
a22 = R1u + kuf;
a12 = -kuf;
a21 = -kfu;

L1 = [(1/2)*((a11+a22)+((a11-a22)^2+4*kfu*kuf).^(1/2))];
L2 = [(1/2)*((a11+a22)-((a11-a22)^2+4*kfu*kuf).^(1/2))];

for i=1:length(tmix)

FF=(Izf*(-(L2-a11)*exp(-L1*tmix(i))+(L1-a11)*exp(-L2*tmix(i)))/(L1-L2));
UU=(Izu*(-(L2-a22)*exp(-L1*tmix(i))+(L1-a22)*exp(-L2*tmix(i)))/(L1-L2));

FU=(Efu+Izf*((a21*exp(-L1*tmix(i)))-(a21*exp(-L2*tmix(i))))/(L1-L2));
UF=(Euf+Izu*((a12*exp(-L1*tmix(i)))-(a12*exp(-L2*tmix(i))))/(L1-L2));

  calc_FF_pk(i)=FF(1);
  calc_UU_pk(i)=UU(1);
  calc_FU_pk(i)=FU(1);
  calc_UF_pk(i)=UF(1);

end;
```

```
ChiFF=sum((calc_FF_pk-DataFF).^2);
ChiUU=sum((calc_UU_pk-DataUU).^2);
ChiFU=sum((calc_FU_pk-DataFU).^2);
ChiUF=sum((calc_UF_pk-DataUF).^2);
chi2=ChiFF+ChiUU+ChiFU+ChiUF;
err2=sqrt(chi2);
```

APPENDIX 7.3. EXCHANGE SPECTROSCOPY PLOTTING SCRIPT.

```
function dummy=chi2_simple_plot(xarg);

global tmix_plot
global calc_FF_pk_plot calc_UU_pk_plot calc_FU_pk_plot calc_UF_pk_plot

kfu=xarg(1);
kuf=xarg(2);
Izf=xarg(3);
Izu=xarg(4);
Efu=xarg(5);
Euf=xarg(6);
%R1f=1.8; % Set to value if desired, ie R1f=[2.4];
%R1u=1.5; % Set to value if desired.
R1f=xarg(7); % Set to value if desired, ie R1f=[2.4];
R1u=xarg(8);

a11 = R1f + kfu;
a22 = R1u + kuf;
a12 = -kuf;
a21 = -kfu;

L1 = [(1/2)*((a11+a22)+((a11-a22)^2+4*kfu*kuf).^(1/2))];
L2 = [(1/2)*((a11+a22)-((a11-a22)^2+4*kfu*kuf).^(1/2))];

for i=1:length(tmix_plot)

FF=(Izf*(-(L2-a11)*exp(-L1*tmix_plot(i))+(L1-a11)*exp(-L2*tmix_plot(i)))/(L1-L2));
UU=(Izu*(-(L2-a22)*exp(-L1*tmix_plot(i))+(L1-a22)*exp(-L2*tmix_plot(i)))/(L1-L2));

FU=(Efu+Izf*((a21*exp(-L1*tmix_plot(i)))-(a21*exp(-L2*tmix_plot(i))))/(L1-L2));
UF=(Euf+Izu*((a12*exp(-L1*tmix_plot(i)))-(a12*exp(-L2*tmix_plot(i))))/(L1-L2));

  calc_FF_pk_plot(i)=FF(1);
  calc_UU_pk_plot(i)=UU(1);
  calc_FU_pk_plot(i)=FU(1);
  calc_UF_pk_plot(i)=UF(1);
end;
```

REFERENCES

1 Zimmerman, S. B. & Trach, S. O. Estimation of macromolecule concentrations and excluded volume effects for the cytoplasm of *Escherichia coli*. *Journal of Molecular Biology* **222**, 599-620 (1991).

2 Theillet, F.-X., Binolfi, A., Frembgen-Kesner, T., Hingorani, K., Sarkar, M., Kyne, C., Li, C., Crowley, P., Gierasch, L. M., Pielak, G. J., Elcock, A. H., Gershenson, A. & Selenko, P. Physicochemical properties of cells and thier effects on intrinsically disordered proteins (IDPs). *Chemical Reviews* **114**, 6661-6714 (2014).

3 Srere, P. A. The infrastructure of the mitochondrial matrix. *Trends in Biochemical Sciences* **5**, 120-121 (1980).

4 Spitzer, J. & Poolman, B. The role of biomacromolecular crowding, ionic strength, and physicochemical gradients in the complexities of life's emergence. *Microbiology and Molecular Biology Reviews* **73**, 371-388 (2009).

5 Waudby, C. A., Camilloni, C., Fitzpatrick, A. W. P., Cabrita, L. D., Dobson, C. M., Vendruscolo, M. & Christodoulou, J. In-cell NMR characterization of the secondary structure populations of a disordered conformation of α-synuclein within *E. coli* cells. *PLoS ONE* **8**, e72286 (2013).

6 London, R. E., Gregg, C. T. & Matwiyoff, N. A. Nuclear magnetic resonance of rotational mobility of mouse hemoglobin labeled with [2-^{13}C] histidine. *Science* **188**, 266-268 (1975).

7 Llinas, M., Wüthrich, K., Schwotzer, W. & Von Philipsborn, W. ^{15}N nuclear magnetic resonance of living cells. *Nature* **257**, 817-818 (1975).

8 Brindle, K. M., Williams, S.-P. & Boulton, M. ^{19}F NMR detection of a fluorine-labelled enzyme *in vivo*. *FEBS Letters* **255**, 121-124 (1989).

9 Daniels, A., Williams, R. J. & Wright, P. E. Nuclear magnetic resonance studies of the adrenal gland and some other organs. *Nature* **261**, 321-323 (1976).

10 Brown, F. F., Campbell, I. D., Kuchel, P. W. & Rabenstein, D. C. Human erythrocyte metabolism studies by 1H spin echo NMR. *FEBS Letters* **82**, 12-16 (1977).

11 Serber, Z. & Dötsch, V. In-cell NMR spectroscopy. *Biochemistry* **40**, 14317-14323 (2001).

12 Serber, Z., Ledwidge, R., Miller, S. M. & Dötsch, V. Evaluation of Parameters Critical to Observing Proteins Inside Living Escherichia coli by In-Cell NMR Spectroscopy. *Journal of the American Chemical Society* **123**, 8895-8901 (2001).

13 Freedberg, D. & Selenko, P. Live cell NMR. *Annual Review of Biophysics* **43**, 171-192 (2014).

14 Hänsel, R., Luh, L. M., Corbeski, I., Trantirek, L. & Dötsch, V. In-cell NMR and EPR spectroscopy of biomacromolecules. *Angewandte Chemie International Edition* (2014).

15 Tochio, H. Watching protein structure at work in living cells using NMR spectroscopy. *Current Opinion in Chemical Biology* **16**, 609-613 (2012).

16 Pielak, G. J. & Tian, F. Membrane proteins, magic-angle spinning, and in-cell NMR. *Proceedings of the National Academy of Sciences USA* **109**, 4715-4716 (2012).

17 Ma, J., McLeod, S., MacCormack, K., Sriram, S., Gao, N., Breeze, A. L. & Hu, J. Real-time monitoring of New Delhi metallo-β-Lactamase activity in living cacterial cells by ^{1}H NMR spectroscopy. *Angewandte Chemie International Edition* **53**, 2130-2133 (2014).

18 Anfinsen, C. B. Principles that govern the folding of protein chains. *Science* **181**, 223-230 (1973).

19 McConkey, E. Molecular evolution, intracellular organization, and the quinary structure of proteins. *Proceedings of the National Academy of Sciences USA* **79**, 3236-3240 (1982).

20 Srere, P. A. The metabolon. *Trends in Biochemical Sciences* **10**, 109-110 (1985).

21 Wirth, A. J. & Gruebele, M. Quinary protein structure and the consequences of crowding in living cells: Leaving the test-tube behind. *BioEssays* **35**, 984-993 (2013).

22 Gershenson, A. Deciphering protein stability in cells. *Journal of Molecular Biology* **426**, 4-6 (2014).

23 Li, C., Charlton, L. M., Lakkavaram, A., Seagle, C., Wang, G., Young, G. B., Macdonald, J. M. & Pielak, G. J. Differential dynamical effects of macromolecular crowding on an intrinsically disordered protein and a globular protein: Implications for in-cell NMR spectroscopy. *Journal of the American Chemical Society* **130**, 6310-6311 (2008).

24 Barnes, C. O. & Pielak, G. J. In-cell protein NMR and protein leakage. *Proteins: Structure, Function, and Bioinformatics* **79**, 347-351 (2011).

25 Waudby, C. A., Mantle, M. D., Cabrita, L. D., Gladden, L. F., Dobson, C. M. & Christodoulou, J. Rapid distinction of intracellular and extracellular proteins using NMR diffusion measurements. *Journal of the American Chemical Society* **134**, 11312-11315 (2012).

26 Reardon, P. N. & Spicer, L. D. Multidimensional NMR spectroscopy for protein characterization and assignment inside cells. *Journal of the American Chemical Society* **127**, 10848-10849 (2005).

27 Sakakibara, D., Sasaki, A., Ikeya, T., Hamatsu, J., Hanashima, T., Mishima, M., Yoshimasu, M., Hayashi, N., Mikawa, T. & Wälchli, M. Protein structure determination in living cells by in-cell NMR spectroscopy. *Nature* **458**, 102-105 (2009).

28 Crowley, P. B., Chow, E. & Papkovskaia, T. Protein interactions in the *Escherichia coli* cytosol: an impediment to in-cell NMR spectroscopy. *ChemBioChem* **12**, 1043-1048 (2011).

29 Crowley, P. B., Kyne, C. & Monteith, W. B. Simple and inexpensive incorporation of 19F-Tryptophan for protein NMR spectroscopy. *Chemical Communications* **48**, 10681-10683 (2012).

30 Hamatsu, J., O'Donovan, D., Tanaka, T., Shirai, T., Hourai, Y., Mikawa, T., Ikeya, T., Mishima, M., Boucher, W., Smith, B. O., Laue, E. D., Shirakawa, M. & Ito, Y. High-resolution heteronuclear multidimensional NMR of proteins in living insect cells using a baculovirus protein expression system. *Journal of the American Chemical Society* **135**, 1688-1691 (2013).

31 Li, C., Wang, G.-F., Wang, Y., Creager-Allen, R., Lutz, E. A., Scronce, H., Slade, K. M., Ruf, R. A. S., Mehl, R. A. & Pielak, G. J. Protein ^{19}F NMR in *Escherichia coli*. *Journal of the American Chemical Society* **132**, 321-327 (2010).

32 Wang, Q., Zhuravleva, A. & Gierasch, L. M. Exploring weak, transient protein-protein interactions in crowded i*n vivo* environments by in-cell nuclear magnetic resonance spectroscopy. *Biochemistry* **50**, 9225-9236 (2011).

33 Xu, G., Ye, Y., Liu, X., Cao, S., Wu, Q., Cheng, K., Liu, M., Pielak, G. J. & Li, C. Strategies for Protein NMR in Escherichia coli. *Biochemistry* **53**, 1971-1981 (2014).

34 Kosol, S., Contreras-Martos, S., Cedeño, C. & Tompa, P. Structural characterization of intrinsically disordered proteins by NMR spectroscopy. *Molecules* **18**, 10802-10828 (2013).

35 Luh, L. M., Haensel, R., Loehr, F., Kirchner, D. K., Krauskopf, K., Pitzius, S., Schaefer, B., Tufar, P., Corbeski, I., Guentert, P. & Dötsch, V. Molecular crowding drives active Pin1 into nonspecific complexes with endogenous proteins prior to substrate recognition. *Journal of the American Chemical Society* **135**, 13796-13803 (2013).

36 Latham, M. P. & Kay, L. E. Is buffer a good proxy for a crowded cell-like environment? A comparative NMR study of calmodulin side-chain dynamics in buffer and *E. coli* Lysate. *PLoS ONE* **7**, e48226 (2012).

37 Latham, M. P. & Kay, L. E. Probing non-specific interactions of Ca^{2+}-calmodulin in *E. coli* lysate. *Journal of Biomolecular NMR* **55**, 239-247 (2013).

38 Reckel, S., Lopez, J. J., Löhr, F., Glaubitz, C. & Dötsch, V. In-cell solid-state NMR as a tool to study proteins in large complexes. *ChemBioChem* **13**, 534-537 (2012).

39 Zhao, X. Protein structure determination by solid-state NMR. *Topics in Current Chemistry* **326**, 187–214 (2012).

40 Latham, M. P. & Kay, L. E. A similar *in vitro* and in cell-lysate folding intermediate for the FF domain. *Journal of Molecular Biology* (2014).

41 Sekhar, A., Latham, M. P., Vallurupalli, P. & Kay, L. E. Viscosity-dependent kinetics of protein conformational exchange: microviscosity effects and the need for a small viscogen. *Journal of Physical Chemistry B* **118**, 4546-4551 (2014).

42 Wang, Y., Li, C. & Pielak, G. J. Effects of proteins on protein diffusion. *Journal of the American Chemical Society* **132**, 9392-9397 (2010).

43 Majumder, S., DeMott, C. M., Burz, D. S. & Shekhtman, A. Using singular value decomposition to characterize protein–protein interactions by in-cell NMR spectroscopy. *ChemBioChem* **15**, 929-933 (2014).

44 O'Hagan, D. & Harper, D. B. Fluorine-containing natural products. *Journal of Fluorine Chemistry* **100**, 127-133 (1999).

45 Gerig, J. T. Fluorine NMR of proteins. *Progress in Nuclear Magnetic Resonance Spectroscopy* **26, Part 4**, 293-370 (1994).

46 Khan, F., Kuprov, I., Craggs, T. D., Hore, P. J. & Jackson, S. E. ^{19}F NMR studies of the native and denatured states of green fluorescent protein. *Journal of the American Chemical Society* **128**, 10729-10737 (2006).

47 Schlesinger, A. P., Wang, Y., Tadeo, X., Millet, O. & Pielak, G. J. Macromolecular crowding fails to fold a globular protein in cells. *Journal of the American Chemical Society* **133**, 8082-8085 (2011).

48 Englander, S. W. & Kallenbach, N. R. Hydrogen exchange and structural dynamics of proteins and nucleic acids. *Quarterly Reviews of Biophysics* **16**, 521-655 (1983).

49 Hernandez, G. & LeMaster, D. M. NMR analysis of native-state protein conformational flexibility by hydrogen exchange. *Methods in Molecular Biology* **490**, 285-310 (2009).

50 Skinner, J. J., Lim, W. K., Bédard, S., Black, B. E. & Englander, S. W. Protein hydrogen exchange: Testing current models. *Protein Science* **21**, 987-995 (2012).

51 Miklos, A. C., Li, C. & Pielak, G. J. Using NMR-detected backbone amide ^{1}H exchange to assess macromolecular crowding effects on globular-protein stability. *Methods in Enzymology* **466**, 1-18 (2009).

52 Smith, A. E., Sarkar, M., Young, G. B. & Pielak, G. J. Amide proton exchange of a dynamic loop in cell extracts. *Protein Science* **22**, 1313-1319 (2013).

53 Benton, L. A., Smith, A. E., Young, G. B. & Pielak, G. J. Unexpected effects of macromolecular crowding on protein stability. *Biochemistry* **51**, 9773-9775 (2012).

54 Smith, A. E., Zhou, L. Z. & Pielak, G. J. Hydrogen exchange of disordered proteins in Escherichia coli. *Protein Science* **24**, 706-713 (2015).

55 Miklos, A. C., Li, C., Sharaf, N. G. & Pielak, G. J. Volume exclusion and soft interaction effects on protein stability under crowded conditions. *Biochemistry* **49**, 6984-6991 (2010).

56 Sanfelice, D., Politou, A., Martin, S. R., Rios, P. D. L., Temussi, P. & Pastore, A. The effect of crowding and confinement: a comparison of Yfh1 stability in different environments. *Physical Biology* **10**, 045002 (2013).

57 Sarkar, M., Smith, A. E. & Pielak, G. J. Impact of reconstituted cytosol on protein stability. *Proceedings of the National Academy of Sciences USA* **110**, 19342-19347 (2013).

58 Inomata, K., Ohno, A., Tochio, H., Isogai, S., Tenno, T., Nakase, I., Takeuchi, T., Futaki, S., Ito, Y., Hiroaki, H. & Shirakawa, M. High-resolution multi-dimensional NMR spectroscopy of proteins in human cells. *Nature* **458**, 106-109 (2009).

59 Sarkar, M., Lu, J. & Pielak, G. J. Protein crowder charge and protein stability. *Biochemistry* **53**, 1601-1606 (2014).

60 Sarkar, M. & Pielak, G. J. An osmolyte mitigates the destabilizing effect of protein crowding. *Protein Science* **23**, 1161-1164 (2014).

61 Monteith, W. B. & Pielak, G. J. Residue level quantification of protein stability in living cells. *Proceedings of the National Academy of Sciences USA* **111**, 11335-11340 (2014).

62 Ghaemmaghami, S. & Oas, T. G. Quantitative protein stability measurement in vivo. *Nature Structural Biology* **8**, 879-882 (2001).

63 Monteith, W. B., Cohen, R. D., Smith, A. E., Guzman-Cisneros, E. & Pielak, G. J. Quinary structure modulates protein stability in cells. *Proceedings of the National Academy of Sciences USA* **112**, 1739-1742 (2015).

64 Bertrand, K., Reverdatto, S., Burz, D. S., Zitomer, R. & Shekhtman, A. Structure of proteins in eukaryotic compartments. *Journal of the American Chemical Society* **134**, 12798-12806 (2012).

65 Kubo, S., Nishida, N., Udagawa, Y., Takarada, O., Ogino, S. & Shimada, I. A gel-encapsulated bioreactor system for NMR studies of protein–protein interactions in living mammalian cells. *Angewandte Chemie International Edition* **52**, 1208-1211 (2013).

66 Banci, L., Barbieri, L., Luchinat, E. & Secci, E. Visualization of redox-controlled protein fold in living cells. *Chemistry and Biology* **20**, 747-752 (2013).

67 Banci, L., Barbieri, L., Bertini, I., Luchinat, E., Secci, E., Zhao, Y. & Aricescu, A. R. Atomic-resolution monitoring of protein maturation in live human cells by NMR. *Nature Chemical Biology* **9**, 297-299 (2013).

68 Barbieri, L., Luchinat, E. & Banci, L. Structural insights of proteins in sub-cellular compartments: in-mitochondria NMR. *Biochimica et Biophysica Acta* **1843**, 2492-2496 (2014).

69 Danielsson, J., Inomata, K., Murayama, S., Tochio, H., Lang, L., Shirakawa, M. & Oliveberg, M. Pruning the ALS-associated protein SOD1 for in-cell NMR. *Journal of the American Chemical Society* **135**, 10266-10269 (2013).

70 Bekei, B. *In-cell NMR spectroscopy in mammalian cells* Doctor rerum naturalium thesis, Freie Universität Berlin, (2013).

71 Kiehn, E. D. & Holland, J. J. Size distribution of polypeptide chains in cells. *Nature* **226**, 544-545 (1970).

72 Minton, A. P. Models for excluded volume interaction between an unfolded protein and rigid macromolecular cosolutes: Macromolecular crowding and protein stability revisited. *Biophysical Journal* **88**, 971-985 (2005).

73 McGuffee, S. R. & Elcock, A. H. Diffusion, crowding & protein stability in a dynamic molecular model of the bacterial cytoplasm. *PLoS Computational Biology* **6**, e1000694 (2010).

74 Zhou, H. X., Rivas, G. & Minton, A. P. Macromolecular crowding and confinement: biochemical, biophysical, and potential physiological consequences. *Annual Review of Biophysics* **37**, 375-397 (2008).

75 Elcock, A. H. Models of macromolecular crowding effects and the need for quantitative comparisons with experiment. *Current Opinion in Structural Biology* **20**, 196-206 (2010).

76 Hvidt, A. & Linderstrøm-Lang, K. Exchange of hydrogen atoms in insulin with deuterium atoms in aqueous solutions. *Biochimica et Biophysica Acta* **14**, 574-575 (1954).

77 Berger, A. & Linderstrøm-Lang, K. Deuterium exchange of poly-DL-alanine in aqueous solution. *Archives of Biochemistry and Biophysics* **69**, 106-118 (1957).

78 Englander, S. W., Mayne, L., Bai, Y. & Sosnick, T. R. Hydrogen exchange: the modern legacy of Linderstrøm-Lang. *Protein Science* **6**, 1101-1109 (1997).

79 Hernández, G., Anderson, J. S. & LeMaster, D. M. Polarization and polarizability assessed by protein amide acidity. *Biochemistry* **48**, 6482-6494 (2009).

80 Hvidt, A. & Nielsen, S. O. Hydrogen exchange in proteins. *Advances in Protein Chemistry* **21**, 287-386 (1966).

81 Bai, Y., Milne, J. S., Mayne, L. & Englander, S. W. Protein stability parameters measured by hydrogen exchange. *Proteins: Structure, Function, and Genetics* **20**, 4-14 (1994).

82 Neira, J. L., Itzhaki, L. S., Otzen, D. E., Davis, B. & Fersht, A. R. Hydrogen exchange in chymotrypsin inhibitor 2 probed by mutagenesis. *Journal of Molecular Biology* **270**, 99-110 (1997).

83 Bai, Y., Milne, J. S., Mayne, L. & Englander, S. W. Primary structure effects on peptide group hydrogen exchange. *Proteins* **17**, 75-86 (1993).

84 Connelly, G. P., Bai, Y., Jeng, M. F. & Englander, S. W. Isotope effects in peptide group hydrogen exchange. *Proteins* **17**, 87-92 (1993).

85 Molday, R. S., Englander, S. W. & Kallen, R. G. Primary structure effects on peptide group hydrogen exchange. *Biochemistry* **11**, 150-158 (1972).

86 Zhang, Y.-Z. *Protein and peptide structure and interactions studied by hydrogen exchange and NMR* Ph.D. thesis, University of Pennsylvania.

87 Charlton, L. M., Barnes, C. O., Li, C., Orans, J., Young, G. B. & Pielak, G. J. Residue-level interrogation of macromolecular crowding effects on protein stability. *Journal of the American Chemical Society* **130**, 6826-6830 (2008).

88 Miklos, A. C., Sarkar, M., Wang, Y. & Pielak, G. J. Protein crowding tunes protein stability. *Journal of the American Chemical Society* **133**, 7116-7120 (2011).

89 Wang, Y., Sarkar, M., Smith, A. E., Krois, A. S. & Pielak, G. J. Macromolecular crowding and protein stability. *Journal of the American Chemical Society* **134**, 16614-16618 (2012).

90 Wang, A., Robertson, A. D. & Bolen, D. W. Effects of a naturally occurring compatible osmolyte on the internal dynamics of ribonuclease A. *Biochemistry* **34**, 15096-15104 (1995).

91 McPhalen, C. A. & James, M. N. Crystal and molecular structure of the serine proteinase inhibitor CI-2 from barley seeds. *Biochemistry* **26**, 261-269 (1987).

92 De Prat Gay, G., Ruiz-Sanz, J., Neira, J. L., Itzhaki, L. S. & Fersht, A. R. Folding of a nascent polypeptide chain in vitro: cooperative formation of structure in a protein module. *Proceedings of the National Academy of Sciences USA* **92**, 3683-3686 (1995).

93 Itzhaki, L. S., Neira, J. L. & Fersht, A. R. Hydrogen exchange in chymotrypsin inhibitor 2 probed by denaturants and temperature. *Journal of Molecular Biology* **270**, 89-98 (1997).

94 Shaw, G. L., Davis, B., Keeler, J. & Fersht, A. R. Backbone dynamics of chymotrypsin inhibitor 2: Effect of breaking the active site bond and its implications for the mechanism of inhibition of serine proteases. *Biochemistry* **34**, 2225-2233 (1995).

95 Hwang, T. L., van Zijl, P. C. & Mori, S. Accurate quantitation of water-amide proton exchange rates using the phase-modulated CLEAN chemical exchange (CLEANEX-PM) approach with a fast-HSQC (FHSQC) detection scheme. *Journal of Biomolecular NMR* **11**, 221-226 (1998).

96 The PyMOL Molecular Graphics System v. Version 1.3 (Schrodinger, LLC, 2010).

97 Cavallo, L., Kleinjung, J. & Fraternali, F. POPS: A fast algorithm for solvent accessible surface areas at atomic and residue level. *Nucleic Acids Research* **31**, 3364-3366 (2003).

98 Li, C., Wang, Y. & Pielak, G. J. Translational and rotational diffusion of a small globular protein under crowded conditions. *Journal of Physical Chemistry B* **113**, 13390-13392 (2009).

99 Chevelkov, V., Xue, Y., Rao, D. K., Forman-Kay, J. D. & Skrynnikov, N. R. $^{15}N^{H/D}$-SOLEXSY experiment for accurate measurement of amide solvent exchange rates: application to denatured drkN SH3. *Journal of Biomolecular NMR* **46**, 227-244 (2010).

100 Li, C. & Pielak, G. J. Using NMR to distinguish viscosity effects from nonspecific protein binding under crowded conditions *Journal of the American Chemical Society* **131**, 1368–1369 (2009).

101 Covington, A. K., Robinson, R. A. & Bates, R. G. The ionization constant of deuterium oxide from 5 to 50°. *The Journal of Physical Chemistry* **70**, 3820-3824 (1966).

102 Mori, S., van Zijl, P. C. M. & Shortle, D. Measurement of water–amide proton exchange rates in the denatured state of staphylococcal nuclease by a magnetization transfer technique. *Proteins: Structure, Function, and Bioinformatics* **28**, 325-332 (1997).

103 Roesler, K. R. & Rao, A. G. Conformation and stability of barley chymotrypsin inhibitor-2 (CI-2) mutants containing multiple lysine substitutions. *Protein Engineering* **12**, 967-973 (1999).

104 Delaglio, F., Grzesiek, S., Vuister, G. W., Zhu, G., Pfeifer, J. & Bax, A. NMRPipe: a multidimensional spectral processing system based on UNIX pipes. *Journal of Biomolecular NMR* **6**, 277-293 (1995).

105 Hernández, G. & LeMaster, D. M. Relaxation compensation in chemical exchange measurements for the quantitation of amide hydrogen exchange in larger proteins. *Magnetic Resonance in Chemistry* **41**, 699-702 (2003).

106 Dedmon, M. M., Patel, C. N., Young, G. B. & Pielak, G. J. FlgM gains structure in living cells. *Proceedings of the National Academy of Sciences USA* **99**, 12681-12684 (2002).

107 Minton, A. P. Quantitative assessment of the relative contributions of steric repulsion and chemical interactions to macromolecular crowding. *Biopolymers* **99**, 239-244 (2013).

108 Zhou, H.-X. Influence of crowded cellular environments on protein folding, binding, and oligomerization: Biological consequences and potentials of atomistic modeling. *FEBS letters* **587**, 1053-1061 (2013).

109 Luh, L. M., Hänsel, R., Löhr, F., Kirchner, D. K., Krauskopf, K., Pitzius, S., Schäfer, B., Tufar, P., Corbeski, I., Güntert, P. & Dötsch, V. Molecular crowding drives active Pin1 into nonspecific complexes with endogenous

proteins prior to substrate recognition. *Journal of the American Chemical Society* **135**, 13796-13803 (2013).

110 Phillip, Y. & Schreiber, G. Formation of protein complexes in crowded environments - From *in vitro* to *in vivo*. *FEBS Letters* **587**, 1046-1052 (2013).

111 McNulty, B. C., Young, G. B. & Pielak, G. J. Macromolecular crowding in the *Escherichia coli* periplasm maintains α-synuclein disorder. *Journal of Molecular Biology* **355**, 893-897 (2006).

112 Croke, R. L., Sallum, C. O., Watson, E., Watt, E. D. & Alexandrescu, A. T. Hydrogen exchange of monomeric α-synuclein shows unfolded structure persists at physiological temperature and is independent of molecular crowding in *Escherichia coli*. *Protein Science* **17**, 1434-1445 (2008).

113 Barnes, C. O., Monteith, W. B. & Pielak, G. J. Internal and global protein motion assessed with a fusion construct and in-cell NMR spectroscopy. *ChemBioChem* **12**, 390-391 (2011).

114 Maroteaux, L., Campanelli, J. T. & Scheller, R. H. Synuclein: a neuron-specific protein localized to the nucleus and presynaptic nerve terminal. *The Journal of Neuroscience* **8**, 2804-2815 (1988).

115 McNulty, B. C., Tripathy, A., Young, G. B., Charlton, L. M., Orans, J. & Pielak, G. J. Temperature-induced reversible conformational change in the first 100 residues of alpha-synuclein. *Protein Science* **15**, 602-608 (2006).

116 Kutsukake, K. & Iino, T. Role of the FliA-FlgM regulatory system on the transcriptional control of the flagellar regulon and flagellar formation in Salmonella typhimurium. *Journal of Bacteriology* **176**, 3598-3605 (1994).

117 Hughes, K. T., Gillen, K. L., Semon, M. J. & Karlinsey, J. E. Sensing structural intermediates in bacterial flagellar assembly by export of a negative regulator. *Science* **262**, 1277-1280 (1993).

118 Daughdrill, G. W., Hanely, L. J. & Dahlquist, F. W. The *C*-terminal half of the anti-sigma factor FlgM contains a dynamic equilibrium solution structure favoring helical conformations. *Biochemistry* **37**, 1076-1082 (1998).

119 Daughdrill, G. W., Chadsey, M. S., Karlinsey, J. E., Hughes, K. T. & Dahlquist, F. W. The *C*-terminal half of the anti-sigma factor, FlgM, becomes structured when bound to its target, sigma 28. *Nature Structural Biology* **4**, 285-291 (1997).

120 Serber, Z., Corsini, L., Durst, F. & Dötsch, V. In-cell NMR spectroscopy. *Methods in Enzymology* **394**, 17-41 (2005).

121 Booth, I. R. Regulation of cytoplasmic pH in bacteria. *Microbiological Reviews* **49**, 359-378 (1985).

122 Shimba, N., Serber, Z., Ledwidge, R., Miller, S. M., Craik, C. S. & Dötsch, V. Quantitative Identification of the Protonation State of Histidines in Vitro and in Vivo. *Biochemistry* **42**, 9227-9234 (2003).

123 Croke, R. L., Patil, S. M., Quevreaux, J., Kendall, D. A. & Alexandrescu, A. T. NMR determination of pKa values in α-synuclein. *Protein Science* **20**, 256-269 (2011).

124 Good, N. E., Winget, G. D., Winter, W., Connolly, T. N., Izawa, S. & Singh, R. M. M. Hydrogen ion buffers for biological research. *Biochemistry* **5**, 467-477 (1966).

125 Harris, D. C. *Quantitative Chemical Analysis*. Seventh edn, (W. H. Freeman and Company, 2007).

126 Maltsev, A. S., Ying, J. & Bax, A. Impact of *N*-terminal acetylation of α-synuclein on its random coil and lipid binding properties. *Biochemistry* **51**, 5004-5013 (2012).

127 Marsh, J. A., Singh, V. K., Jia, Z. & Forman-Kay, J. D. Sensitivity of secondary structure propensities to sequence differences between α- and γ-synuclein: Implications for fibrillation. *Protein Science* **15**, 2795-2804 (2006).

128 Sarkar, M., Li, C. & Pielak, G. J. Soft interactions and crowding. *Biophysical Reviews* **5**, 187-194 (2013).

129 Shortle, D. Assignment of amino acid type in ^{1}H-^{15}N correlation spectra by labeling with ^{14}N-amino acids. *Journal of Magnetic Resonance* **105**, 88-90 (1994).

130 Krishnarjuna, B., Jaipuria, G., Thakur, A., D'Silva, P. & Atreya, H. Amino acid selective unlabeling for sequence specific resonance assignments in proteins. *Journal of Biomolecular NMR* **49**, 39-51 (2011).

131 Muchmore, D. C., McIntosh, L. P., Russell, C. B., Anderson, D. E. & Dahlquist, F. W. Expression and ^{15}N labeling of proteins for proton and ^{15}N nuclear magnetic resonance. *Methods in Enzymology* **177**, 44-73 (1989).

132 Ohki, S.-y. & Kainosho, M. Stable isotope labeling methods for protein NMR spectroscopy. *Progress in Nuclear Magnetic Resonance Spectroscopy* **53**, 208-226 (2008).

133 Kelly, A. E., Ou, H. D., Withers, R. & Dötsch, V. Low-conductivity buffers for high-sensitivity NMR measurements. *Journal of the American Chemical Society* **124**, 12013-12019 (2002).

134 Kang, L., Moriarty, G. M., Woods, L. A., Ashcroft, A. E., Radford, S. E. & Baum, J. *N*-terminal acetylation of α-synuclein induces increased transient helical propensity and decreased aggregation rates in the intrinsically disordered monomer. *Protein Science* **21**, 911-917 (2012).

135 Dyson, H. J., Tennant, L. L. & Holmgren, A. Proton-transfer effects in the active-site region of *Escherichia coli* thioredoxin using two-dimensional proton NMR. *Biochemistry* **30**, 4262-4268 (1991).

136 Jeng, M.-F. & Dyson, H. J. Direct measurement of the aspartic acid 26 pKa for reduced *Escherichia coli* thioredoxin by ^{13}C NMR *Biochemistry* **35**, 1-6 (1996).

137 Markley, J. L. Observation of histidine residues in proteins by nuclear magnetic resonance spectroscopy. *Accounts of Chemical Research* **8**, 70-80 (1975).

138 Bundi, A. & Wüthrich, K. ^{1}H-NMR parameters of the common amino acid residues measured in aqueous solutions of the linear tetrapeptides H-Gly-Gly-X-L-Ala-OH. *Biopolymers* **18**, 285-297 (1979).

139 Glasoe, P. K. & Long, F. A. Use of glass electrodes to measure acidities in deuterium oxide. *The Journal of Physical Chemistry* **64**, 188-190 (1960).

140 Wu, K. P. & Baum, J. Backbone assignment and dynamics of human α-synuclein in viscous 2 M glucose solution. *Biomolecular NMR Assignments* **5**, 43-46 (2011).

141 Eliezer, D., Kutluay, E., Bussell, R. & Browne, G. Conformational properties of α-synuclein in its free and lipid associated states. *Journal of Molecular Biology* **307**, 1061 (2001).

142 Taylor, J. R. *An Introduction to Error Analysis*. Second edn, (University Science Books, 1997).

143 Kauzmann, W. Some factors in the interpretation of protein denaturation. *Advances in Protein Chemistry* **14**, 1-63 (1959).

144 Richards, F. M. Areas, volumes, packing, and protein structure. *Annual Review of Biophysics and Bioengineering* **6**, 151-176 (1977).

145 Fleming, P. J. & Rose, G. D. Do all backbone polar groups in proteins form hydrogen bonds? *Protein Science* **14**, 1911-1917 (2005).

146 Minton, A. P. Excluded volume as a determinant of macromolecular structure and reactivity. *Biopolymers* **20**, 2093-2120 (1981).

147 Ellis, R. J. Macromolecular crowding: obvious but underappreciated. *Trends in Biochemical Sciences* **26**, 597-604 (2001).

148 Zhang, O. & Forman-Kay, J. D. Structural characterization of folded and unfolded states of an SH3 domain in equilibrium in aqueous buffer. *Biochemistry* **34**, 6784-6794 (1995).

149 Evanics, F., Bezsonova, I., Marsh, J., Kitevski, J. L., Forman-Kay, J. D. & Prosser, R. S. Tryptophan solvent exposure in folded and unfolded states of an SH3 domain by ^{19}F and ^{1}H NMR. *Biochemistry* **45**, 14120-14128 (2006).

150 Ye, Y., Liu, X., Zhang, Z., Wu, Q., Jiang, B., Jiang, L., Zhang, X., Liu, M., Pielak, G. J. & Li, C. ^{19}F NMR spectroscopy as a probe of cytoplasmic viscosity and weak protein interactions in living cells. *Chemistry-A European Journal* **19**, 12705-12710 (2013).

151 Becktel, W. J. & Schellman, J. A. Protein stability curves. *Biopolymers* **26**, 1859-1877 (1987).

152 Ebbinghaus, S., Dhar, A., McDonald, J. D. & Gruebele, M. Protein folding stability and dynamics imaged in a living cell. *Nat Meth* **7**, 319-323 (2010).

153 Ignatova, Z., Krishnan, B., Bombardier, J. P., Marcelino, A. M. C., Hong, J. & Gierasch, L. M. From the test tube to the cell: Exploring the folding and aggregation of a β-clam protein. *Peptide Science* **88**, 157-163 (2007).

154 Myers, J. K., Pace, C. N. & Scholtz, J. M. Denaturant m values and heat capacity changes: relation to changes in accessible surface areas of protein folding. *Protein Science* **4**, 2138-2145 (1995).

155 Lim, W. K., Rösgen, J. & Englander, S. W. Urea, but not guanidinium, destabilizes proteins by forming hydrogen bonds to the peptide group. *Proceedings of the National Academy of Sciences USA* **106**, 2595-2600 (2009).

156 Farrow, N. A., Zhang, O., Forman-Kay, J. D. & Kay, L. E. Comparison of the backbone dynamics of a folded and an unfolded SH3 domain existing in equilibrium in aqueous buffer. *Biochemistry* **34**, 868-878 (1995).

157 Hong, J. & Gierasch, L. M. Macromolecular crowding remodels the energy landscape of a protein by favoring a more compact unfolded state. *Journal of the American Chemical Society* **132**, 10445-10452 (2010).

158 Ai, X., Zhou, Z., Bai, Y. & Choy, W.-Y. ^{15}N NMR spin relaxation dispersion study of the molecular crowding effects on protein folding under native conditions. *Journal of the American Chemical Society* **128**, 3916-3917 (2006).

159 Sapir, L. & Harries, D. Is the depletion force entropic? Molecular crowding beyond steric interactions. *Current Opinion in Colloid & Interface Science* (2014).

160 Lipari, G. & Szabo, A. Model-free approach to the interpretation of nuclear magnetic resonance relaxation in macromolecules. 1. Theory and range of validity. *Journal of the American Chemical Society* **104**, 4546-4559 (1982).

161 Lipari, G. & Szabo, A. Model-free approach to the interpretation of nuclear magnetic resonance relaxation in macromolecules. 2. Analysis of experimental results. *Journal of the American Chemical Society* **104**, 4559-4570 (1982).

162 Luck, L. A., Vance, J. E., O'Connell, T. M. & London, R. E. 19F NMR relaxation studies on 5-fluorotryptophan- and tetradeutero-5-fluorotryptophan-labeled E. coli glucose/galactose receptor. *Journal of Biomolecular NMR* **7**, 261-272 (1996).

163 Farrow, N. A., Zhang, O., Forman-Kay, J. D. & Kay, L. E. A heteronuclear correlation experiment for simultaneous determination of ^{15}N longitudinal decay and chemical exchange rates of systems in slow equilibrium. *Journal of Biomolecular NMR* **4**, 727-734 (1994).